ANALYSIS OF FLUID FLOW TO HORIZONTAL AND SLANT WELLS

by

Liangwen Zhang

A thesis

presented to the University of Waterloo
in fulfilment of the
thesis requirement for the degree of
Doctor of Philosophy

in
Earth Sciences

Waterloo, Ontario, Canada, 1997

The University of Waterloo requires the signatures of all persons using or photocopying this thesis. Please sign below, and give address and date.

ABSTRACT

The applications of horizontal and slant wells in the oil industry have increased rapidly for the last decade after successful improvements in horizontal drilling technology. Compared with conventional vertical wells, horizontal or slant wells can significantly improve the per-well productivity because of the longer contact length of the well with the reservoir and a smaller pressure gradient. Horizontal wells are also more effective in controlling problems such as gas or water coning and solids production. Horizontal wells have also been found more effective in phase displacement in cold or hot injection assisted production.

Productivity from a horizontal or slant well is a function of many factors such as well length, orientation and elevation, reservoir thickness, anisotropy, porosity, compressibility, and boundary conditions, both lateral and vertical. To find the relationship between these factors and the productivity of a well is an important task in choosing the proper well pattern in reservoir exploitation. For this purpose, the focus of this thesis is on the analysis of fluid flow to horizontal and slant wells. A new more general solution is developed in this thesis for evaluating per-well productivity of a horizontal or slant well. Compared with the solutions available in the literature, the new solution considers an arbitrarily oriented slant well in a three dimensional anisotropic reservoir. By using the new solution, the direction along which a well obtains the optimum production can be determined.

As we know, reservoir parameters are the most important factors in well productivity prediction. There are several methods (transient solutions) available in the literature for reservoir parameter estimation. However, the parameters estimated from these solutions can deviate from the real field parameters because of poor assumptions, particularly in highly anisotropic reservoirs. A new transient solution is developed considering an arbitrarily oriented well in an anisotropic reservoir, which is not considered in the solutions available. In the new solution, we have presented detailed analysis on the two characteristic times, the upper and lower impermeable boundary effect time t_b and the well length effect time t_w from a horizontal well. We found these two parameters to be as important as the others such as permeability and storativity in characterizing a well-reservoir interaction model.

Wellbore storage and formation alteration are another two important aspects in a horizontal well test and productivity analysis. A brief analysis of the wellbore storage effect on horizontal well

test interpretation is discussed. The storage effect on a horizontal well test is similar to that of a vertical well test, but can mask one or more flow regimes which can destroy possibilities to estimate the parameters which are characterized only by these regimes, such as the vertical permeability characterized in the early time flow regime.

Formation alteration effect has often been simulated by a skin term for both vertical and horizontal well tests. However, the skin term does not always work, particularly when a large size of the formation is altered (improved or damaged). In order to simulate the alteration effect in such situations, a new model is developed in this thesis. The new model considers a more realistic permeability variation model in the altered zone, a continuous variation model. The permeability in the new model is assumed to satisfy a power relationship with radial distance from the well. Experiments indicate that this power permeability model can more closely model the field alteration than the step permeability model widely discussed in the literature. By using the new model, the alteration characteristics such as alteration degree and alteration size can be evaluated.
Because of the more general and detailed analysis on fluid flow to a horizontal or slant well, we believe the conclusions derived from this research will be beneficial to the further applications of horizontal and slant wells in the petroleum and other industries.

ACKNOWLEDGEMENTS

I wish to personally thank my supervisor, Professors Maurice B. Dusseault and John A. Franklin, for their guidance throughout all aspects of preparation of this thesis. Professor Maurice B. Dusseault has been the consistent supporter both financially and technically during this research. I would also like to thank the members of my graduate committee: Dr. Edward A. Sudicky and Dr. Peter Forsyth of Computer Science for their kindly advice and helpful suggestions throughout this research.

I would like to acknowledge the financial support during my graduate studies awarded by the Government of Ontario through Ontario Graduate Scholarships.

I also would like to thank all the members of Geomechanics Group for their assistance and encouragement during my graduate studies in the University of Waterloo.

This thesis is dedicated to the encouragement and contribution of my wife Aiping Huo and the loving memory of my daughter Hui Zhang

TABLE OF CONTENTS

Chapter One

Introduction

1.1 About Horizontal Wells

Vertical wells have been the main tool used for the purpose of natural underground fluid resource exploration and exploitation [Butler, 1989 et al., 1989; Freeze and Cherry, 1979]. A vertical well, however, has its disadvantages in terms of well productivity. The productivity of a well is mainly controlled by two factors, the conducting force, i.e. the pressure gradient, and the resisting force, quantified through appropriate use of parameters such as permeability, viscosity, and saturation. Permeability is a porous medium related lumped parameter expressing the macroscopic effect of microtexture, assuming a representative elementary volume. The larger the permeability, as in the case of a gravel or vuggy limestone, the less resistance force the medium can exert to flow, and the more production can be achieved. The resistant force factors associated with the fluid phase are viscosity and saturation. Issues such as relative permeability arise when there are more than one fluid phase (oil, water, gas), and this relative permeability incorporates both porous medium factors and fluid properties [Dullien, 1979].

To improve well productivity, the basic ideas are to improve the "conducting-factors" and to reduce the "resisting-factors". Reduction of resisting factors involves directly increasing the formation permeability, a highly successful approach to reservoir treatment in the oil industry which includes methods such as hydraulic fracturing, formation acidizing, sand production and so on. Other methods of reducing the resisting factors are related to reduction of viscosity by heating, solvent injection (including soluble gas), or by changing or affecting the surface tension and the fluid saturations. Methods to increase (or maintain) conducting factors include water flood and gas injection to maintain pressure gradient. Other aspects relating to conducting factor improvement had not been successful until the last decade, when horizontal well drilling techniques were substantially improved. Slant and horizontal wells can increase well productivity by reducing the conducting distance over which the formation pressure must act, compared to a convergent vertical flow well. The geometrical configuration of the fluid collector is therefore a basic factor which can change the exploitation strategy of the pressure drive in a reservoir, and also change the pressure distribution of the reservoir. It can

also give substantial advantages in implementation of gravity-dominated production processes.

All these factors are closely related in a full-scale field flow system. Under conditions of constant flow rate, the pressure gradient is the result of the combined effects of permeability, viscosity, well geometric configuration, and boundary conditions. To maintain a specific production rate in a medium of lower permeability generally requires a higher pressure gradient. Similarly, in a high permeability reservoir, a lower gradient can achieve a specific production rate. Changes of well orientation or boundary conditions, on the other hand, will change the pressure distribution, and affect well flow rate.

Horizontal wells can reduce the resisting force because they can have a length as long as the underground reservoir extent. Horizontal wells have been intensively adopted by the oil industry in the last ten years because of advances in horizontal drilling techniques. The potential for horizontal well application in underground fluid resource exploration and production comes from the natural geological formations which are usually much longer horizontally than vertically. The conventional vertical well exploitation scheme seriously limits the optimum per-well productivities because of the tremendous hydraulic gradient required around the well in order to move the resource stream from great distance to the wellbore. A vertical well represents only a point sink in a horizontal reservoir; this makes it very possible that the productivity potential of the well is impaired if a shale lens or a low permeability blockage is located near the well. The natural layered characteristics of underground formations imply that, if a well can be drilled along the horizontal extension of the layer, tremendous energy can saved in the exploitation process. Horizontal wells, therefore, have become the preferred choice for this purpose in many regions of the world.

However, because of the lack of advanced horizontal drilling techniques, horizontal wells were not widely used until the late 1970's, when horizontal drilling for the first time became feasible both economically and technically. The current horizontal drilling cost has dropped almost to the same per-meter level as vertical drilling. The advances in horizontal drilling technology have significantly increased the possibilities for using horizontal wells in various underground engineering constructions, as the applications of horizontal wells are not limited to the oil industry. In environmental engineering, advantages in catching and blocking groundwater contaminants from contaminated aquifers make horizontal wells much more effective than the conventional vertical wells. It is also obvious that horizontal wells are usually the best choice in dewatering systems in slope stability improvement and other similar applications.

Horizontal wells are more and more used in various industries. However, some basic characteristics of horizontal wells in interacting with layered formations remain unsolved, which limits optimum

design in real applications. These problems include horizontal well productivity evaluations, formation parameter estimation from horizontal well tests, horizontal well test interpretation, parameter effects on productivity, and pressure distribution analysis. This research was intended to address most of these questions, and results will be outlined in the following Chapters.

1.2 Objectives of The Research

The objective of this research is to explore the advantages that horizontal wells offer in both engineering and science applications by theoretical analysis. Thus it is hoped to answer some of the questions arising in use of horizontal wells, including horizontal well productivity analysis, well test interpretation, wellbore damage effects on production, and pressure distribution analysis. The effects of various parameters including formation parameters such as anisotropic permeabilities, compressibility, porosity, and geometrical parameters such as well length, reservoir thickness, well elevation and orientation, are important in understanding characteristics of fluid flow behaviour to a horizontal well. The effect of individual parameters and combinations of these parameters should be generally emphasized, and will be studied herein.

Another major goal of this research program is to analyze and solve fluid flow problems commonly encountered in reservoir engineering, ground water exploration and geotechnical engineering. Those problems include formation alteration effects on production, as well as pressure distributions which results from hydraulic fracturing, formation acidizing and reservoir sand production.

Fluid flow in post-treated formations can be simulated by assuming non-uniform permeability. More generally, the fluid collector factor, i.e. horizontal wells, can also be simulated by the formation permeability as "infinite-conductivity", which might be expressed as follows in a "homogeneous isotropic" reservoir:

$$\nabla \left[[k_0 + \delta(r-r')] \nabla p \right] = c_m \phi \mu \frac{\partial p}{\partial t} \qquad (1.2.1)$$

where k_0 is the homogeneous permeability of the porous medium, $\delta(r-r')$ is the Delta function which is infinite for $r = r'$ and is zero for $r \neq r'$, r is the coordinate and r' is where the fluid collector is located, p is fluid pressure (hydraulic head), c_m is formation compressibility, ϕ is formation porosity, μ is fluid viscosity and t stands for time.

Equation (1.2.1) usually can not be solved analytically for generally non-uniform permeabilities. However, the traditional transient flow solution to a bounded vertical well, achieved by assuming a constant permeability, can not be used for cases when one or more of the above described productivity-improvement treatment methods are used. Significant "calibration" or "correction factors" (such as a skin term) have to be introduced to permit use of these conventional equations in any predictive capacity, and this means that the physics of the process is being mis-represented or overly simplified. To give appropriate solutions for these problems, more physical and mathematical analysis is required and this has become a fundamental objective of this research program.

1.3 Research Approaches

Theoretical analysis has been the main approach for this research program. Several theoretical solutions have been obtained related to applications of horizontal wells in engineering. In analyzing fluid flows in an underground porous medium, Darcy's law, describing fluid flow in porous media, and the continuity equation, describing mass conservation, are the basic theoretical foundations. Because of the different conventions in the expression of the governing equations in oil and groundwater industries, they are used alternatively in this research. The main difference between the two conventions is that the gravity effect is neglected in the oil convention compared to the groundwater convention. In the oil industry, fluid pressure is widely used instead of hydraulic head, which is the sum of pressure and gravity effect commonly used in groundwater research. Other differences are in the use of formation parameters, such as reservoir compressibility and porosity in the oil industry, whereas specific storage is used in the groundwater area. Strictly, all the derivations in this thesis are accurate for the groundwater convention; the oil convention is only acceptable when the gravity term can be safely neglected. The relationships for these different expressions are simple and are listed in the following sections.

1.3.1 Darcy's Law

Darcy's law describes fluid flow in a porous medium. It can be written as the following in terms of hydraulic head and conductivity:

$$\vec{q} = K_x\frac{\partial H}{\partial x}\vec{i} + K_y\frac{\partial H}{\partial y}\vec{j} + \frac{\partial H}{\partial z}\vec{k} \qquad (1.3.1)$$

where q is flow rate, K_x, K_y and K_z are the anisotropic hydraulic conductivities and H is hydraulic head.

The hydraulic head and hydraulic conductivity can be expressed in terms of pressure and permeability in the following way:

$$H = \frac{p}{\rho g} + Z \qquad k_i = K_i\frac{\mu}{\rho g} \qquad (1.3.2)$$

where Z is the elevation head.

If we assume that the fluid density is a constant, then by substituting H and k_i of (1.3.2) into equation (1.3.1), the following is obtained:

$$\vec{q} = -\frac{1}{\mu}\left[k_x\frac{\partial p}{\partial x}\vec{i} + k_y\frac{\partial p}{\partial y}\vec{j} + k_z(\frac{\partial p}{\partial z}+\rho g)\right] \qquad (1.3.3)$$

where ρ is fluid density, g is the gravitational acceleration constant and k_x, k_y and k_z are orthogonal anisotropic permeabilities of the porous medium.

If the gravitational term ρg can be neglected, then equation (1.3.3) becomes the same form as equation (1.3.1) in terms of pressure and permeability viscosity ratio instead of hydraulic head and hydraulic conductivity.

1.3.2 Continuity equation

The continuity equation of fluid flow in a porous medium can be written as:

$$div(\rho\vec{q}) = \frac{\partial(\rho\phi)}{\partial t} \qquad (1.3.4)$$

where ϕ is the porosity of the porous medium, ρ is fluid density.

If we substitute the expression of q in equation (1.3.1) into (1.3.4) and assume a slightly compressible fluid, we obtain the following governing equation in terms of hydraulic head:

$$K_x\frac{\partial^2 H}{\partial x^2} + K_y\frac{\partial^2 H}{\partial y^2} + K_z\frac{\partial H}{\partial z^2} = S_s\frac{\partial H}{\partial t} \tag{1.3.5}$$

where:

$$S_s = \rho g(\alpha+\phi\beta) \tag{1.3.6}$$

is the storage coefficient (specific storage), β is the fluid compressibility and α is formation compressibility which is defined as.

$$\alpha = \frac{1}{V_t}\frac{\partial V_t}{\partial p} \tag{1.3.7}$$

where V_t is the total volume of the porous medium.

In the oil industry the fluid compressibility is usually neglected, and instead of using formation compressibility α, formation void compressibility c_m is used which is defined as:

$$c_m = \frac{1}{V_v}\frac{\partial V_v}{\partial p} \tag{1.3.8}$$

where V_v is the pore volume.

From equation (1.3.7) and (1.3.8) we have:

$$\alpha = \frac{1}{V_t}\frac{\partial V_t}{\partial p} = \frac{1}{V_t}\frac{\partial V_v}{\partial p} = \frac{c_m V_v}{V_t} = c_m\phi \tag{1.3.9}$$

therefore the governing equation (1.3.5) becomes the following form in terms of pressure:

$$\frac{k_x}{\mu}\frac{\partial^2 p}{\partial x^2} + \frac{k_y}{\mu}\frac{\partial^2 p}{\partial y^2} + \frac{k_z}{\mu}\frac{\partial p}{\partial z^2} = c_m\phi\frac{\partial p}{\partial t} \qquad (1.3.10)$$

where the fluid is assumed incompressible ($\beta = 0$).

Therefore, the governing equations of the two conventions also have the same form.

1.3.3 Boundary conditions

Two types of boundary conditions are usually used in fluid flow analyses: the first type condition (known head or pressure) and the second type condition (known flux). The first type boundary condition is usually used in specifying a constant head in the wellbore and drainage boundary, which for a horizontal well can be written as the following:

$$\begin{aligned} H(x,y,z)|_{wellbore} &= H_w \\ p(x,y,z)|_{wellbore} &= p_w(Z) \end{aligned} \qquad (1.3.11)$$

$$\begin{aligned} H(x,y,z)|_{drainage} &= H_e \\ p(x,y,z)|_{drainage} &= p_e(Z) \end{aligned} \qquad (1.3.12)$$

where $p_{well\ bore}(Z)$ and $p_{drainage}(Z)$ are the pressure values along the wellbore and drainage boundaries and are functions of the elevation because of the relationships in equation (1.3.2).

For the drainage boundary, if a constant head is maintained, the maximum and minimum pressures are at the lower and upper boundaries of the formation i.e $p_{drainage}$(lower boundary) = $p_e + \rho gh/2$ and $p_{drainage}$(upper boundary) = $p_e - \rho gh/2$, where p_e is the pressure at the middle of the formation. Because the drainage boundary pressure (far-field pressure) in most oil reservoirs is much larger than the terms introduced by the gravity factor, it is usually neglected by only using p_e. However, if the gravity term can not be neglected, the hydraulic head is to be used.

For the same reason, the wellbore boundary condition is also usually approximated by the pressure values along the axis of the well p_w. The maximum and minimum pressures are at the bottom and top sides of the well i.e $p_{wellbore}$(bottom side) = $p_w + \rho g r_w$ and $p_{wellbore}$(upper side) = $p_w - \rho g r_w$.

The second boundary condition is usually specified at impermeable boundaries which are usually the

layers above and below a oil reservoir. The specification of the second boundary condition in terms of hydraulic head and pressure can be written as follows:

$$\left.\frac{\partial H}{\partial z}\right|_{boundaries} = 0 \qquad \left[\frac{\partial p}{\partial z}\right]_{boundaries} = -\rho g \tag{1.3.13}$$

Because of the gravity term ρg, the specifications are different between the two conventions. However, as discussed above, because it is very small compared to the average pressure gradient, the gravity effect is usually neglected in the oil industry, which makes the two conventions identical in the specification.

Obviously, at such boundaries, the hydraulic head instead of pressure should always be used. However, because of the convention used in oil industry, we will still use the pressure terms for problems close to the oil industry in the following chapters, but obviously they can easily be converted into groundwater conventions.

1.4 Thesis Organization

This thesis is divided into eight chapters. Chapter One introduces the objectives of this research and the basic equations used in the research. There are two different conventions currently used by engineers. Oil engineers prefer to use the conventions of the pressure equation, and hydrogeologists prefer to use the hydraulic head equations. Chapter One also introduces the terminologies used for the later chapters. The relationships between the two conventions are presented, because both conventions are used alternately in the analysis in the following Chapters. By using these relationships, one convention can be transferred to another. Chapter Two briefly introduces the development of horizontal wells worldwide. We also discuss some of the advantages of horizontal wells in oil and other industrial applications in this Chapter. Chapter Three discusses the productivity of a horizontal or slant well, and a new solution is derived for this purpose. The new solution considers the effect of three dimensional anisotropic permeability, as well as the orientation of the well, and is a more general solution for an arbitrarily oriented slant well. In this Chapter, the traditional productivity evaluation methods, as well as the solutions used in the evaluation, are also discussed and compared with the new solution. A detailed parametric analysis is presented which gives a clear picture of the productivity

of a slant or horizontal well under various parametric situations. Chapter Four focuses on a discussion of well test interpretation. In this Chapter, a new method is introduced for test interpretation based on a new transient flow solution derived in this Chapter. Compared with the solutions available in the literature, the new solution is more convenient, general and easy to use. The new solution also revealed several new characteristics of horizontal well tests which were not reported in the literature. We will discuss the effect of wellbore storage on test interpretations in Chapter Five. Identification of the effects of wellbore storage from a type curve and a derivative graph are discussed. In Chapter Six, the effect of formation alteration on well tests is analyzed. The formation alteration analysis is based on the assumptions that formation parameters are altered around a vertical well, but can be extended to horizontal well applications because of the similarity at the early vertical radial flow period. A brief summary and some general conclusions are presented in Chapter Seven. Further research and analysis required in horizontal well applications are also summarized. Finally, all the references can be found in Chapter Eight, where they are listed in alphabetic order.

Chapter Two

Horizontal Well Development And Applications

2.1 History of Horizontal Well Applications

The introduction and utilization of horizontal wells is one of the most exciting recent technologies developed in the petroleum and groundwater industries. Horizontal wells are much more effective in underground fluid resource exploitation than vertical wells. This is because the underground fluid reservoirs are natural formations which extend horizontally much longer than vertically, because of the flow limitations caused by layered barriers in the horizontal direction. The convergent flow generated by a vertical well requires a tremendously large potential gradient in order for the fluids to flow rapidly into the well. A horizontal well, on the other hand, does not need a huge gradient because of the longer contact length of the well with the formation. Therefore, horizontal wells have been considered as the preferred choice in oil production for some time, and are being widely used.

Before several stellar and risky experimental successes carried out by Elf Aquitaine in the Rospo Mare field offshore Italy in the late 1970's, horizontal wells were not considered by the industry because of the lack of drilling techniques and the much higher per-foot drilling cost compared to a vertical well. The Rospo Mare case showed that there were a number of advantages to be gained on the productivity and sustainability side from horizontal wells, particularly where the high gradients necessary to achieve adequate production rates led to premature water coning or sand production. With the development of new techniques to control the direction of advance of the drill bit, it has become not only possible to place a horizontal well where desired, but it can also be done at a per-meter cost that is now at the same level as a vertical well.

The number of horizontal wells drilled has been increasing steadily for the last ten years. Figure 2.1 shows the number of horizontal wells drilled in Canada starting with the first of the modern horizontal wells drilled by Esso Resources Canada in its Cold Lake field in 1978. This was drilled to test Esso's

steam assisted gravity drainage process for the recovery of bitumen. This well has now produced more than 52,000 m^3 of oil and its production is continuing. Starting in 1987, the number of horizontal wells drilled each year in Canada increased rapidly. Many of these were in Saskatchewan, where it was found that horizontal wells can produce Lloydminster-type , mobile heavy oil more economically than conventional vertical wells [Butler, 1994].

The largest growth of the use of horizontal wells outside of Canada started in 1989 when horizontal wells drilled by Oryx Energy Co. achieved very high production rates in the generally uneconomic Pearsall reservoir in the Austin Chalk. Figure 2.2 shows data of horizontal-well completions in the United States and Figure 2.3 shows the increase of horizontal well utilization worldwide.

2.2 Productivity Advantages of Horizontal Wells

2.2.1 Productivity of a vertical well

It is widely recognized that for a conventional vertical well, most of the pressure decline occurs near the wellbore because of the convergent flow, and all the streamlines must pass through the limited wellbore entry area to contribute to production. The requirement for two-dimensional convergent flow is thought to be a drawback for thin, extensive, flat-lying reservoirs because most of the flow in these cases must come from a considerable horizontal distance, therefore limiting the production rate capacity of a vertical well.

For reservoirs with great thickness, a vertical well might be the best choice because in such reservoirs the drawdown cone will be limited in size. Therefore, more wells can be added outside of the influence radius. The productivity of wells in such reservoirs may be able to reach a high per-well capacity and a high total productivity.

Vertical well productivity also can become effective in reservoirs where horizontal permeability is much larger than vertical permeability, for example, if intense horizontal fractures are present, or if there are many thin horizontal beds. In such situations, the horizontal fractures act as horizontal conduits which help to transport the fluid from the far field to the wellbore.

However, because most reservoirs have a relatively small thickness and can be made more conductive

vertically because of artificial simulation, e.g., hydraulic fracturing, horizontal wells are suitable in most cases.

2.2.2 Productivity of horizontal and slant wells

Most moderate thickness horizontal reservoirs with vertical wells can be approximated by two-dimensional (radially symmetrical) flow to each well, so that once again the pressure drop is concentrated in the near wellbore vicinity, particularly so if there is permeability impairment in the zone just around the wellbore. The requirement for two-dimensional convergent flow is thought to be a particular drawback for thin, extensive, flat-lying reservoirs because most of the flow in these cases must come from a considerable horizontal distance, therefore limiting the production rate capacity of a vertical well.

Therefore, an efficient way to improve productivity in thin reservoirs is to reduce the average travel distance of the fluid; use of a horizontal well is an effective way to do this. Economic studies invariably show that quick profits are more valuable than delayed profits because of the possibility of re-investment and the meeting of capital equipment costs. Therefore, the issue of production rate over time is at least as important as the issue of resource recovery (total percent of original oil in place produced). Both of these issues must be addressed in a general assessment of the economic viability of vertical versus horizontal drilling.

Slant wells are also important in a general well productivity assessment process. Clearly, it is impossible to drill precisely horizontal or precisely vertical wells because of drilling deviations (drift) and measurement errors. The most common case is that wells are somewhat inclined and can be called slant wells. However, the effect of a few degrees of inclination on production rate is negligible. It is important to decide the best choice of well types (horizontal, vertical or slant) and their geometric lay out before developing a particular reservoir, in view of the economic constraints on the exploitation strategy for a reservoir. For example, many slant wells are deliberately drilled because it is simply easier (more economical) than vertical wells. A common example is in heavy oil operations in Alberta and Saskatchewan reservoirs at depths of 300-700 m, where from 8 to 24 wells may be drilled from a single pad. In these cases, horizontal well techniques are usually not used, and only the central wells are approximately vertical. In offshore platform drilling, steeply inclined wells, long-reach or extended-reach horizontal wells, vertical access wells with short turning radius sections and several horizontal drains, and other variations are all used for efficient reservoir access because it is far cheaper to drill horizontal boreholes than it is to build new platforms.

In view of the need for quantitative evaluation, several questions arise: how will a slant well differ from a horizonal well or a vertical well in terms of sustained production rate and how will the directional permeabilities with respect to a particular well orientation and inclination affect the production rate in those cases?

Multi-horizontal or slant well systems are major tools to increase the per well productivity in a field, as one can exploit the reservoir pressure gradient more effectively and sooner than in the case of a single horizontal well or a series of vertical wells. One such case was reported by Karakas et al., [1991]; however the productivity increase is not linearly proportional to the increase in the number of wells drilled, therefore a optimization criterion must exist between the productivity increase and the drilling cost increase. However, this is not the case if horizontal holes can be "self-produced" during the process of oil production, such as has been suggested as an explanation for the enhanced productivity of wells experiencing cold production (oil production with continuous solids co-production). It has been suggested that piping channels are propagated as the result of an internal erosion of sand, and these piping channels serve as (approximately) horizontal collector tubes, bringing in oil from distance to the vertical wellbore. If this is indeed the mechanism which dominates cold production, we need to consider a case of many horizontal wells instead of one. There could conceivably be so many such horizontal "worm holes" in a case of massive sand production (1000 m^3 in three years for example for several cases in Alberta) that it becomes necessary to consider that the sanded area permeated by the horizontal drains has a general permeability increase. There is need for solutions which can analyze these cases, permitting at least qualitative assessment of the effect of a small number of drain holes leading to a vertical well, versus a zone of large permeability change, using either a continuous permeability change function, or a step-permeability model with several zones.

2.3 Other Advantages of Horizontal Wells

2.3.1 Horizontal wells in water or gas coning reservoirs

Many reservoirs have a gas cap above the oil body because of the natural geological history of petroleum and gas migration. The gas cap sometimes can be the most important factor limiting the production of oil from the reservoir. This is because when the reservoir pressure decreases the gas in the gas cap begins to move vertically in the decreased pressure direction, which eventually reaches the

production well as a gas cone. If a water body exists below the oil reservoir, a similar situation also can happen to produce a water cone. Horizontal wells can have substantial advantages in a gas cap drive reservoir. The conventional way of reducing the effect of coning is to complete the vertical well over a limited vertical distance to maximize the standoff from the underlying water or overlying gas cap, as the case may be. In this circumstance, the contact of the vertical well with the reservoir is reduced even further than it would be for a full thickness completion. The effect of reservoir thickness on the relative performance of a horizontal well is much smaller.

Because of its extended contact with the reservoir, a horizontal well usually has less pressure drawdown for a given production rate than does a vertical well. This reduced drawdown lessens the tendency for coning of water or gas with the produced oil. Thus, for example, horizontal wells may be operated at the same rate as a conventional vertical well but with less, and sometimes much less coning, i.e. with better water-oil ratios or gas-oil ratios or both. In some cases, production without coning may be economic using horizontal wells, where it would be prohibitively slow with conventional wells. In situations where the initial rate for production without free gas coning would be impractical with vertical wells, it may be possible with horizontal wells to achieve economic production by gravity drainage with only a small rate of gas injection to maintain gas cap pressure through voidage replacement.

Even if operation below the critical rate for coning is impractical because of economics, there can still be large advantages for horizontal wells. This situation is common when viscous, heavy oil deposits such as those in Saskatchewan, are produced from above a water layer. Here, the high oil viscosity and the low difference in density between the oil and water makes water coning, or more correctly fingering, occur even at very low production rates. In these cases, the volume of oil that is produced is approximately proportional to the volume swept by the water fingering. Horizontal wells have advantages over vertical wells here because the fingers have much larger volume, and the large crest simply displaces a much large volume of oil.

This application is being developed enthuastically, particularly in Canada. For instance, it has been reported that in Saskatchewan heavy oil fields, horizontal wells can produce about ten times the volume of oil than can be produced by conventional wells [Butler, 1994]. In some Saskatchewan reservoirs, it is economic to produce oil with horizontal wells but not with conventional vertical wells.

2.3.2 Horizontal wells in fractured reservoirs

Many reservoirs consist of a fine-grained, low-permeability matrix penetrated by approximately parallel natural vertical fractures. Connection of a production well with these fractures is important if higher productivity is to be obtained. When the fractures are vertical or nearly vertical, their intersection by vertical wells is difficult. On the other hand, the length of a horizontal well, particularly if it is drilled at a right angle to the fracture planes, can provide contact with multiple fractures and greatly improve productivity. A related field is in karstic reservoirs, which contain interconnecting solution cavities and passages. Production from such reservoirs is dependent upon intersecting these flow systems. The chances of doing this are much greater with a longer horizontal well.

In reservoirs where fractures do not occur naturally, it is sometimes possible to create vertical artificial fractures. Preferably, these should extend at right angles to the well, although in some cases, for example, with horizontal wells drilled like spokes of a wheel from an offshore platform in a uniform stress field, this may not be practical. Success has been obtained in making multiple fractures along the length of a horizontal well so that each fracture contributes to the well's productivity . For example, a well with five artificial, equally spaced fractures originating from it can have an initial productivity approximately five times that of a vertical well with a single artificial fracture in the same reservoir.

2.3.3 Horizontal wells in heavy oil production

Probably the most promising area for using horizontal wells lies in the field of heavy oil recovery, particularly thermal recovery using steam. There are enormous opportunities here. For example, the bitumen deposits in Canada, which are impossible to recover economically by conventional vertical wells, have a volume of oil in place approximately equal to that of all the known conventional crude oil in the world. One approach used to recover these resources is open pit mining. However, this is limited to the small fraction of the Athabasca reservoir that is close to the surface and the approach involves handling vast quantities of material. In situ thermal recovery is more generally applicable, cheaper and less damaging environmentally. Because the deposits are shallow (< 700 m), wells are economical and thermal effectiveness is high.

Thermal recovery normally requires close well spacing. Typical projects have a spacing of 1 to 2 hectares (2.5 to 5 acres) per well and, in many cases, these are later infilled to improve recovery. Steamflood projects in California with spacing as low as 0.25 ha are being operated. In such

circumstances, a single horizontal well can replace a row of as many as ten or more conventional vertical wells. This may become one of the most important applications of horizontal wells. The successful operation of field pilots in Cold Lake, the Lloydminster area and in Athabasca using horizontal wells and steam - assisted gravity drainage (SAGD) are discussed by Butler [1994]. A particularly important feature of the use of horizontal wells for steam recovery is that it is possible to operate and obtain higher recoveries with little steam production, i.e. with little steam bypassing by cresting. With horizontal wells, it is possible to produce economically below the critical rate for steam bypass. With vertical wells, steam-flooding is impractical without the bypass of steam, except on very close spacing.

2.3.4 Horizontal wells in sand production reservoirs

Solids production is another problem in both conventional and heavy oil reservoirs. Because of the high viscosity of heavy oil, sand is usually co-produced with production of oil in uncemented reservoirs. The amount of sand produced from a well also increases with increasing production rate of oil. Several ways have been employed to lessen sand production; however, it is observed that decreasing the amount of sand production, for instance by utilizing a gravel filter, will decrease the oil production at the same time. Sand production has also been a serious problem for the environment as it is required to be disposed of.

Massive sand production is a special case of solid production, which usually is introduced when the pressure gradient becomes higher than the cohesive force of the solid. This partially explains why the solids production increases with increasing oil production. Horizontal wells can lessen the amount of sand production, and at the same time maintain or even increase the oil production. This is because the pressure gradient around a horizontal well can be much smaller than a conventional vertical well, therefore decreasing the sand production rate. Also, because of the much longer length of horizontal wells compared with conventional vertical wells, a higher per well production rate can be maintained.

2.3.5 Horizontal wells in environmental applications

Groundwater resources are often contaminated by use of agricultural chemicals, spills of industrial chemicals, leakage from waste disposal facilities, or leakage from underground storage tanks. Contaminants can migrate hundreds of meters per year and reach groundwater discharge zones, water supply wells, or cross property boundaries, leading to environmental or legal problems.

Much research has been carried out to develop physical, chemical and biological methods to control or remediate contaminated groundwater. One of the most common physical remediation methods is the pump-and-treat (P&T) method. P&T systems have been widely used in groundwater remediation programs for many years. These systems involve the installation of groundwater extraction wells within a contaminated zone and removing contaminants with groundwater, followed by above-ground treatment of the contaminated water. P&T is intended to capture and prevent further expansion of contaminated plumes. The effectiveness of a P&T system will depend on the size of the capture zone and the amount of contaminants captured per unit well length. The effectiveness can be influenced by many factors, such as the well orientation, hydrogeological features, the nature of the contamination and the pumping well design. Among those, the orientation and elevation of the well relative to the contaminant plume is probably the most important.

Groundwater contaminants usually migrate from the contaminant source as a plume with higher concentration around the centre of the plume and a gradual decrease outward. Depending on the hydrogeological features of the aquifer and properties of the contaminants, the plume can be at different elevation and with different sizes at different times. Obviously, if a well can be oriented along the longer axis of the cross section of the plume and placed at the elevation of the plume centre, the optimum capture zone can be obtained. A horizontal well or a slant well is the best choice for this purpose.

2.4 Horizontal Drilling Development

The potential advantage of horizontal wells for draining reservoirs has been recognized for a long time. As early as the 1930's, Ranney [1939] indicated that horizontal wells could have particular advantages if they could be drilled for a long distance in a thin reservoir [Ranney, 1939]. Although he drilled some wells of this type, the idea did not become popular because of directional control difficulties and high cost.

With equipment advances and better drilling approaches, the horizontal well concept was successfully established in recent years (based on pioneering work by Elf Aquitaine). As an example of the technical level reached in the 1980's, a case reported by MacDonald [1985] was drilled with an open horizontal length in the reservoir of over 1000 m, with the well bore staying within 2 m of the desired elevation. Current practice is even better.

Wells having long horizontal sections are now regularly drilled using conventional deviated drilling

methods; techniques which have contributed to the success of such projects are summarised by Butler [1989] as follows:

1. The use of downhole mud motors with bent housings is necessary. If a hole is drilled with such a motor, it tends to deviate in the direction of the bend, and can be steered by orienting the drill pipe so that the bend from the "tool face" is in the desired direction. Relatively straight holes can also be drilled by rotating the drill pipe as the hole is drilled. The use of the bent sub assembly connected to a straight motor has been replaced in most recent practice by the use of a motor with the bend in the motor housing itself.

2. Heavy drill collars are commonly used in the more vertical part of the well during drilling so as to exert a large compressive load on the bit. High drill-string weight in horizontal and near-horizontal sections of the hole is undesirable as it contributes to friction. The obvious use of light (aluminium) drill pipe has been considered for the near-horizontal portion of the hole, but is not generally used for reasons of cost, durability and availability.

3. MWD (measurement while drilling) techniques are required to locate the bit position and advance direction. These involve measurements of the direction of the earth's gravity and magnetic fields at the bit location, and non-magnetic metallic drill collars or steering tools are used.

4. Swivel-drive (top-drive) rigs rather than conventional rotary table rigs are preferred, mainly to allow mud circulation and drillstring rotation during trips. This tends to prevent sticking and helps keep drill cuttings suspended rather than letting them settle in the bottom of the horizontal sections of the hole.

Using these techniques, wells can be deviated with a radius of curvature of about 600 ft. To drill shallow horizontal holes it may be necessary to employ an inclined drilling rig mast rather than a conventional vertical one. With some modifications, such as the use of smaller diameter, compressive service drill pipe and drill motors having two bends rather than one, holes can have a radius of curvature of about 300 to 500 ft, and it is possible to drill several horizontal drains at the base of a vertical well section.

2.5 Cost of Horizontal and Slant Wells

The costs of earlier horizontal wells were much higher than comparable vertical wells drilled in the same reservoir. As in any new field of technology, early prototypes may be expected to be much more costly than later, well-established operations because of additional precautions involved in experimental projects, rig down time for periodic hole location, and the use of non-optimum equipment and methods. It has been found by companies drilling horizontal wells that the costs decrease as experience is gained. It was reported that the costs per foot of horizontal drilling decreased from US$462 to US$282 as

compared to US$233 for a conventional well [Butler, 1994]. This shows that with the acquisition of corporate knowledge, unit length costs of long horizontal wells can be expected to be much less than double the costs of a vertical well, and in some cases it can almost approach equality [Butler, 1989]. There are additional costs associated with geophysical logging and completing horizontal wells which are not fully accounted for in this analysis, but the per foot cost ratios are probably similar. Workover costs of horizontal wells are in general much more expensive than for vertical wells. Figure 2.4 shows the decreases of cost in drilling a horizontal well with time. Given that the reservoir intersection length of a horizontal well can be anywhere from several times to more than 20 times that of a vertical well, and that production capacity will rise as some function of the intersection length, the economics of horizontal wells are quite appealing, provided that the reservoir properties are appropriate. Clearly, to assess the economics of horizontal wells properly, methods of estimating the potential productive capacity of such wells are necessary.

The costs of slant wells are intermediate between those of horizontal and vertical wells. For heavy oil development, it is common for 8-24 wells to be drilled from a single pad, saving on rig moving costs and on the cost of surface production facilities. Typically, reservoir intersection angles will be from 30° to 70° from vertical, so that the intersection length may be as much as three times the reservoir thickness. As stated above, to optimise the investment rationally, the best possible predictive approaches for reservoir productivity should be used. These predictions even include the possibility of orienting horizontal sections in particular directions to take advantage of natural permeability anisotropy.

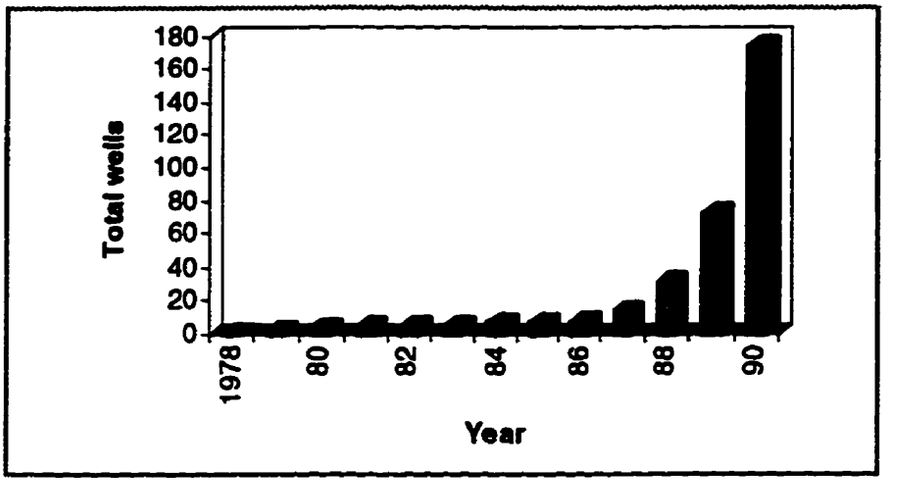

Figure 2.1 Horizontal wells drilled in Canada up to the year 1990 (after Butler, 1994).

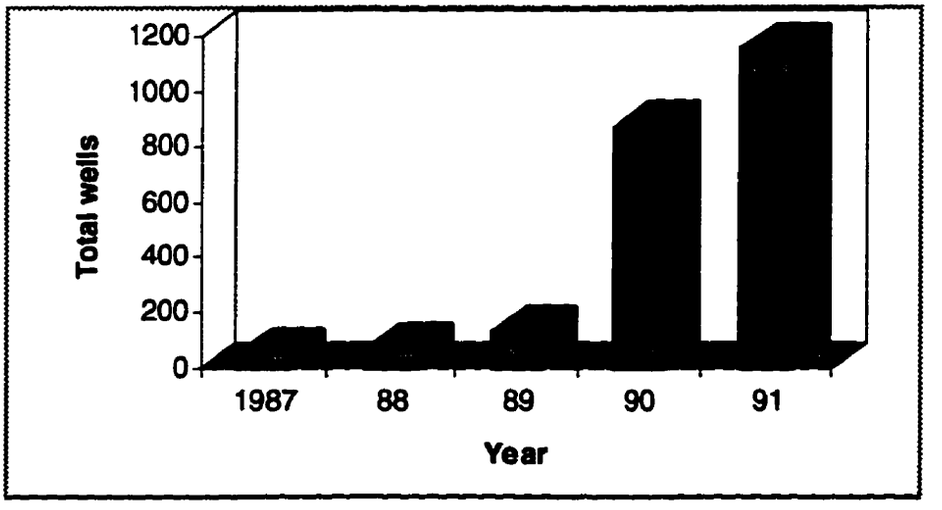

Figure 2.2 Horizontal wells drilled in the United States up to the year 1991 (after Butler, 1994).

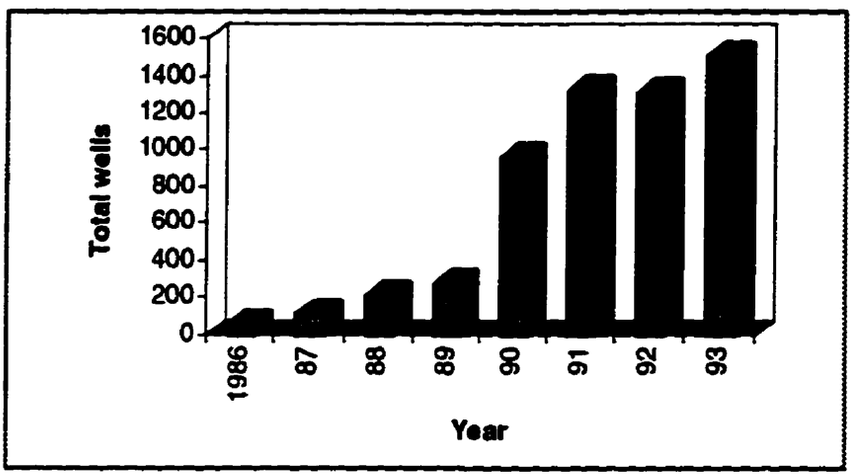

Figure 2.3 Horizontal wells drilled in the world up to the year 1993 (after Butler, 1994).

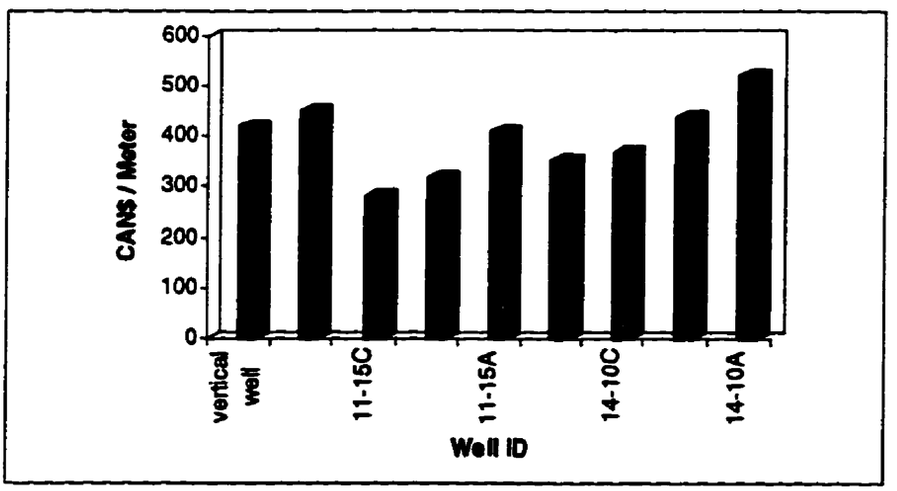

Figure 2.4 Cost of drilling and completing horizontal wells at Pelican Lake, Alberta (after Butler, 1994)

Chapter Three

Productivity of A Horizontal Well

3. 1 Horizontal well productivity

One of the main purposes of horizontal and slant wells is to achieve higher per well fluid production from oil, gas, and water reservoirs, as discussed in Chapter Two. This is particularly the case in off-shore development where highly inclined and horizontal wells are necessary for economical field development. Other advantages include reduced tendencies for premature water coning and solid production. The advantages and production improvements offered by horizontal wells have been discussed by various authors [Butler, 1989; Cinco et al., 1975; Joshi, 1988, 1987; Lee and Milliken, 1993]. For the same well length, the production improvement by a horizontal well is usually less than 10% compared with a vertical well, if the medium has isotropic permeability. This indicates that, in addition to the longer well intersection length with reservoir, the anisotropic permeability is another important factor in slant well analysis. This includes not only the permeability magnitude, but also its principal directions relative to the well orientation.

Borisov reported a mathematical solution to predict steady-state horizontal well production with no mention of anisotropic permeability [Borisov, 1984]. One augmentation solution for steady-state flow to a horizontal well which mentioned the anisotropic permeability effect was derived by Joshi [1988] where he considered only the transverse isotropic case, i.e., the horizontal permeability differs from the vertical, but with $k_x = k_y = k_h$. The anisotropic permeability was incorporated by substituting isotropic permeability with the square root of the product of the vertical and horizontal permeability, which is a commonly employed transformation.

Lee [1989] reported some results of the effects of anisotropic permeability on slant well production, but his results were based on numerical simulation.

A new analytical solution for fluid flow to a slant well in a medium with permeability anisotropy is derived in this thesis. Three dimensional anisotropy is considered in this new solution, and the effect of this anisotropy on fluid production is discussed.

3.2 Productivity Evaluation Scheme

3.2.1 Vertical well productivity evaluation

The evaluation of well productivity is one of the most important tasks in the exploration for underground resources. The productivity capacity of a well directly affects well pattern design. Well productivity is a function of not only the well geometry but most importantly is also a reflection of the reservoir characteristics.

Conventional vertical well productivity is evaluated by assuming radial flow and constant pressure boundary conditions both at the wellbore and at the drainage radius. The productivity of a vertical well under this condition is in the form of a very simple solution. Therefore, the conventional solution only reflects the capacity of a well as well as the transmissivity of the reservoir. The various boundary conditions are not considered in it. However, for simple boundary conditions such as no flow or linear constant flow boundaries, the solution can be modified by superposition of the boundary effects. However, the constant boundary conditions are not always satisfied, particularly in pressurized (confined) reservoirs. The real pressure in such reservoirs decreases and the influence radius moves outward with time during production. The distance from the well where the pressure is just beginning to decrease at a given time is referred to as the influence radius of the wellbore at that time. However, pseudo steady-state solutions which satisfy the constant boundary conditions can be developed around the well after a period of production.

Other conventional vertical well productivity solutions and modifications developed over the years were mostly based on the modelling of natural physical flow cases by considering various more complicated boundary conditions, such as the aquitard models, free phreatic surfaces (water-table) models, or multi-layered reservoir models.

3.2.2 Horizontal well productivity evaluation

It is widely recognized that a horizontal well can yield more fluid than a conventional vertical well, in particular if the reservoir is thin and extensive. Some of the advantages and production improvements offered by horizontal wells have been discussed in the previous chapter, and several

approximate solutions for horizontal well productivity have been derived [Borosov, 1984; Joshi, 1988, 1987]. For inclined (slant) wells, however, there seems to be no systematic analysis yet available except for the numerical analysis reported by Lee [1989].

To best utilize the advantages provided by a horizontal well, the effect of various parameters such as the true three-dimensional anisotropic permeability need to be evaluated.

Several productivity evaluation methods have been reported in the literature. Borisov [1984] reported the following steady-state solution for predicting fluid flow to a horizontal well:

$$Q = \frac{2\pi k h \Delta p}{\mu} \cdot \frac{1}{\ln(\frac{4r_e}{L}) + \frac{h}{L}\ln(\frac{h}{2\pi r_w})} \qquad (3.2.1)$$

where h is the reservoir thickness, L is the horizontal well length, r_e is the drainage radius of the reservoir, r_w is the well bore radius, Δp is the pressure difference between the well-bore and the drainage boundary, k is the homogeneous isotropic permeability of the reservoir, and μ is the fluid viscosity.

Borisov's solution has a very simple form and is convenient in use, however, the solution is limited in general analysis because of the isotropic assumption.

Another commonly used solution for horizontal well production is the augmentation solution derived by Joshi [1988] in the following form:

$$Q = \frac{2\pi k_h h \Delta p/(\mu B_0)}{\ln[\frac{a+\sqrt{a^2-(L/2)^2}}{L/2}] + \frac{\beta^2 h}{L}\ln(\frac{h}{2r_w})} \qquad (3.2.2)$$

where B_0 is formation factor, $\beta = \sqrt{k_h/k_v}$, and a is the maximum axis length of the drainage ellipse of the well and has the following relationship with the drainage radius r_e:

$$a = \frac{L}{2}\left[\frac{1}{2} + \sqrt{\frac{1}{4} + \left(\frac{2r_e}{L}\right)^4}\right]^{\frac{1}{2}} \qquad (3.2.3)$$

with other parameters the same as in Borisov's solution.

Joshi derived this solution by separating the three-dimensional problem into two two-dimensional ones, relating to vertical and horizontal cross-sections. The solutions are combined using an electrical analog concept.

Joshi modified his isotropic solution to account for horizontal well eccentricity by using Muskat's method, initially developed for a vertical well located eccentric to a circular drainage boundary [Muskat, 1937]. Finally, he arrived at the following result for the isotropic case:

$$Q = \frac{2\pi k h \Delta p/(\mu B_o)}{\ln\left[\frac{a + \sqrt{a^2 - (L/2)^2}}{L/2}\right] + \frac{h}{L}\ln\left[\frac{(h/2)^2 - \delta^2}{(h r_w/2)}\right]} \qquad (3.2.4)$$

where the term δ is the distance of the horizontal well from the midheight of the reservoir.

Joshi also compared horizontal and slant well productivities using some results provided by Cinco et al., [1975] and Van Der Vlis et al., [1979] and presented some information on slant well productivity for wells inclined in the range of zero to 75° from vertical.

However, Joshi has over-simplified the effect of anisotropic permeability in his solution (3.2.2), and his solution has also some difficulty in analyzing both the eccentricity and the inclination effects because of the singularity at $\delta = h/2$, where one cannot recover the original solution (3.2.2).

Lee [1989] provided a semi-numerical simulation of a slant well in a thin reservoir, obtained using by analytically integrating around the boundaries and using numerical boundary integral methods in the calculation. Because of the introduction of a numerical technique, the solution lost its analytical characteristics, and it becomes inconvenient to use by engineers.

In this chapter we will present a new analytical solution which predicts slant and horizontal well

production in an 3-D anisotropic reservoir, and will show that the cases of vertical and horizontal wells are the two limits for this new solution. A series of parametric analyses and comparisons of horizontal, slant and vertical wells is also presented. To conclude, we will discuss the results and address the anisotropic permeability effect implied by the new solution.

3.3 Flow Rate Changes Under Coordinate Transformations

Anisotropic permeability can usually be transformed to an equivalent isotropic permeability by coordinate transformation in solving the governing equations. The primary variable, such as the fluid pressure in the flow equation, will be an invariant with the transformation; however, other variables such as the flow rate are not necessarily the same. This is particularly so when the transformation is not conformal, so care must be taken in the transformation.

Assume a cartesian coordinate system is chosen with its axes being parallel to the principal anisotropic permeability directions. Then, the steady-state flow equation under such a coordinate system can be written as (equation 1.3.10):

$$\frac{\partial}{\partial x}[\frac{k_x}{\mu}\frac{\partial p}{\partial x}] + \frac{\partial}{\partial y}[\frac{k_y}{\mu}\frac{\partial p}{\partial y}] + \frac{\partial}{\partial z}[\frac{k_z}{\mu}\frac{\partial p}{\partial z}] = 0 \qquad (3.3.1)$$

where k_x, k_y and k_z are the principal permeabilities and p is fluid pressure.

Suppose a new cartesian coordinate system (u,v,w) is related to the old system (x,y,z) by the following relationship:

$$u = I_x\, x \qquad v = I_y\, y \qquad w = I_z\, z \qquad (3.3.2)$$

and assuming the reservoir is homogeneous in permeability and viscosity, then equation (3.3.1) can be written in the following form under the new system:

$$k_s \left[\frac{\partial^2 p}{\partial u^2} + \frac{\partial^2 p}{\partial v^2} + \frac{\partial^2 p}{\partial w^2}\right] = 0 \qquad (3.3.3)$$

which becomes the three-dimensional Laplace equation with an equivalent isotropic permeability k_s,

which appears as an arbitrary constant only if the transformation factors satisfy the relationships:

$$I_x = \sqrt{\frac{k_s}{k_x}} \qquad I_y = \sqrt{\frac{k_s}{k_y}} \qquad I_z = \sqrt{\frac{k_s}{k_z}} \tag{3.3.4}$$

It is obvious that the pressure p is indeed an invariant under this transformation if the relationships of the two coordinate systems expressed in equation (3.3.2) are applied.

For the flow rate we can do the following analysis. Suppose the flow through a arbitrary surface S is Q in the (x,y,z) system and is Q' in the (u,v,w) system; then we have $Q = Q_x\boldsymbol{i} + Q_y\boldsymbol{j} + Q_z\boldsymbol{k}$, $Q' = Q_u\boldsymbol{i} + Q_v\boldsymbol{j} + Q_w\boldsymbol{k}$ and:

$$Q_x = \frac{1}{\mu}\int_S k_x \frac{\partial p}{\partial x}dydz \qquad Q_y = \frac{1}{\mu}\int_S k_y \frac{\partial p}{\partial y}dxdz \qquad Q_z = \frac{1}{\mu}\int_S k_z \frac{\partial p}{\partial z}dxdy \tag{3.3.5}$$

where:

$$Q_x = \frac{1}{\mu}\int_S k_x \frac{\partial p}{\partial x}dydz = \frac{1}{\mu}\int_S k_x I_x \frac{\partial p}{\partial u}\frac{dvdw}{I_y I_z} = \frac{1}{\mu}\int_S \frac{k_s}{I_x I_y I_z}\frac{\partial p}{\partial u}dvdw \tag{3.3.6}$$

and similarly we obtain:

$$Q_y = \frac{1}{\mu}\int_S \frac{k_s}{I_x I_y I_z}\frac{\partial p}{\partial v}dudw \qquad Q_z = \frac{1}{\mu}\int_S \frac{k_s}{I_x I_y I_z}\frac{\partial p}{\partial w}dudv \tag{3.3.7}$$

therefore the flow rate obtained from the two coordinates have the following relationships:

$$Q = \frac{Q'}{I_x I_y I_z} \tag{3.3.8}$$

This equation indicates that if the coordinate transformation factors expressed in equation (3.3.2) are

used, then the flow rate calculated from the (u,v,w) system is not the true flow rate, but needs to be multiplied by the reciprocal product of the transformation factors.

For the two-dimensional vertical well flow case we have:

$$Q = \frac{Q'}{I_x I_y} = \frac{k_s \ 2\pi h \Delta p}{I_x I_y \ \mu \ln(\frac{r_e}{r_w})} = \frac{\sqrt{k_x k_y}\ 2\pi h \Delta p}{\mu \ln(\frac{r_e}{r_w})} \qquad (3.3.9)$$

which shows that the isotropic equivalent permeability can be represented by the square root of the product of the two principal permeabilities.

3.4 Mathematical Model of Flow to a Slant Well

3.4.1 Problem formulation

To obtain a solution for a slant well in an anisotropic reservoir, we will utilize the transformation techniques outlined in section 3.3. Upper and lower boundaries will be simulated using the image principle, and the results will be simplified using a Laplace transformation result.

To derive a productivity evaluation solution for a slant or horizontal well, we also assume that the simple constant pressure boundary conditions are satisfied. The problem here is described as follows: the reservoir has a constant thickness h, the horizontal dimension is much larger than the vertical thickness, such that the horizontal boundary drainage condition can be assumed to be constant pressure, very far away with respect to the well intersection length. The upper and lower reservoir boundaries are parallel no-flow planes, corresponding to relatively impermeable strata. The well has a length L, is inclined with an angle β to the vertical upward direction (z axis in Figure 3.1), and one end of the well is located in the reservoir at a distance b from the lower boundary, which is defined as z = 0, and the well is orientated with an angle of α to the x axis. The anisotropic permeability values in the principal directions, corresponding to the cartesian axes, are k_x, k_y, and k_z. The governing equation for the steady-state and incompressible fluid flow satisfies the Laplace equation (1.3.10):

$$k_x\frac{\partial^2 p}{\partial x^2} + k_y\frac{\partial^2 p}{\partial y^2} + k_z\frac{\partial^2 p}{\partial z^2} = 0 \qquad (3.4.1)$$

and the boundary conditions for the problem can be described as:

$$p(x,y,z)|_{x^2+y^2=r_e^2} = p_e$$
$$\frac{\partial p}{\partial z}|_{z=0} = 0 \ , \quad \frac{\partial p}{\partial z}|_{z=h} = 0 \qquad (3.4.2)$$

the wellbore condition should be a constant pressure around the wellbore, which if written in mathematical terms, satisfies the following:

$$p(x,y,z)\Big|_{\substack{(x-x')^2+(y-y')^2+(z-z')^2=r_w^2 \\ (x-x')\cos(\alpha)+(y-y')\sin(\alpha)+(z-z')\tan(\beta)=0}} = p_w \qquad (3.4.3)$$

where x', y' and z' are the coordinates of a point at the well axis where a sink is located, r_e is the drainage radius, r_w is the well radius, p is fluid pressure, and p_e and p_w are the pressures at r_e and r_w respectively. We assume that the amount of fluid that flows into a well through the two ends of the well is negligible; that is, we assume that $L >> r_w$.

As noted in Chapter One, the above boundary conditions are only approximations in terms of pressure; the exact conditions should consider the gravity effect which give the same form as above if hydraulic head is used.

If l is defined as a distance along the well, then x', y' and z' can be written as:

$$x' = l\cos(\alpha)\sin(\beta) \ , \quad y' = l\sin(\alpha)\sin(\beta) \ , \quad z' = b + l\cos(\beta) \qquad (3.4.4)$$

To simplify equation (3.4.1) the following coordinate transformation is applied:

$$u = I_x x \,, \quad v = I_y y \,, \quad w = I_z z$$
$$I_x = \sqrt{\frac{k_s}{k_x}} \quad I_y = \sqrt{\frac{k_s}{k_y}} \,, \quad I_z = \sqrt{\frac{k_s}{k_z}} \tag{3.4.5}$$

where k_s is the three dimensional equivalent isotropic permeability. If we let $I_x I_y I_z = 1$, which makes the productivity calculated from both systems identical, then we obtain the equivalent permeability $k_s^3 = k_x k_y k_z$.

The governing equation (3.4.1) under this transformation becomes:

$$\frac{\partial^2 \phi}{\partial u^2} + \frac{\partial^2 \phi}{\partial v^2} + \frac{\partial^2 \phi}{\partial w^2} = 0 \tag{3.4.6}$$

and the boundary conditions (3.4.2) become:

$$\phi(u,v,w)\Big|_{(\frac{u}{I_x})^2 + (\frac{v}{I_y})^2 = r_e^2} = \phi_e$$
$$\frac{\partial \phi}{\partial w}\Big|_{w=0} = 0 \quad , \frac{\partial \phi}{\partial w}\Big|_{w=h_m} = 0 \tag{3.4.7}$$

the wellbore condition (3.4.3) becomes:

$$\phi(u,v,w)\Big|_{\substack{(\frac{u-u'}{I_x})^2 + (\frac{v-v'}{I_y})^2 + (\frac{w-w'}{I_z})^2 = r_w^2 \\ \frac{(u-u')\cos(\alpha_m)}{I_x^2} \frac{(v-v')\sin(\alpha_m)}{I_y^2} + \frac{(w-w')\cot(\beta_m)}{I_z^2} = 0}} = \phi_w \tag{3.4.8}$$

where

$$\phi = \frac{4\pi \Delta p k_s}{\mu} \tag{3.4.9}$$

is the pressure potential, μ is fluid viscosity, α_m and β_m are the transformed angles, h_m is the transformed reservoir thickness under the (u,v,w) system and $\Delta p = p_e - p$ is the pressure drawdown between the drainage boundary pressure and the wellbore pressure.

Because the components in the x, y and z direction must satisfy the relationships of $xI_x = u$, $yI_y = v$ and $zI_z = w$, if we take the point on the well axis of distance l from the origin as the study point, then the relation between the two systems can be obtained:

$$\begin{aligned} l\cos(\alpha)\sin(\beta)I_x &= l_m\cos(\alpha_m)\sin(\beta_m) \\ l\sin(\alpha)\sin(\beta)I_y &= l_m\sin(\alpha_m)\sin(\beta_m) \\ l\cos(\beta)I_z &= l_m\cos(\beta_m) \end{aligned} \tag{3.4.10}$$

where l_m is the distance corresponding to l in the (u, v, w) system.

From the relationships in (3.4.10) we obtain:

$$\tan(\alpha_m) = \frac{I_y}{I_x}\tan(\alpha)\ , \quad \tan(\beta_m) = \frac{\sin(\alpha)I_y}{\sin(\alpha_m)I_z}\tan(\beta) \tag{3.4.11}$$

It is easy to find the following relationships from equations (3.4.10) and (3.4.11):

$$\begin{aligned} \sin(\alpha_m) &= \frac{I_y\sin(\alpha)}{I_1}\ , \quad \cos(\alpha_m) = \frac{I_x\cos(\alpha)}{I_1} \\ \sin(\beta_m) &= \frac{I_1\sin(\beta)}{I_2}\ , \quad \cos(\beta_m) = \frac{I_z\cos(\beta)}{I_2} \\ l_m &= lI_z\ , \quad L_m = LI_z \quad h_m = I_z h \quad b_m = I_z b \end{aligned} \tag{3.4.12}$$

and

$$\begin{aligned} I_1 &= \sqrt{I_y^2\sin^2(\alpha) + I_x^2\cos^2(\alpha)} = \sqrt{\frac{k_s}{k_\alpha}} \\ I_2 &= \sqrt{I_1^2\sin^2(\beta) + I_z^2\cos^2(\beta)} = \sqrt{\frac{k_s}{k_\beta}} \end{aligned} \tag{3.4.13}$$

where k_α is the horizontal permeability in the direction of the well projection, k_β is the directional

permeability in the direction of the well and they have the following forms:

$$\frac{1}{k_\alpha} = \frac{\cos^2(\alpha)}{k_x} + \frac{\sin^2(\alpha)}{k_y} \qquad \frac{1}{k_\beta} = \frac{\cos^2(\beta)}{k_z} + \frac{\sin^2(\beta)}{k_\alpha} \tag{3.4.14}$$

3.4.2 Solution of the problem

The problem described by equation (3.4.6) for a reservoir with infinite thickness and a sink point located at (u', v' w') can be described by the Green's function [Muskat 1937]:

$$d\phi = \frac{q'(l_m)dl_m}{\sqrt{(u - u')^2 + (v - v')^2 + (w - w')^2}} \tag{3.4.15}$$

where u', v' and w' are the sink locations, $q'(l_m)$ is the sink strength in the (u, v, w) system and is Q/L_m if the total flow rate from the well is Q, dl_m is the differential well segment which produces a potential fraction $d\phi$ at the point (u,v,w). This is the basic solution for our problem.

The two impermeable boundaries can be simulated by applying the image principle. Figure 3.2 shows the image principle for the case of a horizontal well. The same approach can be used to solve for the slant well.

By applying the superposition results presented in Figure 3.2, the effect of the two no-flow boundaries can be simulated by the following infinite series:

$$\frac{d\phi}{q'(l_m)dl_m} = \sum_{n=-\infty}^{+\infty}\left[\frac{1}{\sqrt{L_z^2 s^2 + (w + 2h_m n + w')^2}} + \frac{1}{\sqrt{L_z^2 s^2 + (w + 2h_m n - w')^2}}\right] \tag{3.4.16}$$

where $s^2 = [(u-u')^2 + (v-v')^2]/L_z^2$.

A closed form expression of this series is not available. There have been several methods used to obtain an approximation of this series. Muskat [1937] used two series to approximate a vertical well not totally penetrating the reservoir, which is only a special case of the problem here. One series arises when u + v is very small, and the other when it is very large. This is possible because for a vertical

well u + v can be taken as very small when the well bore boundary is considered, and u + v can be taken as very large when the drainage boundary is considered. However this method becomes invalid here because u + v for a horizontal well can never be considered a small quantity, either for the well bore dimension or for those of the drainage boundary. Haitjema [1985] used another method to approximate the above series in which he only considered the first several terms, employing a "strip" to simulate the effects of the rest of the terms. This approach works because the effects of the terms decrease as n becomes larger; however, many terms still need to be considered if such accuracy is to be achieved, particularly for the thin reservoirs common in stratified formations. This makes the application of Haitjema's solution inconvenient.

The following alternative method transforms the infinite series into an integral form by applying the results of Laplace transformation. In fact equation (3.4.16) can be written as the following integral:

$$\frac{d\phi}{q\,dl_m} = \sum_{-\infty}^{+\infty}\left[\int_0^{\infty} e^{-t|w+2h_m n+w'|} J_0(l_z t)dt + \int_0^{\infty} e^{-t|w+2h_m n-w'|} J_0(l_z t)dt\right] \qquad \textbf{(3.4.17)}$$

It is obvious that for the problem depicted above, we always have positive values of w, w' and h_m, and also $(w + w') \le 2h_m$ for all possible values of (u, v, w) in the reservoir. This fact guarantees that the following relationships is satisfied:

$$\begin{aligned}\sum_{-\infty}^{+\infty} e^{-t|w+2h_m n+w'|} &= \sum_{0}^{\infty} e^{-t|w+2h_m n+w'|} + \sum_{1}^{\infty} e^{-t|w-2h_m n+w'|} \\ &= \sum_{0}^{\infty} e^{-t(w+w')}[e^{-2h_m t}]^n + \sum_{1}^{\infty} e^{t(w+w')}[e^{-2h_m t}]^n\end{aligned} \qquad \textbf{(3.4.18)}$$

Now, the above series can be written as the following:

$$\begin{aligned}\sum_{-\infty}^{+\infty} e^{-t|w+2h_m n+w'|} &= \left[\frac{e^{2h_m t}}{e^{2h_m t}-1}\right]e^{-t(w+w')} + \left[\frac{e^{2h_m t}}{e^{2h_m t}-1} - 1\right]e^{t(w+w')} \\ &= \frac{e^{-h_m t}\cosh[t(w+w')]}{\sinh[h_m t]} + e^{-t(w+w')}\end{aligned} \qquad \textbf{(3.4.19)}$$

and for the same reason, the second series can be written as:

$$\sum_{0}^{+\infty} e^{-t|w+2h_m t-w'|} = \frac{e^{-h_m t}\cosh[t(w-w')]}{\sinh[h_m t]} + e^{-t(w-w')} \tag{3.4.20}$$

and therefore equation (3.4.17) becomes:

$$\frac{d\phi}{q'(l_m)\,dl_m} = \int_0^{\infty} e^{-hv}[e^{tw'} + e^{-tw'}]J_0(l_z s t)\,dt + 2\int_0^{\infty}\frac{e^{-h_m t}\cosh[t(w+w')]\cosh[t(w-w')]}{\sinh(h_m t)}J_0(l_z s t)\,dt \tag{3.4.21}$$

which leads to the following form:

$$\frac{d\phi}{q'(l_m)\,dl_m} = 2\int_0^{\infty}\left[\frac{\cosh[t(w-h_m)]\cosh(tw')}{\sinh(h_m t)}\right]J_0(l_z s t)\,dt \tag{3.4.22}$$

From equations (3.4.4) and (3.4.12) we know that u', v' and w' satisfy the following relationships:

$$u' = l_m\cos(\alpha_m)\sin(\beta_m) \quad v' = l_m\sin(\alpha_m)\sin(\beta_m) \quad w' = b_m + l_m\cos(\beta_m) \tag{3.4.23}$$

and therefore s can be written as:

$$s = \frac{l_1}{l_z}\sqrt{[\frac{l_m\sin(\beta_m)}{l_1} - A']^2 + [\frac{u\sin(\alpha_m) - v\cos(\alpha_m)}{l_1}]^2} \tag{3.4.24}$$

where parameter A' is defined as:

$$A' = \frac{u\cos(\alpha_m) + v\sin(\alpha_m)}{l_1} \tag{3.4.25}$$

If we substitute x, y, z and l back to solution (3.4.22) we obtain:

$$\frac{1}{I_x I_y I_z}\frac{d\phi}{q(l)\,dl} = 2\int_0^{\infty}\left[\frac{\cosh[I_z t(z-h)]\cosh(I_z t z')}{\sinh(I_z h t)}\right]J_0(I_z s t)\,dt \qquad (3.4.26)$$

where $q(l_m)\,dl_m = q(l)\,dl$ and q(l) is the flow rate per unit well length in the (x, y, z) system, and s of equation (3.4.24) in terms of x, y and z becomes :

$$s = \frac{I_1}{I_z}\sqrt{[\sin(\beta)l - A']^2 + C} \qquad (3.4.27)$$

where parameter A' and C become :

$$A' = \frac{1}{I_1^2}[x I_x^2\cos(\alpha) + y I_y^2\sin(\alpha)] \qquad C = \frac{(I_x I_y)^2}{I_1^4}[x\sin(\alpha) - y\cos(\alpha)]^2 \qquad (3.4.28)$$

If we define $\xi = I_z t$ then solution (3.4.26) becomes:

$$\frac{1}{I_x I_y}\frac{d\phi}{q(l)\,dl} = 2\int_0^{\infty}\left[\frac{\cosh[\xi(z-h)]\cosh(\xi z')}{\sinh(h\xi)}\right]J_0(s\xi)\,d\xi \qquad (3.4.29)$$

The flow rate distribution q(l) along the well bore can have several forms depending on the assumptions. The assumption that q is a constant implies uniform flow. This assumption, however, cannot generate a uniform pressure along the well. To meet this condition, i.e. for an uniform pressure assumption, other distributions have to be used, such as a parabolic or a discrete function [Muskat, 1937, Haitjema, 1985]. Theoretically, q in equation (3.4.29) can be specified by any rational function without too much difficulty; however, here we will maintain the uniform flow assumption to permit comparison with published solutions. The fluid production will be approximately the same as that calculated by a uniform pressure assumption if the well bore pressure is taken as the pressure that exists three-quarters way along the well [Muskat, 1937] and, as explained later in this paper, by using this assumption we can obtain good agreement with conventional vertical well production rates by

letting $\beta \rightarrow 0°$. Also, when $\beta = 90°$, it gives good agreement with Borisov's and Joshi's solutions for the isotropic case.

The solution for a slant well with length L and a uniform production rate q along the well can be obtained by integrating equation (3.4.29) with respect to the sink length dl from 0 to L which gives the following form:

$$\phi = I_x I_y q \psi \tag{3.9.30}$$

where ψ is the integral term, and if use z' as defined in (3.4.4), it becomes:

$$\psi = 2\int_0^{\infty}\int_0^{L}\left[\frac{\cosh[\xi(z - h)]\cosh[\xi(b + l\cos(\beta))]}{\sinh(h\xi)}\right]J_0(s\xi)\,dl\,d\xi \tag{3.4.31}$$

To determine the production rate q, the drainage and wellbore boundary conditions of (3.4.2) and (3.4.3) need to be used. When $x^2 + y^2$ becomes very large, the integral ψ tends to zero, and therefore ϕ_e is the pressure potential at the drainage boundary, and ϕ_w is the pressure potential at the wellbore. Therefore we obtain the following:

$$\phi_e = I_x I_y q \psi_e \,, \qquad \phi_w = I_x I_y q \psi_w \tag{3.4.32}$$

where ψ_e and ψ_w are the theoretical integral value obtained by equation (3.4.31).

Because usually $r_e >> L$, we can neglect the effect of the well length and reservoir thickness effect in approximating the drainage boundary, and take a representative point of r_e distance away in the well direction, which can be written as $(r_e\cos(\alpha), r_e\sin(\alpha), h/2)$. If we substitute this point into the parameters A', C and s in equation (3.4.28) and (3.4.27), we have:

$$A' = \frac{k_s r_e}{I_1^2 k_\alpha} = r_e \,, \qquad C = 0 \,, \qquad s_e = \sqrt{\beta_z}\,(l\sin(\beta) - r_e) \tag{3.4.33}$$

and, by substituting A', C and s_e into equation (3.4.31), we obtain the drainage boundary integral value:

$$\psi_e = 2\int_0^{-L}\int_0^{\infty}\frac{\cosh[\xi(b + l\cos(\beta))]}{2\sinh(\frac{h\xi}{2})}J_0(\xi s_e)\,d\xi\,dl \qquad (3.4.34)$$

where $\beta_z = k_z/k_\alpha$,

The well bore boundary has to be determined from the following equation:

$$\begin{aligned}(x-x')^2 + (y-y')^2 + (z-z')^2 &= r_w^2 \\ (x-x')\cos(\alpha) + (y-y')\sin(\alpha) + (z-z')ctan(\beta) &= 0\end{aligned} \qquad (3.4.35)$$

The wellbore boundary condition also can be represented by choosing a representative point at the elevation of well axis and distance δL along the well, with δ being the position parameter, which may take a value between 0.75 and 0.866 [Muskat, 1937, Goode et al., 1987].

This representative point (x_w, y_w, z_w) therefore can be written as:

$$\begin{aligned}x_w &= \delta L\sin(\beta)\cos(\alpha) + r_b\sin(\alpha)\,, \\ y_w &= \delta L\sin(\beta)\sin(\alpha) - r_b\cos(\alpha)\,, \\ z_w &= b + \delta L\cos(\beta)\end{aligned} \qquad (3.4.36)$$

If we substitute this point into the parameters A' and C defined in 3.4.28, we obtain:

$$A' = \delta L\sin(\beta) + \frac{r_b\sin(2\alpha)(I_x^2 - I_y^2)}{2I_1^2} = \delta L\sin(\beta) \qquad C = \frac{(I_xI_y)^2}{I_1^4}r_b^2 \qquad (3.4.37)$$

and the parameter s at the wellbore becomes:

$$s_w = \sqrt{\beta_z\left[\sin^2(\beta)(l - \delta L)^2 + (\frac{r_b}{\beta_h})^2\right]} \qquad \textbf{(3.4.38)}$$

where $\beta_h = k_h/k_\alpha = \sqrt{k_x k_y}\ / k_\alpha$ and r_b is the permeability weighted wellbore radius [Goode et al., 1987].

Therefore the integral term ψ of (3.4.31) at the wellbore becomes:

$$\psi_w = 2\int_0^{\infty}\int_0^{L}\left[\frac{\cosh[\xi(b + l\cos(\beta) - h)]\cosh(\xi(b + l\cos(\beta)))}{\sinh(h\xi)}\right]J_0(s_w\xi)\,dl\,d\xi \qquad \textbf{(3.4.39)}$$

Obviously, the well production q can be obtained by applying ψ_e of (3.4.34) and ψ_w of(3.4.39) in solution 3.4.32), which leads to the following:

$$q = \frac{1}{I_x I_y}\frac{\phi_e - \phi_w}{(\psi_e - \psi_w)} = \frac{4\pi\sqrt{k_x k_y}\,\Delta p}{\mu(\psi_e - \psi_w)} \qquad \textbf{(3.4.40)}$$

$$Q = Lq = \frac{4\pi\sqrt{k_x k_y}\,L\Delta p}{\mu(\psi_e - \psi_w)}$$

Thus by using solution (3.4.40), the well productivity Q can be determined.

For a horizontal well $\beta = 90°$, then the drainage boundary integral term ψ_e becomes:

$$\psi_e = 2\int_0^{\infty}\int_0^{L}\frac{\cosh[\xi(b)]}{2\sinh(\frac{h\xi}{2})}J_0(\xi s_e)\,d\xi\,dl \qquad \textbf{(3.4.41)}$$

and ψ_w becomes:

$$\psi_w = 2\int_0^{\infty}\int_0^{L}\left[\frac{\cosh[\xi(b-h)]\cosh(\xi b)}{\sinh(h\xi)}\right]J_0(s_w\xi)\,dl\,d\xi \qquad (3.4.42)$$

where parameter s_e and s_w becomes:

$$s_e = \sqrt{\beta_z}(l - r_e), \qquad s_w = \sqrt{\beta_z[(l-\delta L)^2 + \frac{r_b^2}{\beta_h^2}]} \qquad (3.4.43)$$

If we further assume that the well is located at the middle of the reservoir, i.e. b = h/2 then ψ_e and ψ_w under this condition become:

$$\psi_e = \int_0^{\infty}\int_0^{L} J_0(\xi s_e)\coth(\xi b)\,dl\,d\xi \qquad \psi_w = \int_0^{\infty}\int_0^{L} J_0(s_w\xi)\coth(\xi b)\,dl\,d\xi \qquad (3.4.44)$$

if we define $l_l = l\sqrt{\beta_z}$, $L_l = L\sqrt{\beta_z}$,then ψ_e and ψ_w of (3.4.44) become:

$$\psi_e = \frac{1}{\sqrt{\beta_z}}\int_0^{\infty}\int_0^{L_l} J_0(\xi s_e)\coth(\xi b)\,d\xi\,dl_l \qquad \psi_w = \frac{1}{\sqrt{\beta_z}}\int_0^{\infty}\int_0^{L_l} J_0(\xi s_w)\coth(\xi b)\,dl_l\,d\xi \qquad (3.4.45)$$

then the production rate (3.4.40) becomes:

$$Q = \frac{4\pi L\sqrt{k_x k_y}\,\Delta p}{\mu\left[\int_0^{\infty}\int_0^{L_l} J_0(\xi s_e)\coth(\xi b)\,dl_l\,d\xi - \int_0^{\infty}\int_0^{L_l} J_0(\xi s_w)\coth(\xi b)\,dl_l\,d\xi\right]} \qquad (3.4.46)$$

where

$$s_e = l_I - \sqrt{\beta_z}\, r_e, \quad s_w = \sqrt{(l_I - \delta L_I)^2 + \frac{\beta_z r_b^2}{\beta_h^2}} \tag{3.4.47}$$

Equation (3.4.46) implies that the anisotropic permeability effect on horizontal well productivity can be considered using the following modified well length, well radius and permeability as the isotropic parameters and used in isotropic solutions such as Borisov's or Joshi's solution.

$$L_I = L\sqrt{\frac{k_z}{k_a}}, \quad r_{wI} = r_b\sqrt{\frac{k_a k_z}{k_x k_y}}, \quad r_{eI} = r_e\sqrt{\frac{k_z}{k_a}} \tag{3.4.48}$$

3.4.3 Verification of the solution

To validate the solution developed in this chapter, we compared the two extreme cases of the new solution with the ones available in the literature. Figure 3.3 shows the horizontal well production curves of the new solution compared with Borisov's and Joshi's solutions under isotropic permeability conditions. Figure 3.4 compares the new solution of $\beta = 0°$ (vertical well) with the conventional vertical solution. In all these figures, the vertical axes (y axis) are the relative production Q_d which is defined as $Q_d = Q\mu/\pi\Delta p$ with Q being the real production, μ the fluid viscosity, and Δp the pressure difference between the well bore and drainage boundaries, maintained constant. From Figure 3.3 we find that the new solution agrees very well with Borisov's solution except for a small difference (< 5%) when the well length becomes less than the reservoir thickness. However, a consistent difference between Joshi's solution is present, but still within the range of a good engineering approximation. Joshi developed his solution by superposition of the vertical and horizontal flow, which might cause this difference.

From Figure 3.4 we also found that the new solution agrees with the conventional vertical well solution very well when $\beta = 0$ is used. This confirms the validity of our new solution because it replicates the well formulated and accepted conventional vertical solution.

3.5 Productivity of a slant well

Production rates in the following analysis are obtained by applying solution (3.4.40) with ψ_e and ψ_w defined in (3.4.33) and (3.4.39), and are also expressed in the form of relative production $Q_d = Q\mu/\pi\Delta P$. To show the productivity of a slant well, the relative production Q_d is plotted versus the inclination angle β when various other parameters are varied. The two geometric parameters r_e and r_w have been fixed in all the analyses and take the value of $r_e = 1000$ m, which is four to five times larger than the longest well length used in the analyses, and $r_w = 0.2$ m, which is 20 times less than the shortest well we have used in the analysis. Also if k_α is the flow permeability in the direction α, then the gradient permeability (usually used in flow analysis) can be written k_h^2/k_α. Therefore, if k_α is fixed, then increase k_h is equivalent to increase the gradient permeability in the direction perpendicular to the well. Therefore, in the following discussions we use k_h whenever the gradient permeability perpendicular to the α direction is considered.

3.5.1 The effect of well inclination

A large inclination toward the vertical direction (small value of β) is only possible in thick reservoirs because thin reservoirs significantly limit the possible length of a slant well. Horizontal or slightly inclined wells ($\beta > 85°$) are most likely to be used in thin reservoirs. Therefore, we will only discuss thick reservoirs where the well length can be approximately the same or less than the reservoir thickness. Figure 3.5 shows a case of an isotropic reservoir with thickness of $h = 50$m. To compare the production changes relative to the vertical well of the same length, the vertical axis in the figure is expressed as the production ratio between the slant well and the vertical well (Q/Q_v). It becomes obvious that the production rate increases as the slant well becomes more horizontal, and also the increase caused by inclination changes is larger for longer wells than short ones. However, generally the production increase caused by the inclination change is insignificant (less than 8% from the figure). We also note that the amount of production increase mostly happens when the slant angle is at $20° < \beta < 80°$. The production of a slant well with $\beta > 80°$ is almost the same as a horizontal well, and for $\beta < 20°$ it is almost the same as for a vertical well. This agrees with the numerical simulation results presented by Lee [1989].

In reality, horizontal and slant wells have longer intersection lengths in all practical cases, and therefore have much higher sustainable production rates. This tells us that, for constant pressure boundary conditions, the increased production of a horizontal well comes mostly from the longer contact length

of the well with the reservoir, with only a small part from the inclination effect.

We may conclude that the horizontal well always has larger production compared with the vertical well in an isotropic reservoir. The production advantages most come from the longer contact length of the well with reservoir, but also from the inclination effect.

3.5.2 The effect of vertical permeability

The anisotropic permeability effect also plays an important part in the productivity evaluation. The effect of vertical permeability is studied by fixing the horizontal and varying the vertical permeability. The slant well production in such a situation is shown in Figure 3.6, where $k_x = k_y = k_h = 1$ is used, and different curves in the figure represent different values of the k_v/k_h (k_z/k_α) ratio.

The vertical permeability effect is best demonstrated in Figure 3.6 where even though the isotropic production ($k_v/k_h = 1$) increases with increasing slant angle (become more horizontal), as discussed above, the production for $k_v/k_h = 0.5$ increases with β only when $\beta < 20°$. In other cases, however, the production decreases with β, except when β becomes very large. As is expected, the production for a vertical well ($\beta = 0°$) becomes identical and is independent of the vertical permeability values.

To more clearly observe the anisotropic permeability effect by eliminating the inclination effects, we also plotted Q/Q_I versus β in Figure 3.7, where Q/Q_I stands for the ratio of anisotropic permeability production Q to the isotropic production Q_I. It is found that by decreasing the vertical permeability by half, the horizontal well production decreases by about 8%; decreasing it by five times results in a production decrease of about 21%. Also we found that the vertical permeability effects decrease if a slant well becomes more vertical (Figure 3.7).

3.5.3 The effect of horizontal permeability

Figure 3.8 shows the well production changes while the permeability in the direction perpendicular to the well is varied while maintaining k_z and k_α as unit values. From Figure 3.8 we find that k_h has approximately the same effect on all differently inclined wells. The production increases about 1.4 times if the magnitude of k_h is doubled, and is about 2.2 to 2.4 times if we increase k_h by five times. This indicates that the effect of a permeability change perpendicular to the well is approximately the

same for all well inclinations.

Figure 3.9 shows the results when the k_z and k_h are fixed, i.e. $k_z = k_h = 1$, and the permeability in the α (well projection) direction k_α is increased. Compared with Figure 3.8, the production increase in these cases is approximately the same only for vertical wells. For slant wells, the production increase caused by an increase in k_α is less than when k_h is increased. The production increase for the horizontal well is the least and shows a 14% to 30% difference, depending on the amount of permeability increase, compared with the results in Figure 3.8. This indicates that a larger α-direction permeability increases vertical well production more effectively than horizontal well production.

3.6 Productivity of a horizontal well

3.6.1 Reservoir thickness and well length effect

The well length and reservoir thickness have significant effects on horizontal well production because most of the horizontal well advantages come from the longer contact length of the well with the reservoir, as discussed above. Figures 3.10 and 3.11 show the production changes versus reservoir thickness and well length. From Figure 3.10, we find that the production rate increases with increasing thickness. However, the increase is not a linear function with h. The production increases rapidly with h only for thin reservoirs. When h becomes very large, a quasi-steady state can be reached and under this state, the production rate predicted is no longer affected significantly by reservoir thickness. Long wells require a greater thickness value for reaching this quasi-steady state than short wells (Figure 3.11). This indicates, logically, that for exceptionally thick reservoirs, the optimum extraction method may require several horizontal wells located at different pre-designed heights in the reservoir. Provided that the drive mechanism is pressure-field dominated, this should increase both production efficiency and total resource access.

Well production increases with well length, but again the relationship is not linear, as in the case of a vertical well. The increase of production with well length is greater when the well is short, and lesser when the well becomes long. A log-log relationship may approximately describe this variation with L (Figure 3.10).

3.6.2 The effect of eccentric placement

The location of a horizontal well in the producing stratum can affect well performance; intuitively, for the solutions derived herein which have constant pressure boundary conditions at a large distance from the wellbore, one would expect that the best production rates would be found at the midpoint. The parametric analysis results are shown in Figure 3.12 for different well lengths. The vertical axis in this figure is the value of Q/Q_m where Q_m is the production when the well is located in the middle of the reservoir (b = h/2), and Q stands for production of an off-midheight well. The horizontal axis of the figure is the ratio between well location and reservoir thickness b/h. If b/h = 0, it means a horizontal well is on the bottom boundary, b/h = 0.5 means it is at the midheight, and b/h = 1 means it is at the top boundary.

The locations of the horizontal wells in the reservoir indeed affect the steady-state production rate. The maximum production rate is given when the wells are at the middle of the reservoir, as would be expected, and decreases 28% if the wells are shifted to the impervious boundaries for a well with h/L = 0.5). This difference also would increase if h/L > becomes larger than 0.5. Thus, we may conclude that for long wells in a thin reservoir (h/L < 0.1), deviation of the well location from the middle of the reservoir does not significantly affect the sustainable production, but for short wells in a thick reservoir, the effect is more pronounced.

3.6.3 Advantages of horizontal wells in production

We have discussed the effect of well length and reservoir thickness on horizontal well production, but did not discuss the production of a vertical well in the same reservoir. To analyze the advantages of horizontal wells in production relative to vertical wells, it is better to obtain the ratio between the horizontal and vertical well production under the same conditions.

Figure 3.13 shows the Q/Q_v relationships under various values of well length and reservoir thickness in an isotropic reservoir. Q is the horizontal well production and Q_v is the production of a vertical well which penetrates the reservoir. Figure 3.13 clearly shows that for an isotropic permeability reservoir, horizontal wells are always better than vertical wells if the well length is larger than the reservoir thickness. However, we also can see that even though production increases with well length, the increase becomes insignificant when the well is quite long. For instance, for a 30 m thick reservoir, an increase in production of about 2 times requires an increase in the horizontal well length of about 4-5 times. This may not economically viable if the drilling cost is also considered. Also, because of the viscosity effect, the capability for transportation of fluid within the wellbore may also limit the production if a well is too long. Therefore a optimum production design is required.

The effect of vertical permeability on productivity of long horizontal wells largely depends on reservoir thickness. Decreasing vertical permeability will decrease the horizontal well production, and this decrease can be significant for thick reservoirs. Figure 3.14 shows the case of a 30 m reservoir, where the horizontal well becomes worse than the vertical well when k_z/k_α becomes less than 0.05 if h/L is less than 0.2. This indicates that for thick reservoirs with a very small vertical permeability, vertical wells are still the preferred choice. For thin reservoirs, horizontal wells are better and it does not heavily depend on the permeability ratio.

Figure 3.15 shows the results when $k_z = k_h = 1$ and the permeability in the well direction is increased. Increasing k_α can increase production more for a vertical well than for a horizontal well. This can be seen from Figure 3.15, where if k_α increases 20 times, the Q/Q_v ratio decreases from 2.7 to 1.8. This indicates that larger axial permeability (parallel to the well axis) does not have a significant effect on the well production, even though, in general, horizontal wells are still much better than vertical wells.

The case of increasing k_h is different from that of increasing k_α. Increasing k_h does increase the Q/Q_v ratio, even though the increase is not great. Figure 3.16 shows the results where $k_z = k_\alpha = 1$ and k_h is increased. The effect of k_h on horizontal well production is less significant for short wells than for long ones. This indicates that the effect of the permeability perpendicular to the well is almost the same for both slant and vertical wells, as was discussed above.

We may conclude from this section that horizontal wells are always better than vertical wells if the h/L is not too large (< 0.2) and the vertical permeability is not too small (> $k_h/20$). Generally speaking, increasing k_z or k_h and decreasing k_α can permit us to exploit the advantages of a horizontal well, and this can also be seen from Figure 3.17. We conclude that to best use the advantages of a horizontal well, it is best to place the well along the minimum permeability direction, and perpendicular to the maximum permeability direction in the horizontal plane. For very thick reservoirs, multilevel horizontal wells at different heights are probably a good idea no matter what the vertical and horizontal permeability ratios are.

3.7 Conclusions

A new analytical solution has been developed to analyze the sustainable (steady-state) production rates from wells in an anisotropic reservoir with a constant inclination angle. This solution avoids some of the assumptions that others have found necessary in order to achieve a useful approximation. Instead,

a definite integration term is introduced which can be evaluated easily by numerical integration. We show that for the well-known limiting case of a vertical well, our solution gives almost identical results, and for horizontal wells, good agreement has been obtained compared with previous published solutions, through our solution is more rigorous.

Using sustainable production rate as the comparison, and for the case of constant far-field pressure boundary conditions, horizontal wells are always better than vertical wells if the well length is larger than the reservoir thickness in an isotropic case, regardless of the reservoir thickness. However if the horizontal well length is less than the reservoir thickness, the production becomes almost the same for wells of any angle. The production rate decrease for an inclined well is insignificant to sustainable production rates, particularly when α is less than 20°. A horizontal well located other than in the midheight of the reservoir will decrease the production rate, but this effect is usually less than 25% and the effect decreases with increasing well length and decreasing reservoir thickness. Because horizontal or inclined wells always have longer intersection lengths in the reservoir, compared to vertical wells, a proper economic comparison should be normalised to a unit length of intersection of the reservoir. In general, the results herein confirm clearly that the longer the horizontal well, the greater the benefits, leaving aside costs arising from other sources. However the increase of production is not proportional to the increase of the well length.

We must be aware that all the conclusions obtained above are for steady-state flow. These conclusions will not in general apply to transient cases directly, as will be discussed in Chapter 4. Anisotropic permeability has been incorporated in the newly developed analytical solution to analyze the sustainable (steady-state) production rates from a slant well at any angle. For the well-known limiting case of a vertical well, our solution gives identical results, and for horizontal wells, if we take an isotropic permeability, good agreement has been obtained with previous published solutions. A general anisotropic analysis has never been done before in a analytical formulation, therefore, the new solution presents advantages for analysis of anisotropy.

Anisotropic permeability has significant effects on the production rate of a horizontal or a slant well. The permeability in the well direction has less effect on small angle wells than for large angle ones. The permeability in the direction perpendicular to the well increases horizontal well production better than for vertical ones, but the difference is insignificant. The anisotropic permeability effect may be approximately simulated by using the reservoir anisotropy modified parameters defined in equation (3.4.47) in a isotropic solution such as Borisov's solution.

Generally speaking, vertical wells are most suitable for thick reservoirs or where there is very small

vertical permeability, whereas horizontal wells are suitable for thin reservoirs, particularly when the vertical permeability is larger.

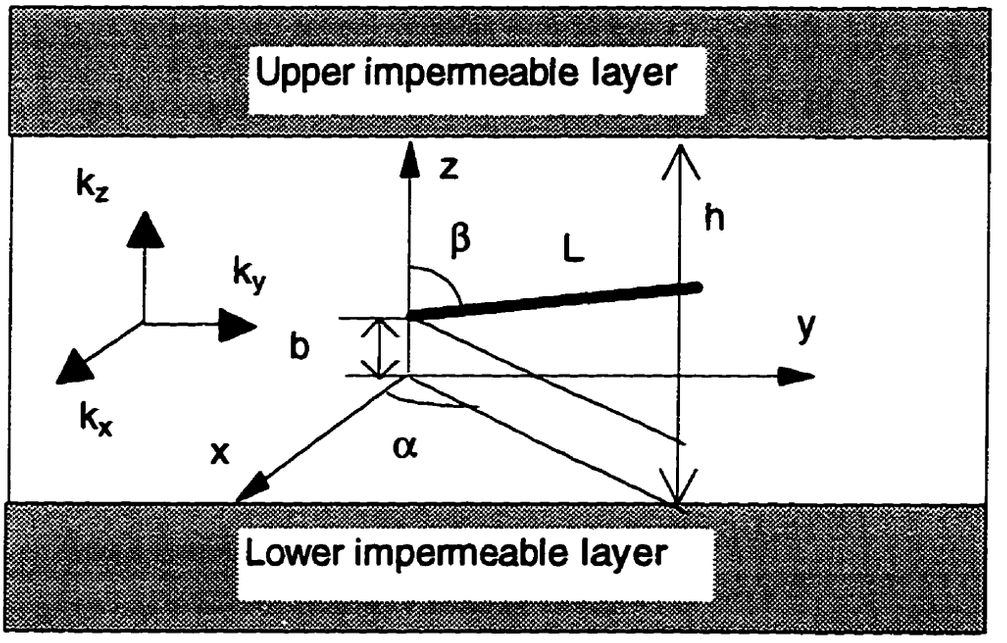

Figure 3.1 Configuration of a slant well in a three dimensional anisotropic reservoir.

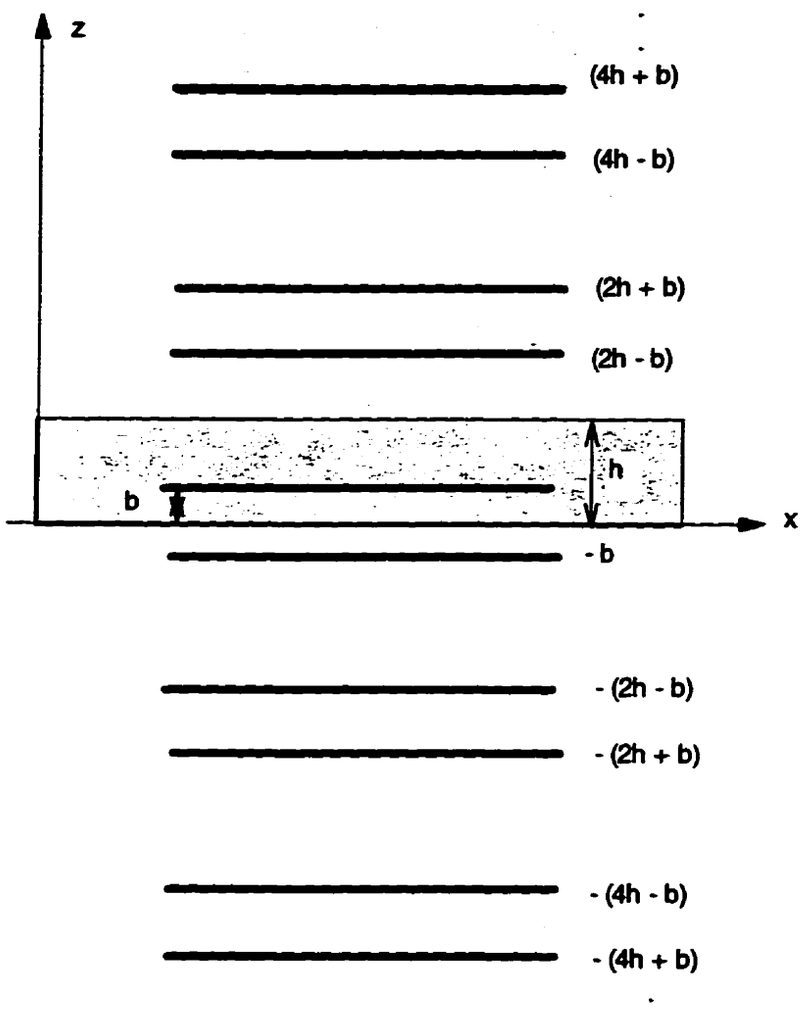

Figure 3.2 Image superposition to simulate the impervious upper and lower boundaries (at y = 0 and y = h) of a slant well.

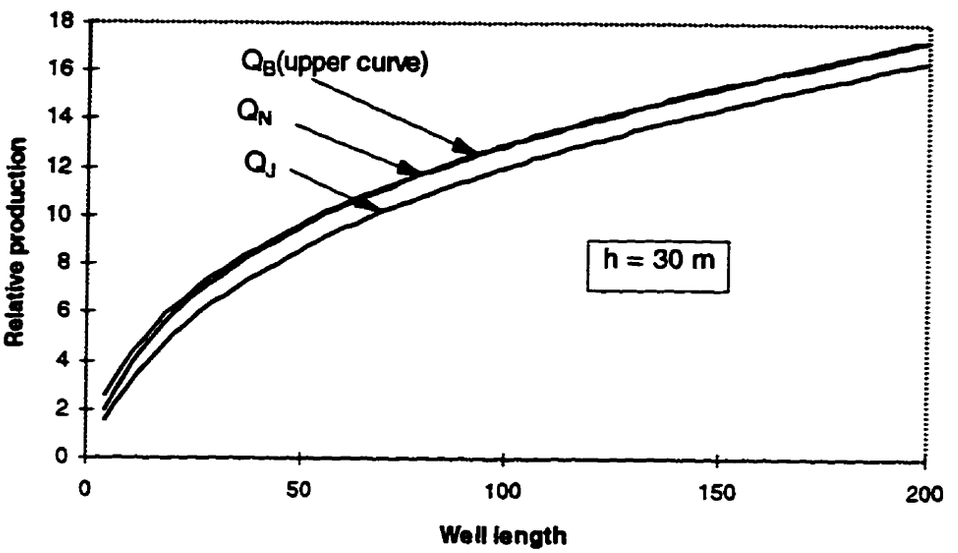

Figure 3.3 Comparisons between Borisov (1984), Joshi (1988) and the new solutions for horizontal well productivity.

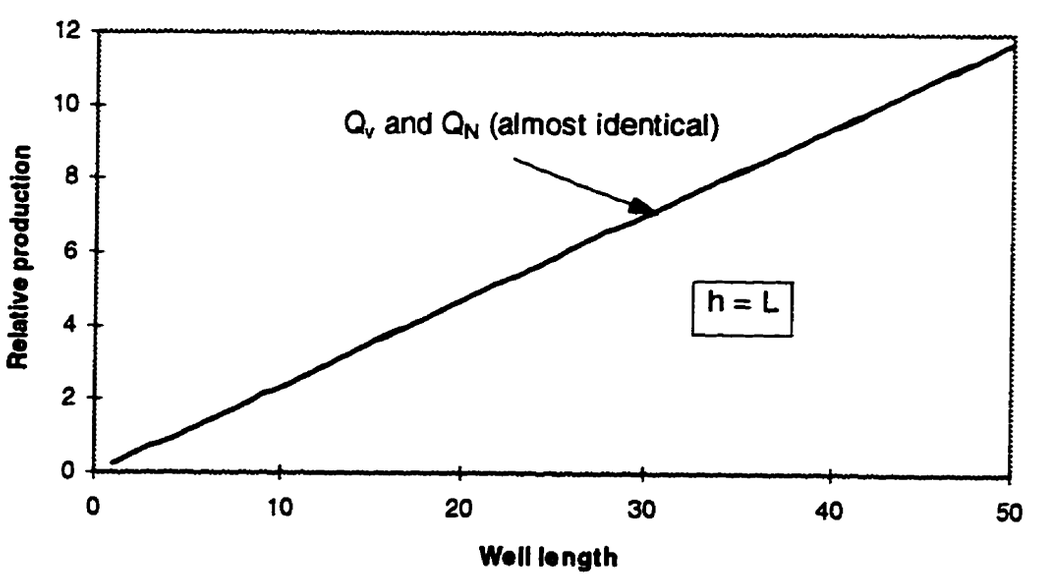

Figure 3.4 Comparison of production between the new solution and the conventional vertical well solution.

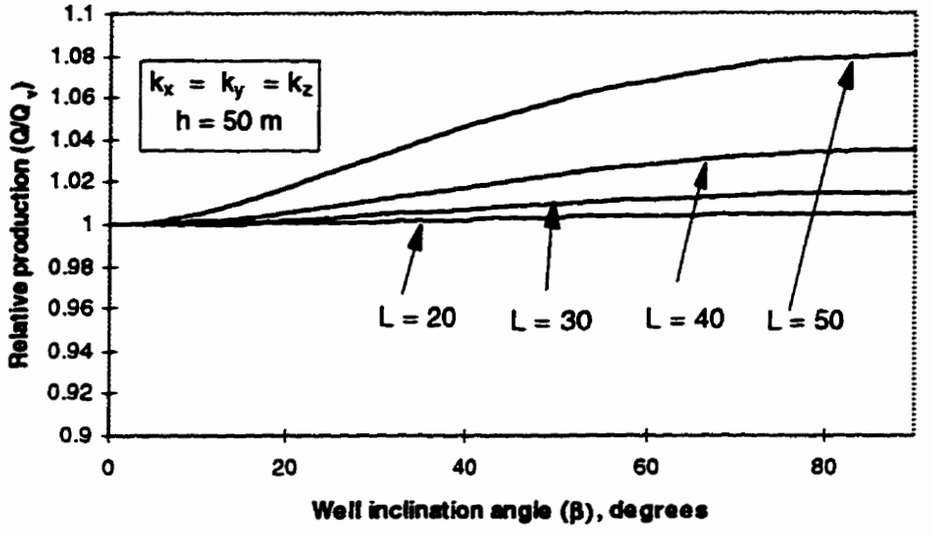

Figure 3.5 The effect of inclination of a slant well on well production with different well lengths.

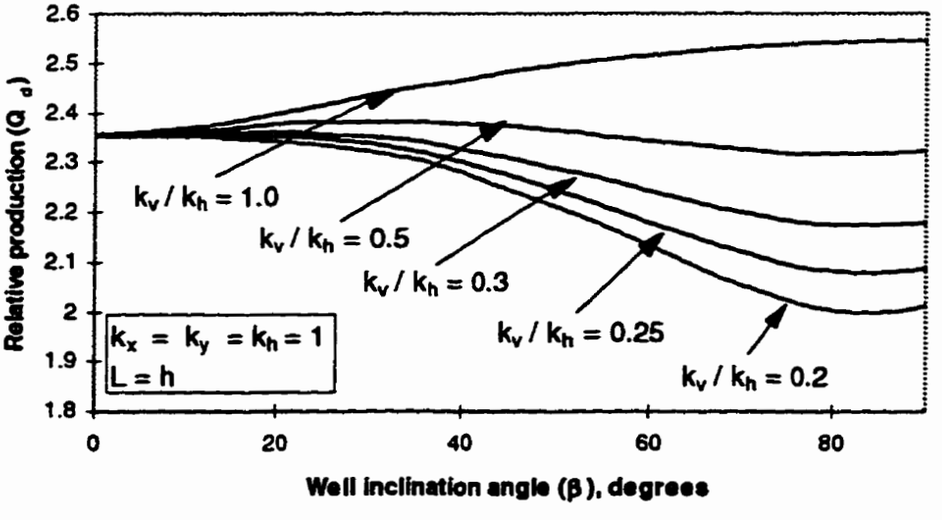

Figure 3.6 The effect of vertical permeability on production of wells at different degree of inclinations.

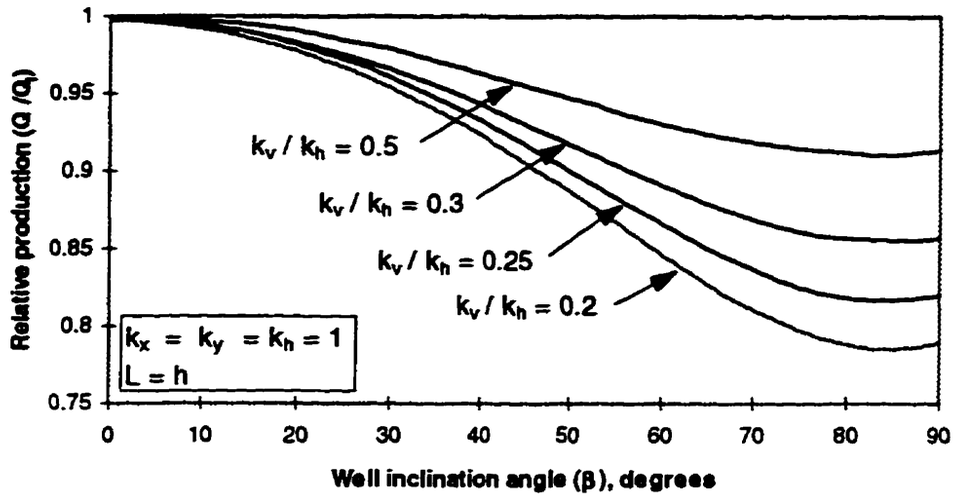

Figure 3.7 The effect of vertical permeability on slant well production compared with normalized isotropic production.

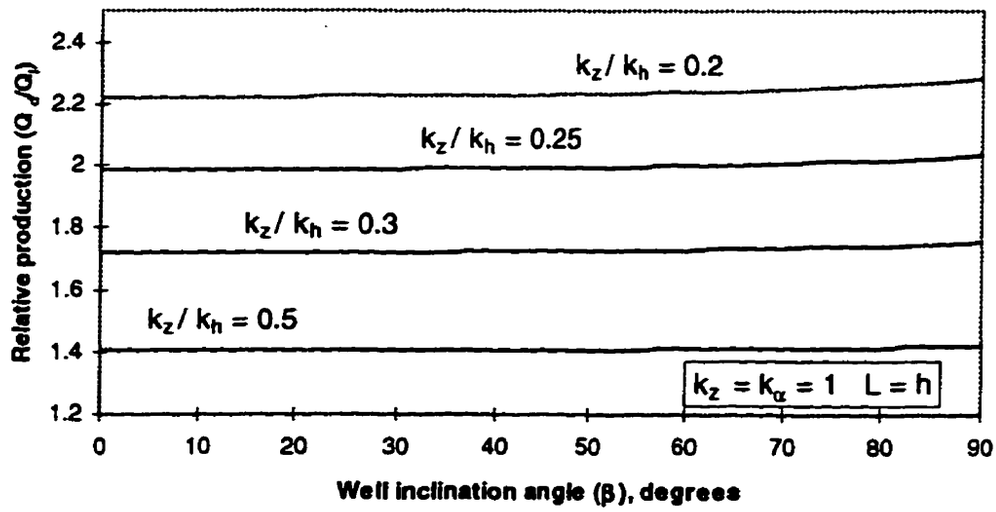

Figure 3.8 The effect of horizontal permeability on slant well production compared with normalized isotropic production.

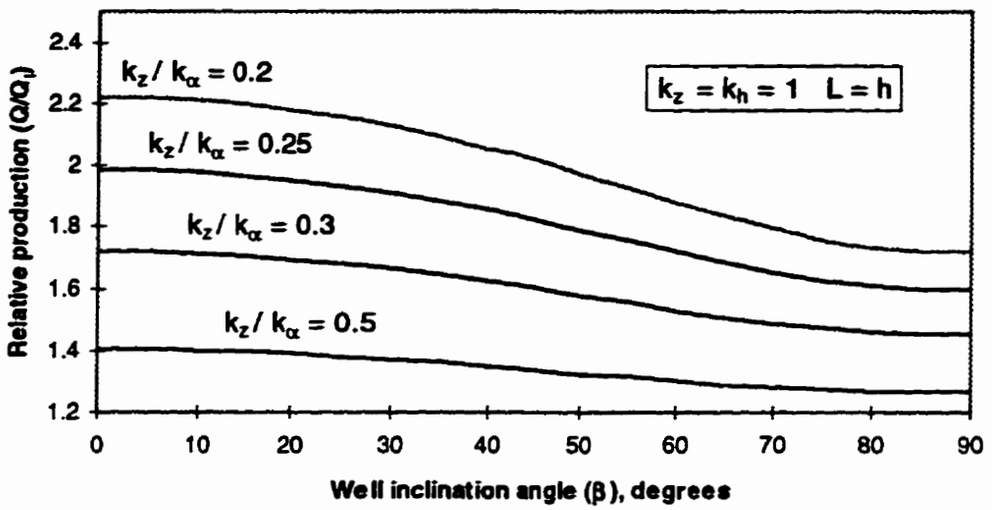

Figure 3.9 The effect of permeability in the α direction on slant well production.

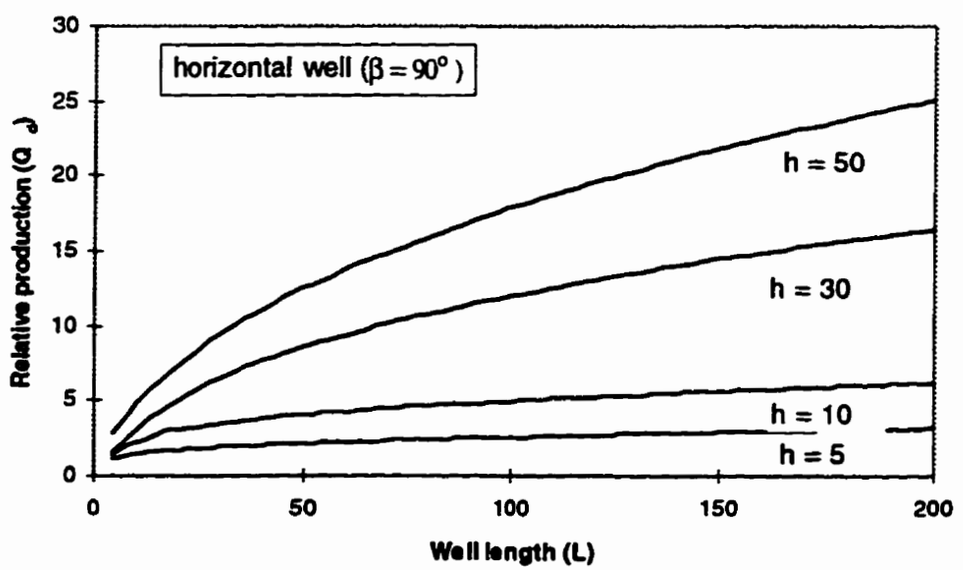

Figure 3.10 Effect of well length on horizontal well production with different reservoir thicknesses.

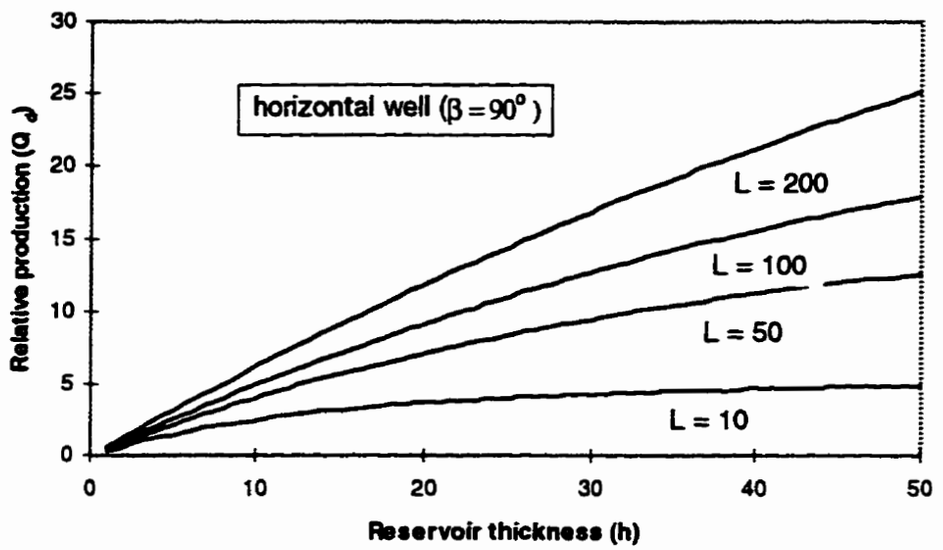

Figure 3.11 Effect of reservoir thickness on horizontal well production with different well lengths.

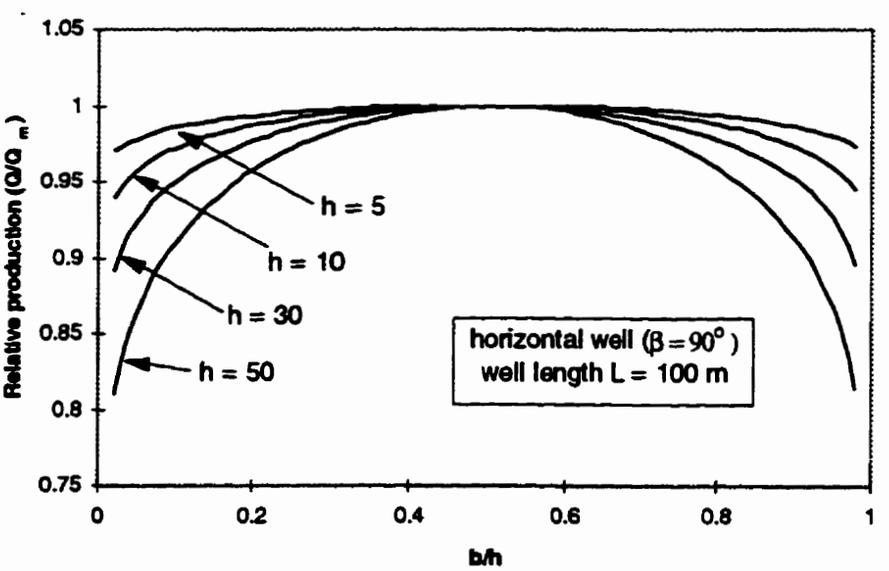

Figure 3.12 Effect of eccentric placement on horizontal well production with different reservoir thicknesses.

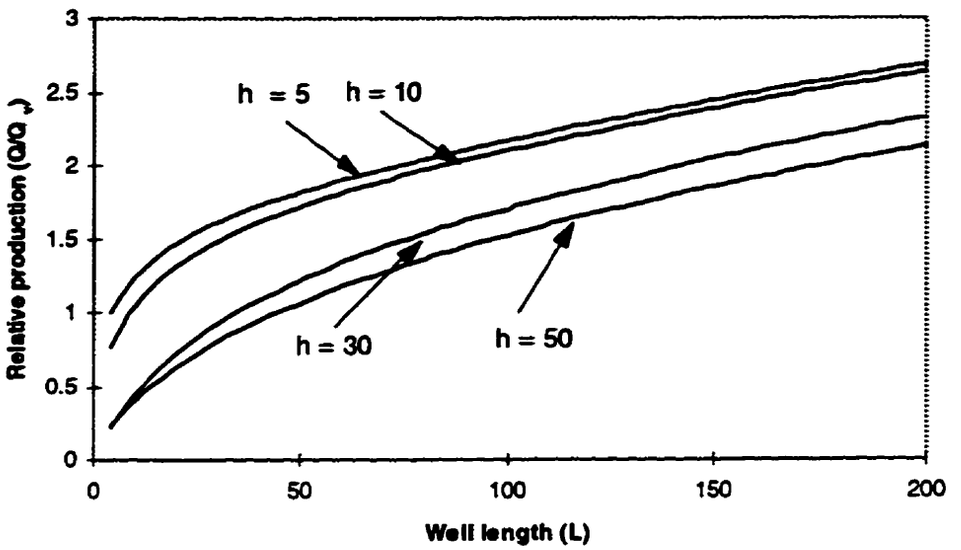

Figure 3.13 Advantages of horizontal well production compared with a vertical well in an isotropic reservoir.

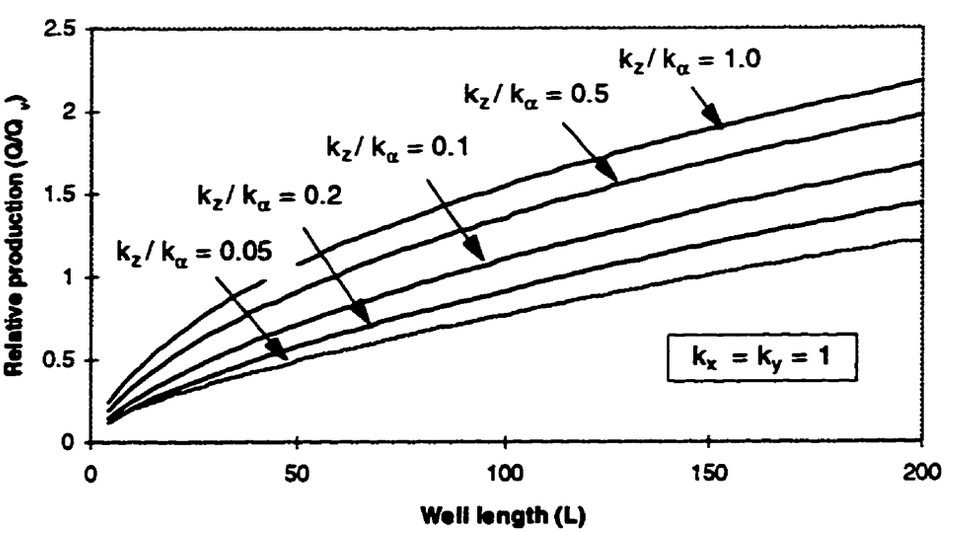

Figure 3.14 The effect of vertical permeability on horizontal well production.

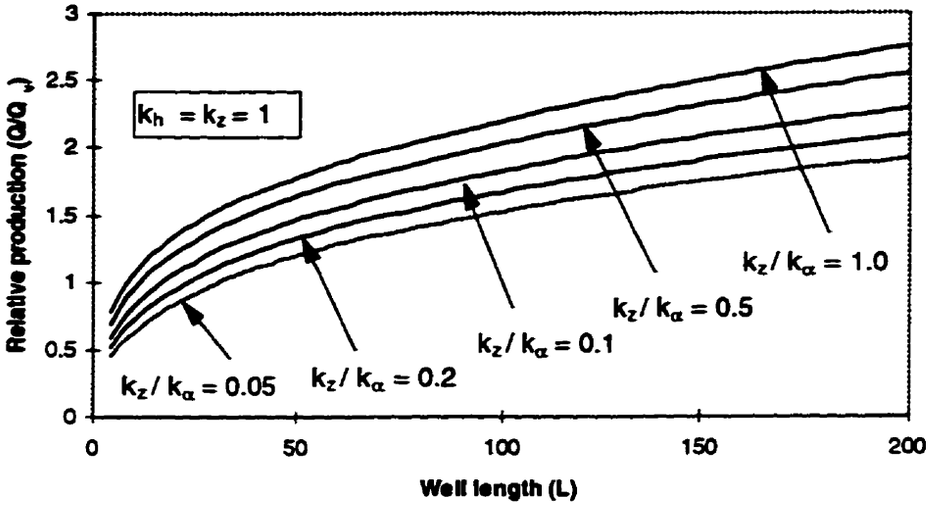

Figure 3.15 The effect of permeability in the well direction on horiozntal well production.

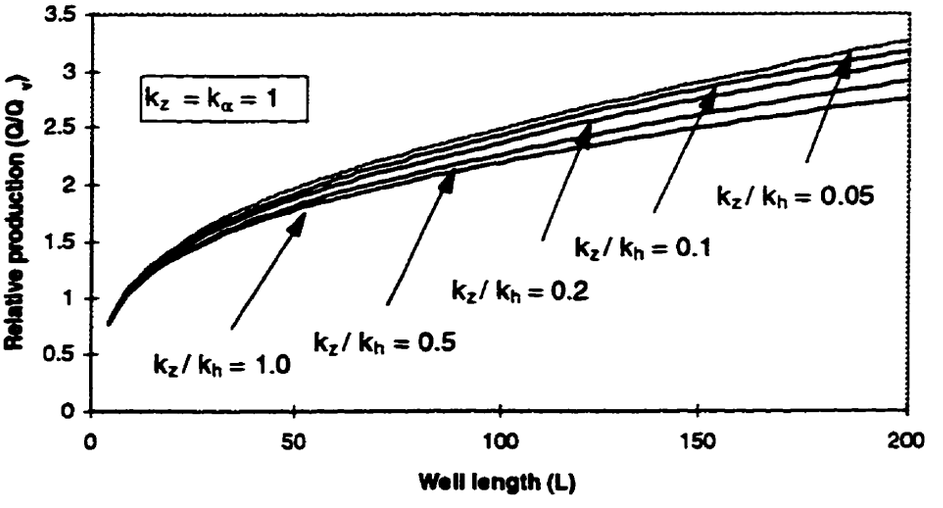

Figure 3.16 The effect of permeability in the direction perpendicular to the well on horizontal well production.

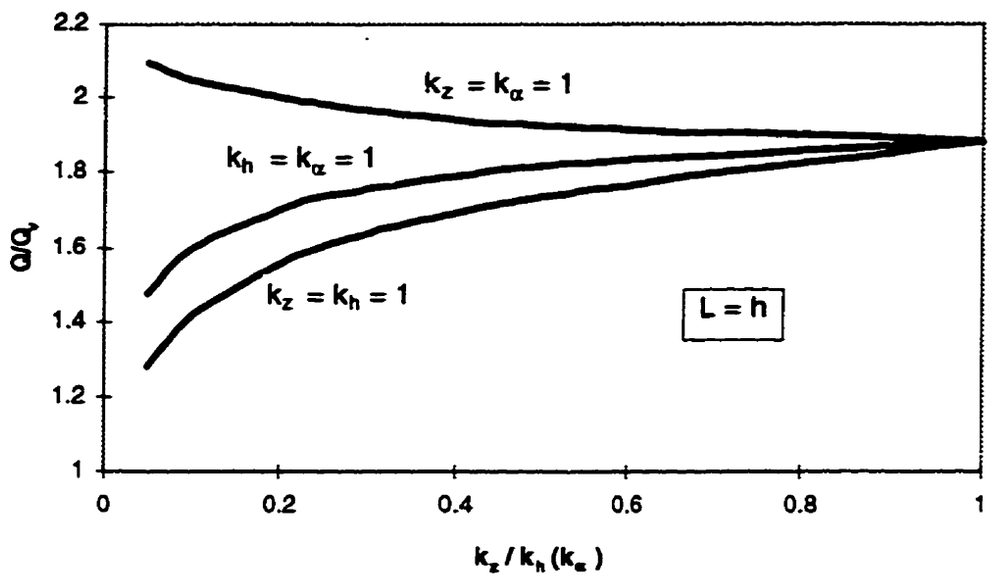

Figure 3.17 Horizontal well production variations with anisotropic permeability values.

Chapter Four

Horizontal Well Test Interpretation

4.1 Interpretation of Horizontal Well Test

4.1.1 Literature review

Interpretation of a horizontal well test is more difficult than for a vertical well test because of the 3D geometrical nature and the evolution into different flow regimes. Horizontal well test results will not only depend on the reservoir characteristics, but also on the well geometry and orientation. Even though a number of well defined horizontal well pressure analyses have been reported in the literature [Daviau et al., 1988; Goode et al., 1987; Kuchuk et al., 1988; Mattar and Santo, 1995] some of the issues are still not clearly resolved. Well test behaviour in a highly anisotropic reservoir seems to be one of these issues which has not received enough attention. It has been observed that a complete horizontal well test in an infinite acting reservoir can usually be segmented into three flow regimes (neglecting the wellbore storage effect): the vertical radial flow regime, the linear flow regime and the horizontal radial flow regime as shown in Figure 4.0 [Daviau et al., 1988; Goode,et al., 1987]. However, under certain conditions, such as when the vertical permeability is very small compared to the horizontal one, linear flow could be absent, and instead, a spherical flow regime can develop. However, the criteria for linear flow to be replaced by spherical flow and the corresponding test behaviour during the spherical flow period have not, as far as we are aware, been discussed in the literature.

Another example of a deficiency in many existing analyses is that most of the horizontal solutions were developed by assuming the well was drilled along the k_x direction, therefore leading to the conclusion that by using the vertical radial flow regime the combined permeability $[k_y k_z]^{1/2}$ can be determined. This conclusion is only acceptable in a horizontally isotropic reservoir or if the well is truly drilled along the k_x direction; otherwise, errors are introduced, and the magnitude of these errors increases with increasing anisotropy.

In this Chapter we present a interpretation method which considers a well in an anisotropic reservoir,

oriented arbitrarily in the horizontal plane. By using the new solution, accurate test interpretation can be obtained for all possible horizontal well orientations. Also, if two tests are carried out in wells of two different orientations from the same reservoir, then the permeability anisotropy can be determined.

We will also try to outline some guidelines for flow regime identification based on our analysis. The criteria for such identification differ in the literature [Daviau et al., 1988; Goode et al., 1987; Mattar, and Santo, 1995] which makes it difficult and confusing to use in flow regime identification, which is the foundation for using the segmental analysis method in interpreting test [Zhang and Dusseault, 1996].

4.1.2 Limitations of traditional interpretation methods

Many analyses of transient horizontal well pressures have been reported in the literature, and several test interpretation methods have also been developed based on these solutions. However, several problems still exist in using the available solutions. As we have discussed above, most available solutions assume the reservoir is isotropic horizontally, or if a horizontally anisotropic reservoir is encountered, then the well is assumed to be parallel to the k_x direction. These assumptions make it difficult to determine the true reservoir anisotropies from arbitrarily oriented horizontal wells.

Another limitation of the available solutions is that the characteristic times, such as the time when the no flow boundaries take effect, or when the length of the well begins to take effect, are not used. In fact, such times give important information on the characteristics of the reservoir and the well configuration, and sometimes could be the only information available. We will in the following sections develop a new set of solutions which takes advantage of all possible information and which also provides important data concerning the reservoir and the well behaviour.

4.2 Horizontal Well Drawdown Test Interpretation

4.2.1 Theoretical derivation of the solution

The horizontal well problem discussed here is similar to that discussed by others [Daviau et al., 1988; Goode et al., 1987] except that an arbitrary horizontal well is drilled at α degrees from the k_x direction. Other assumptions are as follows: 1) the reservoir is an infinite, horizontal reservoir with constant

thickness h; 2) the reservoir has no-flow upper and lower boundaries; 3) the reservoir has primary anisotropic permeabilities k_x, k_y and k_z which coincide with the three axes of the coordinate system and, 4) a well of length L is located at a distance b from the lower boundary (Figure 4.1). The following equation is used to model this problem:

$$c_m\phi\frac{\partial\Delta p}{\partial t} - \frac{k_x}{\mu}\frac{\partial^2\Delta p}{\partial x^2} - \frac{k_y}{\mu}\frac{\partial^2\Delta p}{\partial y^2} - \frac{k_z}{\mu}\frac{\partial^2\Delta p}{\partial z^2} = q(t')\delta(x-x',y-y',z-z',t-t') \tag{4.2.1}$$

where k_x, k_y, k_z are the primary permeabilities in the three-dimensional space, x', y', z' define the position of the well, μ is viscosity, ϕ is porosity, c_m is compressibility, $\Delta p = p_i - p_{wf}$ is defined as the pressure drop between wellbore and far field, q is flow rate per unit well length, and t is time.

The boundary conditions for such a problem are:

$$\Delta p(x,y,z,t)|_{x=\pm\infty} = 0 \quad \Delta p(x,y,z,t)|_{y=\pm\infty} = 0$$
$$\Delta p(x,y,z,t)|_{t=0} = 0 \quad \frac{\partial\Delta p}{\partial z}|_{z=0} = 0, \quad \frac{\partial\Delta p}{\partial z}|_{z=h} = 0 \tag{4.2.2}$$

To solve the boundary value problem defined by (4.2.1) and (4.2.2), we define new variables $x_d = x\sqrt{k_z/k_x}$, $y_d = y\sqrt{k_z/k_y}$, and $z_d = z$, then equation (4.2.1) becomes:

$$\frac{c_m\phi\mu}{k_z}\frac{\partial\Delta p}{\partial t} - \frac{\partial^2\Delta p}{\partial x_d^2} - \frac{\partial^2\Delta p}{\partial y_d^2} - \frac{\partial^2\Delta p}{\partial z_d^2} = \frac{q(t')\mu}{k_h}\delta(x_d-x_d',y_d-y_d',z_d-z_d',t-t') \tag{4.2.3}$$

where $k_h = \sqrt{k_x k_y}$ is the horizontal average permeability.

The boundary conditions (4.2.2) become:

$$\Delta p(x_d,y_d,z_d,t)|_{x_d=\pm\infty} = 0 \qquad \Delta p(x_d,y_d,z_d,t)|_{y_d=\pm\infty} = 0$$
$$\Delta p(x_d,y_d,z_d,t)|_{t=0} = 0 \qquad \frac{\partial \Delta p}{\partial z_d}|_{z_d=0} = 0,\ \frac{\partial \Delta p}{\partial z_d}|_{z_d=h} = 0 \tag{4.2.4}$$

If we apply the following exponential transform:

$$G(\alpha_1,\alpha_2,z_d,t) = \int_{-\infty}^{\infty}\int_{-\infty}^{\infty} \Delta p(x_d,y_d,z_d,t) e^{i(\alpha_1 x_d + \alpha_2 y_d)} dx_d dy_d \tag{4.2.5}$$

to equation (4.2.3) and boundary conditions (4.2.4) for x_d and y_d, we obtain:

$$\frac{c_m \phi \mu}{k_z}\frac{\partial G}{\partial t} + \alpha_1^2 G + \alpha_2^2 G - \frac{\partial^2 G}{\partial z_d^2} - \frac{q(t')\mu}{k_h} e^{-i(\alpha_1 x_d' + \alpha_2 y_d')}\delta(z_d - z_d', t-t') = 0 \tag{4.2.6}$$

and the transformed initial and boundary conditions become:

$$G(\alpha_1,\alpha_2,z_d,t)|_{t=0} = 0$$
$$\frac{\partial G}{\partial z_d}|_{z_d=0} = 0,\ \frac{\partial G}{\partial z_d}|_{z_d=h} = 0 \tag{4.2.7}$$

If we further apply the following Fourier transform :

$$\bar{G}(\alpha_1,\alpha_2,n,t) = \int_0^h G(\alpha_1,\alpha_2,z_d,t)\cos(\frac{n\pi z_d}{h})dz_d \tag{4.2.8}$$

to equation (4.2.6) and the boundary conditions (4.2.7) we have:

$$\frac{c_m \phi \mu}{k_z}\frac{\partial \bar{G}}{\partial t} + \alpha_1^2 \bar{G} + \alpha_2^2 \bar{G} + \frac{n^2\pi^2}{h^2}\bar{G}$$
$$= \frac{q(t')\mu}{k_h} e^{-i(\alpha_1 x_d' + \alpha_2 y_d')}\cos(\frac{n\pi z_d'}{h})\delta(t-t') \tag{4.2.9}$$

Solving for G from equation (4.2.9) we obtain:

$$\bar{G} = \frac{k_z q(t')}{k_h c_m \phi} e^{-i\alpha_1 x'_d} e^{-\frac{k_z}{c_m \phi \mu}\alpha_1^2 (t-t')} e^{-i\alpha_2 y'_d} e^{-\frac{k_z}{c_m \phi \mu}\alpha_2^2 (t-t')} \cos\left(\frac{n\pi z'_d}{h}\right) e^{-\frac{k_z}{c_m \phi \mu}\frac{n^2\pi^2}{h^2}(t-t')} \tag{4.2.10}$$

If α_1 and α_2 in equation (4.2.10) are inverted back to x_d and y_d, we obtain the following point sink solution:

$$\Delta\bar{p} = \frac{k_z q(t')}{k_h c_m \phi} \frac{1}{4\pi C_z (t-t')} e^{-\frac{(x_d - x'_d)^2 + (y_d - y'_d)^2}{4C_z(t-t')}} \cos\left(\frac{n\pi z'_d}{h}\right) e^{-\frac{C_z n^2 \pi^2}{h^2}(t-t')} \tag{4.2.11}$$

which can be written as:

$$\Delta\bar{p} = \frac{q(t')\mu}{4\pi k_h (t-t')} e^{-\frac{(x_d - x'_d)^2 + (y_d - y'_d)^2}{4C_z(t-t')}} \cos\left(\frac{n\pi z'_d}{h}\right) e^{-\frac{C_z n^2 \pi^2}{h^2}(t-t')} \tag{4.2.12}$$

where $C_z = k_z/(c_m \phi \mu)$.

If we invert n back to z_d, then the point sink solution becomes:

$$\Delta p' = \frac{q(t')\mu}{4\pi k_h h (t-t')} e^{-\frac{(x_d - x'_d)^2 + (y_d - y'_d)^2}{4C_z(t-t')}} \left[1 + 2\sum_{n=1}^{\infty} e^{-\frac{C_z n^2 \pi^2}{h^2}(t-t')} \cos\left(\frac{n\pi z'_d}{h}\right)\cos\left(\frac{n\pi z_d}{h}\right)\right] \tag{4.2.13}$$

Substituting the variables $x_d = x\sqrt{k_z/k_x}$, $y_d = y\sqrt{k_z/k_y}$,and $z_d = z$ back into solution (4.2.13), we obtain the following:

$$\Delta p' = \frac{q(t')\mu\, e^{-\frac{1}{4s_s(t-t')}\left[\frac{(x-x')^2}{k_x}+\frac{(y-y')^2}{k_y}\right]}}{4\pi k_h h(t-t')} \left[1+2\sum_{n=1}^{\infty} e^{-\frac{C_z n^2\pi^2(t-t')}{h^2}} \cos\left(\frac{n\pi z'}{h}\right)\cos\left(\frac{n\pi z}{h}\right)\right] \tag{4.2.14}$$

where $s_s = 1/c_m\phi\mu$.

For a slant well defined in Figure 3.1, with l being measured radially outward from the coordinate center, the following relationships are satisfied:

$$\begin{aligned} x' &= l\sin(\theta)\cos(\alpha)\ , \\ y' &= l\sin(\theta)\sin(\alpha)\ , \\ z' &= b + l\cos(\theta) \end{aligned} \tag{4.2.15}$$

If we substitute the relationships of (4.2.15) into (4.2.14) and let $\tau = t - t'$, we obtain:

$$\Delta p = \frac{\mu}{4\pi h k_h L}\int_0^L\int_0^t \frac{Q(t-\tau)}{\tau} e^{-\frac{1}{4s_s\tau}\left[\frac{[l\sin(\theta)\cos(\alpha)-x]^2}{k_x}+\frac{[l\sin(\theta)\sin(\alpha)-y]^2}{k_y}\right]} \left[1+2\sum_{n=1}^{\infty} e^{-\frac{C_z n^2\pi^2\tau}{h^2}} \cos\left(\frac{n\pi(b-l\cos(\theta))}{h}\right)\cos\left(\frac{n\pi z}{h}\right)\right] dl\ d\tau \tag{4.2.16}$$

where $Q(t-\tau) = q(t-\tau)L$ is the total flow rate along the full length of wellbore if wellbore storage is neglected.

Solution (4.2.16) is the pressure drawdown solution for a slant well defined in Figure 3.1 in a layered reservoir. Solution (4.2.16) has a exponential term and a series term included in the double integral; each term reflects different geometric aspects of the problem. Because the double integral can not be solved analytically, a numerical scheme must be applied to evaluate the solution.

For a horizontal well as defined in Figure 4.1, because $\theta = 90°$, the series term becomes independent of l, and the exponential term becomes:

$$\frac{[l\cos(\alpha) - x]^2}{k_x} + \frac{[l\sin(\alpha) - y]^2}{k_y}] = [Al - A'L]^2 + CA^2L^2 \qquad (4.2.17)$$

where

$$A = \sqrt{\frac{\cos^2(\alpha)}{k_x} + \frac{\sin^2(\alpha)}{k_y}} = \frac{1}{\sqrt{k_\alpha}}$$

$$A' = \frac{1}{AL}[\frac{x\cos(\alpha)}{k_x} + \frac{y\sin(\alpha)}{k_y}] \qquad (4.2.18)$$

$$C = \frac{1}{L^2A^4k_xk_y}[y\cos(\alpha) - x\sin(\alpha)]^2$$

and k_α is the permeability along the direction of well with α being defined as the angle between the well and the x axis, which has the following form:

$$\frac{1}{k_\alpha} = \frac{\cos^2(\alpha)}{k_x} + \frac{\sin^2(\alpha)}{k_y} \qquad (4.2.19)$$

Equation (4.2.19) implies that the directional permeability in the horizontal plane forms an ellipse with $\sqrt{k_x}$ and $\sqrt{k_y}$ as its major and minor axis respectively [Hantush, 1966]. The square root of the permeability in any direction therefore can be determined from the ellipse shown in Figure 4.2

If $Q(t-\tau)$ is a constant Q, then by integrating l from 0 to L, solution (4.2.16) becomes:

$$\Delta p = \frac{Q\mu}{4\pi k_h hL}\int_0^t \frac{1}{\sqrt{\tau}} e^{-\frac{CA^2L^2}{4s_s\tau}} \left[erf\left[\frac{AL - A'L}{\sqrt{4s_s\tau}}\right] + erf\left[\frac{A'L}{\sqrt{4s_s\tau}}\right]\right] \qquad (4.2.20)$$
$$\frac{\sqrt{\pi s_s}}{A}\left[1 + 2\sum_{n=1}^{\infty} e^{-\frac{n^2\pi^2C_s\tau}{h^2}} \cos(\frac{n\pi b}{h})\cos(\frac{n\pi z}{h})\right]d\tau$$

We can introduce dimensionless pressure P_d and dimensionless time t_d as :

$$P_d = \frac{4\pi h k_h}{\mu Q}\Delta p \qquad t_d = \frac{4k_\alpha t}{L^2 c_m \phi \mu} \tag{4.2.21}$$

and by applying P_d and t_d to solution (4.2.20) we have:

$$P_d = \int_0^{t_e} Z(u)du \tag{4.2.22}$$

where the function inside the integral $Z(t_d)$ is defined as:

$$Z(t_d) = \sqrt{\frac{\pi}{4t_d}}\, e^{-(\frac{C}{t_d})^2}\left[erf[\frac{(A - A')}{A\sqrt{t_d}}] + erf[\frac{A'}{A\sqrt{t_d}}]\right] \left[1 + 2\sum_{n=1}^{\infty} e^{-\frac{n^2\pi^2 L^2 \beta_z t_d}{4h^2}} \cos(\frac{n\pi b}{h})\cos(\frac{n\pi z}{h})\right] \tag{4.2.23}$$

where $\beta_z = k_z/k_\alpha$

Solution (4.2.22) can be used in evaluation of pressure at any point (x, y, z) as long as the parameters A, A' and C in equation (4.2.18) are used. This solution can also be used to determine reservoir parameters by test data from an observation well (point).

For the pumping well, if we use the point (x_w, y_w, b) from the wellbore with :

$$\begin{aligned} x_w &= \delta L\cos(\alpha) + r_b\sin(\alpha) \\ y_w &= \delta L\sin(\alpha) - r_b\cos(\alpha) \end{aligned} \tag{4.2.24}$$

where r_b is the permeability weighted equivalent radius which considers the effect of the anisotropic permeability and takes the form [Goode et al., 1987]:

$$r_b = \frac{r_w}{2}\left[\left(\frac{k_x k_y}{k_z k_\alpha}\right)^{\frac{1}{4}} + \left(\frac{k_z k_\alpha}{k_x k_y}\right)^{\frac{1}{4}}\right] \qquad (4.2.25)$$

then the geometrical parameters A' and C can be approximately written:

$$A' = \delta A + \frac{(k_y - k_x) r_b \sin(2\alpha)}{2AL} \approx \delta A \qquad C = \frac{r_b^2}{L^2 A^4 k_x k_y} = \frac{r_b^2}{L^2 \beta_h^2} \qquad (4.2.26)$$

where $\beta_h = k_h/k_\alpha$ and δ is the location parameter which can take a value between 0.75-0.886 [Muskat, 1937; Goode et al., 1987].

Substituting A and A' into $Z(t_d)$, equation (4.2.23) becomes:

$$Z(t_d) = \sqrt{\frac{\pi}{4t_d}}\, e^{-\left[\frac{r_b^2}{L^2\beta_h^2 t_d}\right]}\left[erf\left[\frac{(1-\delta)}{\sqrt{t_d}}\right] + erf\left[\frac{\delta}{\sqrt{t_d}}\right]\right] \left[1 + 2\sum_{n=1}^{\infty} e^{-\frac{n^2\pi^2 L^2 \beta_h t_d}{4h^2}} \cos^2\left(\frac{n\pi b}{h}\right)\right] \qquad (4.2.27)$$

The solution expressed in equations (4.2.22) with (4.2.27) and its derivative are usually used in well test interpretation if the integrated method (curve matching) method is used. Figures 4.3 and 4.4 show the type curves and their derivatives generated by this solution. The parameter HV in the figures is the flow criterion from which the flow pattern can be determined, and this will be discussed in section 4.4.4

The skin term for a horizontal well can be obtained by analogy to a vertical well, and can be added to the pressure drawdown term as:

$$\Delta p = \frac{\mu Q}{4\pi h k_h}\left[P_d + \frac{2h}{L}\sqrt{\frac{k_\alpha}{k_z}}\, S\right] \qquad (4.2.28)$$

where S can be written as (see the average permeability expression in the segmentation approximation

section later in this Chapter):

$$S = \left[\frac{1}{k_a}\sqrt{\frac{k_x k_y k_z}{k_\alpha}} - 1\right]\ln\left(\frac{r_a}{r_w}\right) \qquad (4.2.29)$$

where k_a is the skin permeability in the skin zone from r_w to r_a around the well. The pseudoskin term can also be added into (4.2.28) if it needs to be considered [Goode et al., 1987].

4.2.2 Type curves and curve matching method

The dimensionless solution given by (4.2.22) and (4.2.27) is the type curve generator in estimating reservoir parameters by the integrated method (curving matching) method. Generally, two parameters must be provided to generate the horizontal well test type curves, one to describe the horizontal anisotropy (β_h) and the other to describe the vertical anisotropy (β_z). However, multi-parameter matching usually is difficult and time consuming because many parameters need to be altered during simulation in order to find a good match. One of the advantages of the solution given in (4.2.27) is that only one parameter β_z is significant in type curve generation, because the horizontal anisotropic characteristics are separated from the solution to the dimensionless variables P_d and t_d. The appearance of β_h in the exponential term can be added into the permeability weighted well radius r_b, which does not have much effect on the results except at a very short early time period. The main effect caused by horizontal anisotropy in this solution is represented in the definition of dimensionless pressure P_d and time t_d.

Therefore, the type curves generated with different β_z values such as those shown in Figure 4.3 and the derivative curves in Figure 4.4 can be used to estimate reservoir parameters by log-log curve matching.

If a matching point (P_d^m, t_d^m, Δp^m, t^m, β_z^m) has been determined for a horizontal well test data, then the parameters can be determined by the following equations:

$$k_\alpha = \frac{L^2 c_m \phi \mu t_d^m}{4t^m} \quad k_z = \beta_z^m k_\alpha \quad k_h = \frac{\mu Q P_d^m}{4\pi h \Delta p^m} \qquad (4.2.30)$$

The dimensionless pressure P_d defined in (4.2.21) is only related to the horizontal average permeability k_h and therefore, at late times of a test, the effect of β_z will become insignificant. This is evident as all type curves with different β_z fall into a curve single or very closely spaced ones. This can be helpful in curve matching if a test curve can not be matched uniquely to the type curves in the early separated sections. Obviously, this characteristic is only available when the horizontal radial flow regime is present. However, if the horizontal radial flow regime is not present, a modified dimensionless pressure P_{dv} can produce type curves which are independent of β_z in the early time vertical radial flow regime.

In fact, the type curves in the vertical radial flow regime will be independent of β_z if the new dimensionless pressure (P_{dv}) and the type curve generator $Z_v(t_d)$ are redefined as:

$$P_{dv} = P_d\sqrt{\beta_z} = \frac{4\pi h\Delta p}{\mu Q}\sqrt{\frac{k_x k_y k_z}{k_\alpha}}, \qquad Z_v(t_d) = \sqrt{\beta_z}\, Z(t_d) \tag{4.2.31}$$

Because P_{dv} is related to the three dimensional average permeability, which is characterized by the early vertical radial flow regime, the type generator $Z_v(t_d)$ is therefore independent of β_z at early times. Figures 4.5 and 4.6 show the type curves and their derivative generated by $Z_v(t_d)$.

If a matching point (P_{dv}^m, t_d^m, Δp^m, t^m, β_h^m) has been obtained, either from the type curve matching or from the derivative curve matching, then the parameters can be obtained by the following:

$$k_\alpha = \frac{L^2 c_m \phi \mu t_d^m}{4t^m}, \quad k_h = \sqrt{k_x k_y} = \beta_h^m k_\alpha, \quad k_z = \frac{\mu Q P_{dv}^m}{4\pi h\Delta p^m}\frac{k_\alpha}{k_x k_y} \tag{4.2.32}$$

Ambiguity has often been one of the difficulties encountered in the curve matching method. This problem exists because the test data are often contaminated (affected by other unexpected processes such as flow rate fluctuation, electricity voltage variation and so on). The direct effect of contaminated test data is that it becomes difficult to identify (match) to a unique type curve in the main flow regime. This difficulty can be partially eased by using the sectional curve match methods discussed above.

Another advantage of solution (4.2.27) we want to highlight is that the well length effect time t_{dw} is a constant $1/\pi$. Therefore, by determining the value of the well length effect time t_w from a well test which matches to a unique type curve can help to determine the parameters included in the definition of t_w such as well directional permeability k_α, formation compressibility c_m and porosity.

4.2.3 Characteristic times for a horizontal well test

It has been noted that three flow regimes can be recognized from a complete horizontal well test if wellbore storage is neglected. However, the criteria for identification of these regimes differ in the literature [Daviau et al., 1988; Goode et al., 1987; 1988; Mattar and Santo, 1995]. Because flow regime identification is an essential part of segmental analysis, we would like to first discuss some aspects of these criteria.

The logarithmic derivative of P_d ($dP_d/d(\log(t_d))$) in equation (4.2.22) is $Z(t_d)*t_d$. If wellbore storage is neglected, $Z(t_d)$ is composed of three parts: the exponential term, the error function term, and the series term. The square root term of t_d will be combined into one of the above three parts in different times to generate the required result. The exponential term is similar to the expression for a vertical well and accounts for the pressure drop with radial flow toward a well. The error function term accounts for the well length and orientation effects in the horizontal plane. The series term accounts for the effect of the upper and lower no-flow boundaries.

Two important time criteria are needed in the identification of flow regimes; the effect of the no-flow boundary time t_b, and the effect of well length time t_w. Therefore, based on t_b and t_w, three flow regimes can be recognized. The early time vertical radial flow regime is maintained when $t < min(t_b, t_w)$ and the horizontal radial flow regime is maintained when $t > max(t_b, t_w)$. Between t_b and t_w, the middle transitional flow regime develops.

In the vertical flow regime, the exponential term is dominant; it varies exponentially at very early times and becomes a constant when C/t_d becomes greater than 0.01 [Muskat, 1937]. In the following discussion, we always assume this criterion is satisfied. In fact, because $y\cos(\alpha) - x\sin(\alpha)$ is the distance from the observation point to the well, which is usually very small compared to the well length L, this criterion is usually satisfied at relatively early times. Before the well length (error function term) takes effect, the derivative of P_d is dominated only by the series term.

If we define the series term $f(\beta_z*t_d)$ as:

$$f(\beta_z * t_d) = 1 + 2\sum_{n=1}^{\infty} e^{-\frac{n^2\pi^2 L^2 \beta_z t_d}{4h^2}} \cos\left(\frac{n\pi b}{h}\right)\cos\left(\frac{n\pi z}{h}\right) \tag{4.2.33}$$

then we find that $f(\beta_z * t_d)$ gives a value of unity for large t_d. For small t_d, $f(\beta_z * t_d)$ varies linearly with the square root of $\beta_z * t_d$, which can be expressed as:

$$f(\beta_z * t_d) = \frac{h}{L\sqrt{\pi t_d \beta_z}}\, g(\beta_z * t_d)$$
$$g(\beta_z * t_d) = \sum_{n=-\infty}^{\infty}\left[e^{-\frac{(b-z+2nh)^2}{L^2\beta_z t_d}} + e^{-\frac{(b+z+2nh)^2}{L^2\beta_z t_d}}\right] \tag{4.2.34}$$

where $g(\beta_z * t_d)$ gives a value of unity for small t_d.

If we assume that the well is located in the middle of the reservoir, i.e. b = h/2, then we find there exists a unique point below which $g(\beta_z * t_d)$ becomes unity, and above which $f(\beta_z * t_d)$ becomes unity (Figure 4.7). Because the no-flow boundaries effect is only dependent on the series term, this point clearly defines the no-flow boundary effects, and therefore gives t_b as:

$$t_{db} = \frac{k_a}{\pi k_z}\left(\frac{h}{L}\right)^2 \tag{4.2.35}$$

The effect of the well length, on the other hand, can be obtained by applying t_{db} to equation (4.2.59) by noting the fact that the slope of the linear flow straight line of the logarithmic derivative is 0.5 in a log-log graph. It is easy to show that t_{dw} has the following value:

$$t_{dw} = \frac{1}{\pi} \tag{4.2.36}$$

However, we should be aware that the effect of well length is a more complicated and lengthy process, and takes a time of about one half to 2 cycles of logarithmic time. The t_{dw} obtained above is approximately in the middle of this process. By evaluating the error function term in equation (4.2.27), we find that the error caused by segmentation approximation becomes only non-negligible (relative

error larger than 0.1%) when t_d is in the range of (Appendix 4.1):

$$\frac{0.1A^2}{\pi} < t_d < \frac{10A^2}{\pi} \tag{4.2.37}$$

therefore error corrections are necessary in the segmentation approximation in this range around t_{dw}.

In the derivative graph, t_{db} is the intersection point between the early vertical flow horizontal line and the middle transitional straight line (linear or spherical flow, see the discussion below), and t_{dw} is the intersection between the middle transitional straight line and the late time horizontal radial flow line (Figure 4.4).

If we write the error function term of $Z(t_d)$ in equation (4.2.27) as $e(t_d)$:

$$e(t_d) = \sqrt{\frac{\pi}{4t_d}}\left[erf[\frac{A-A'}{A\sqrt{t_d}}] + erf[\frac{A'}{A\sqrt{t_d}}]\right] \tag{4.2.38}$$

then, based on the derivation of t_{db} and t_{dw}, we are led to the following approximate expressions for the terms contained in $Z(t_d)$:

$$f(\beta_z^* t_d) = 1 \quad t_d > t_{db} \qquad f(\beta_z^* t_d) = \frac{h}{L}\sqrt{\frac{k_a}{\pi k_z t_d}} \quad t_d < t_{db} \tag{4.2.39}$$

$$e(t_d) = \frac{1}{t_d} \quad t_d > t_{dw} \qquad e(t_d) = \sqrt{\frac{\pi}{t_d}} \quad t_d < t_{dw} \tag{4.2.40}$$

Therefore, $Z(t_d)$ can be simplified as follows when $t_d > 100C$:

$$Z(t_d) = \frac{1}{t_d}\frac{h}{L}\sqrt{\frac{k_a}{k_z}} = \frac{1}{t_d}\sqrt{\frac{t_{db}}{t_{dw}}} \quad (t_d < t_{db} < t_{dw}) \tag{4.2.41}$$

and

$$Z(t_d) = \sqrt{\frac{\pi}{t_d}} = \sqrt{\frac{1}{t_{dw} t_d}} \quad (t_{db} < t_d < t_{dw}) \tag{4.2.42}$$

$$Z(t_d) = \frac{h}{L}\sqrt{\frac{k_a}{\pi k_z t_d^3}} = \sqrt{\frac{t_{db}}{t_d^3}} \quad (t_{dw} < t_d < t_{db}) \tag{4.2.43}$$

$$Z(t_d) = \frac{1}{t_d} \quad (t_d > t_{dw} > t_{db}) \tag{4.2.44}$$

The segmentation solutions discussed below will be based on these relationships.

We have neglected the effect of wellbore storage in the discussion. Wellbore storage usually masks parts or all of one or more flow regimes. If the criteria time t_b or t_w are masked by the storage effect, it then becomes impossible to identify flow regimes from a derivative graph. The wellbore storage effect will be analyzed and discussed in Chapter 5.

4.2.4 Flow regimes and segmentation

4.2.4.1 Solutions in forms of dimensionless variables

Segmental approximation provides a convenient approach to well test interpretation. The approximate solutions derived by Goode [Goode et al., 1987] do not use the characteristic times t_b and t_w, and therefore are more complicated than the solutions we derive in the following. It is also difficult to obtain the geometric skin from Goode's solution if the vertical radial flow regime is masked [Domzalski and Yuer, 1992].

We will try to eliminate those requirements by integrating $Z(t_d)$ with each individual flow regime, based on t_{db} and t_{dw} values discussed above. Two situations can arise: either $t_{db} < t_{dw}$ or $t_{db} > t_{dw}$. If $t_{db} < t_{dw}$, which occurs if $L^2/h^2 > k_z/k_a$ (see equation (4.2.59) in the following), the common Vertical-Linear-Horizontal flow pattern (VLH) is generated. If $t_{db} > t_{dw}$, which occurs if $L^2/h^2 < k_z/k_a$, the

Vertical-Spherical-Horizontal flow pattern (VSH) is generated. We give the segmentation solutions for both patterns.

The Vertical-Linear-Horizontal flow pattern

The vertical radial flow regime in the VLH flow pattern is maintained when $t_d < t_{db}$, and if $t_d > 100C$. Solution (4.2.22) then can be approximately expressed as:

$$P_d = \sqrt{\frac{t_{db}}{t_{dw}}}\left[\ln\left(\frac{t_d}{C}\right) - \gamma\right] \qquad (4.2.45)$$

where $\gamma = 0.5772$.

The linear flow regime is observed when $t_{db} < t_d < t_{dw}$. The solution for P_d and Δp in this regime can be obtained by integrating equation (4.2.22) using the time criterion t_{db}:

$$P_d = 2\sqrt{\frac{t_d}{t_{dw}}} + \sqrt{\frac{t_{db}}{t_{dw}}}\left[\ln\left(\frac{t_{db}}{C}\right) - (\gamma+2)\right] \qquad (4.2.46)$$

When t_d becomes greater then t_{dw}, the horizontal radial flow regime starts, and P_d in this regime is approximated as:

$$P_d = \ln\left(\frac{t_d}{t_{dw}}\right) + 2 + E_f + \sqrt{\frac{t_{db}}{t_{dw}}}\left[\ln\left(\frac{t_{db}}{C}\right) - (\gamma+2)\right] \qquad (4.2.47)$$

where $E_f = -0.93$ is the error correction term for VLH flow pattern caused by the approximation of t_w (Appendix 4.1).

The Vertical-Spherical-Horizontal flow pattern

If $t_{db} > t_{dw}$, which occurs if $L^2/h^2 < k_r/k_z$ (see equation (4.2.59)), a Vertical-Spherical-Horizontal flow

pattern (VSH) will be generated. The vertical radial flow regime is maintained for $t_d < t_{dw}$, and solutions for $t_d > 100C$ are the same as in (4.2.45).

The spherical flow regime starts when $t_d = t_{dw}$ and ends when $t_d = t_{db}$. The pressure P_d in the spherical flow regime is:

$$P_d = -2\sqrt{\frac{t_{db}}{t_d}} + \sqrt{\frac{t_{db}}{t_{dw}}}\left[\ln\left(\frac{t_{dw}}{C}\right) - (\gamma - 2 - E_g)\right] \qquad (4.2.48)$$

and $E_g = -0.56$ is the VSH pattern error correction term caused by the approximation of t_{dw} (Appendix 4.1).

The horizontal flow regime starts when $t_d > t_{db}$, and the equations are:

$$P_d = \ln\left(\frac{t_d}{t_{db}}\right) - 2 + \sqrt{\frac{t_{db}}{t_{dw}}}\left[\ln\left(\frac{t_{dw}}{C}\right) - (\gamma - 2 - E_g)\right] \qquad (4.2.49)$$

4.2.4.2 Solutions in forms of oil field units(darcy, psi...)

If the dimensionless pressure P_d and time t_d are expressed in oil field units, they become:

$$P_d = \frac{h\sqrt{k_x k_y}}{70.6\mu BQ}\Delta p \qquad t_d = \frac{k_x t}{948 L^2 c_m \phi \mu} \qquad (4.2.50)$$

where B is the formation volume factor.

The boundary effect time t_b and well length effect time t_w therefore become:

$$t_b = \frac{301.75 h^2 c_m \phi \mu}{k_z} \qquad t_w = \frac{301.75 L^2 c_m \phi \mu}{k_a} \qquad (4.2.51)$$

The Vertical-Linear-Horizontal flow pattern

The segmentation solution of the VLH flow pattern for the vertical radial flow regime (4.2.45) becomes:

$$\Delta p = \frac{162.6\mu BQ}{h\sqrt{k_x k_y}}\sqrt{\frac{t_b}{t_w}}\left[\log_{10}\left(\frac{t}{t_b}\right) + 0.866\right] + F \qquad (4.2.52)$$

the linear flow solution (4.2.46) becomes:

$$\Delta p = \frac{141.2\mu BQ}{h\sqrt{k_x k_y}}\sqrt{\frac{t}{t_w}} + F \qquad (4.2.53)$$

and the horizontal radial flow solution (4.2.47) becomes:

$$\Delta p = \frac{162.6\mu BQ}{h\sqrt{k_x k_y}}\left[\log_{10}\left(\frac{t}{t_w}\right) + 0.463\right] + F \qquad (4.2.54)$$

where F is the VLH total skin term at $t = t_b$ which has the following form:

$$F = \frac{162.6B\mu Q}{h\sqrt{k_x k_y}}\sqrt{\frac{t_b}{t_w}}\left[\log_{10}\left(\frac{k_a t_b}{L^2 c_m \phi\mu C}\right) - 4.084 + 0.868S\right] \qquad (4.2.55)$$

The Vertical-Spherical-Horizontal flow pattern

For the VSH flow pattern we have the following form for the spherical flow regime solution (4.2.28)

$$\Delta p = -\frac{141.2\mu BQ}{h\sqrt{k_x k_y}}\sqrt{\frac{t_b}{t}} + G \qquad (4.2.56)$$

and the horizontal radial flow regime solution (4.2.49) :

$$\Delta p = \frac{162.6\mu BQ}{h\sqrt{k_x k_y}}\left[\log_{10}\left(\frac{t}{t_b}\right) - 0.866\right] + G \qquad (4.2.57)$$

where G is the total skin term for the VSH pattern, given by:

$$G = \frac{162.6\mu BQ}{h\sqrt{k_x k_y}}\sqrt{\frac{t_b}{t_w}}\left[\log_{10}\left(\frac{k_a t_w}{L^2 c_m \phi\mu C}\right) + 0.374 + 0.868S\right] \qquad (4.2.58)$$

Note that if we take the logarithmic derivative we find that all the coefficients of the solutions in dimensionless forms become 2.3, and in oil field terms become $162.6B\mu Q/k_h h$.

These solutions do not require calculation of the slope of a well test in interpretation, but employ some degree of approximation around well-length time t_w. Figure 4.8 shows the comparison between the segmentation approximations with the system solution. From this figure we find that satisfactory results are obtained from the segmentation solutions. However, non-negligible errors exist within the two logarithmic cycle area around t_w. If all the test data fall into this area, then the segmentation solutions derived in this thesis are not valid.

If we define the derivative ratio HV as the ratio between the horizontal radial flow derivative and the vertical radial flow derivative :

$$HV = \sqrt{\frac{t_w}{t_b}} = \frac{L}{h}\sqrt{\frac{k_z}{k_a}} \qquad (4.2.59)$$

then it becomes obvious that if HV > 1, the linear flow regime will be present and the larger HV, the longer is the period. If HV < 1, then the spherical flow regime will be present, and the smaller HV, the longer is the period. Finally, if HV = 1, neither linear nor spherical flow regimes will be present. In such situations, the vertical radial flow transfers to the horizontal radial flow directly and t_b becomes identical to t_w. It has therefore become clear that the derivative ratio is a measure of the duration of the transitional flow period. A small value of HV either means a small vertical permeability is encountered or the effective well length is reduced. If a small effective well length is encountered in a long horizontal well, this may mean that production is dominantly from the heel of the well. The

VLH flow pattern is the most often encountered in field and Figure 4.9 shows one such example of a horizontal well test from Mattar and Santo [1995]. However, we also frequently encounter the VSH flow pattern is the field tests. Figure 4.10 is one VSH flow pattern well test reported by Domzalski and Yuer [1992].

4.2.5 Well eccentricity effect

The boundary effect time t_b in (4.2.35) is obtained by assuming b = h/2. If the well is not located in the middle of the reservoir, two different time effects can sometimes be observed because of the effects of the two boundaries at different distances. From the derivative graph, this effect is indicated by two horizontal line sections in the vertical flow regime (Figure 4.11). The end of the first horizontal line section indicates that the first boundary (the one closest to the well) is taking effect, and the second section indicates that the second boundary is taking effect.

The time criterion for the first boundary effect can be obtained by substituting b for h (or h - b for h if b > h/2) in equation (4.2.35), which gives t_{dbl} and t_{bl} (in oil field units) :

$$t_{dbl} = \frac{4k_a}{\pi k_z}\left(\frac{b}{L}\right)^2 \qquad t_{bl} = \frac{1207 b^2 c_m \phi \mu}{k_z} \tag{4.2.60}$$

The time criterion for the second boundary effect is approximately four times larger than t_{db} i.e.:

$$t_{db2} = 4t_{db} = \frac{4k_a}{\pi k_z}\left(\frac{h}{L}\right)^2 \qquad t_{b2} = \frac{1207 h^2 c_m \phi \mu}{k_z} \tag{4.2.61}$$

This indicates that the effect time of the second impermeable boundary presented in a derivative graph is dependent only on the reservoir thickness, and the actual elevation of the well does not affect the value of t_{b2}. This conclusion may come from that fact that after the first boundary begins to take effect, the pressure propagation speed is doubled, which results in approximately the same t_b regardless of the actual location of the first boundary.

As indicated by Kuchuk et al. [1990], if a horizontal well is located much closer to one boundary than to the other, then a obvious two-line derivative could be obtained in the early vertical radial flow regime (Figure 4.11). If this is the case, then the derivative value of the second line section is twice as large as the one obtained by solution (4.2.45) and (4.2.56).

4.2.6 Observation Wells

Most of the approximate solutions discussed above are for the active pumping well. For observation wells the measuring point (x, y, z) considered in the parameters A' and C of equation (4.2.18) are different from the wellbore, and therefore can not be simplified to equation (4.2.26).

However, the boundary effect time t_b and well length effect time t_w are still the same as in equation (4.2.35) and (4.2.36) because their derivations are independent of the wellbore condition. From the analyses of the series term $f(\beta_z t_d)$ and error function term $e(t_d)$ in equation (4.2.33) and (4.2.38) we also find that the approximate solutions derived in section 4.2.4 are true for observation wells.

However, we note that the parameter C is proportional to the distance between the observation and the pumping well, therefore the criterion for $C/t_d < 0.01$ requires a longer time to satisfy then for the wellbore case. One effect of this criterion change is that the boundary effect time t_b may become un-observable from the derivative graph due to the masking effect.

Figure 4.12 shows observation results of a point with a distance of 3L/8 from one end of the well (origin) and at the height of z/b = 0.2. Because this observation point is close to the lower impermeable boundary, the boundary effect time t_b becomes difficult to identify.

Figure 4.13 also shows observation results of a point of 3L/8 from one end of the well (origin), but at the height of z/b = 0.8. Compared to the results of Figure 4.3.12, it is obvious that the boundary effect time t_b in this case is identifiable.

Both figures also indicate that the well length effect time t_w can be identified easily. However, if a more remote observation point is considered, the well length effect time also can be masked, and in such cases, both t_b and t_w can become difficult to identify.

4.3 Horizontal Well Buildup Test

4.3.1 Interpretation methods from the literature

Pressure buildup tests usually can provide more smooth and noise-free test data for evaluation of reservoir characteristics than pressure drawdown tests. However, some of the flow regimes presented in a drawdown test can be masked by the effect of buildup superposition. The superposition of the various flow regimes makes a horizontal buildup test much more difficult to interpret than a vertical well buildup test. The common superposition results for a horizontal well buildup test shows that the late time flow regimes are masked. If the early time flow regime is also serious masked by wellbore storage, then the test interpretation becomes almost impossible.

Analyses of horizontal well buildup tests in the literature are rare. Goode presented a set of segmentation solutions for a horizontal well buildup test [Goode, et al., 1987]. Those solutions requires that the shut-in time t_p be larger than the well length effect time t_{wf}, and, therefore that the effect of buildup superposition in early time can be neglected. Under this assumption, a buildup test usually can be considered as equivalent to a drawdown test for the recovery time periods $t < 0.1\ t_p$, and the interpretation using these periods becomes the same as for a drawdown test. However, if these periods appear insufficient for interpreting the test, such as when the early part is seriously masked by wellbore storage, the interpretation is unsuccessful.

Another problem in horizontal well buildup test interpretation is the identification of the test flow sequence pattern, as presented in section 4.2. A horizontal well test can be a Vertical-Linear-Horizontal sequence (VLH), or a Vertical-Spherical-Horizontal flow sequence (VSH) depending on the magnitude of the parameter HV. The logarithmic derivative of pressure recovery for the VSH sequence will decrease with increased recovery time t' in the spherical flow regime. This decrease can sometimes be difficult to distinguish from decreases caused by the buildup superposition.

An alternative approach would be to decompose the pressure superposition effect from the horizontal buildup test by restoring those flow regimes masked by the superposition effect, and obtain an equivalent drawdown derivative curve. If this buildup restoration is successful, then the interpretation of a buildup test for late time periods becomes identical to that of a drawdown test.

Unfortunately, an accurate restoration equation for the masked horizontal buildup test periods is very unlikely because of the complicated effect of various flow regimes. Instead, we want to develop an approximate method in this section to restore the flow regimes masked by the buildup superposition, and hope that the restoration can make the interpretation of a horizontal buildup test more practical and reliable.

4.3.2 Pressure buildup test analysis

4.3.2.1 Buildup test model

A transient well pressure solution for a horizontal well test with variable flow rate was obtained in dimensionless variables in section 4.2 , with the following form

$$P_d = \int_0^{t_d} \frac{Q_{sf}(t_d - \tau)}{Q} Z(\tau) d\tau \qquad (4.3.1)$$

where $Z(t_d)$ is expressed as:

$$Z(t_d) = \sqrt{\frac{\pi}{4t_d}} e^{-(\frac{c}{t_d})} \left[erf[\frac{(1-\delta)}{\sqrt{t_d}}] + erf[\frac{\delta}{\sqrt{t_d}}] \right] \left[1 + 2\sum_{1}^{\infty} e^{-\frac{n^2\pi^2 L^2 \beta_z t_d}{4h^2}} \cos^2(\frac{n\pi b}{h}) \right] \qquad (4.3.2)$$

For a horizontal well buildup test, if we assume that the pressure shut-in time is t_{dp} and neglect the wellbore storage effect , the bottom-hole flow rate can be written as (the wellbore storage effect is discussed in Chapter 5):

$$Q_{bh}(t_d) = \begin{bmatrix} Q - 0 & (t_d < t_{dp}) \\ Q - Q & (t_d \geq t_{dp}) \end{bmatrix} \qquad (4.3.3)$$

where $t_{dp} = 4k_\alpha t_p/(L^2 c_m \phi \mu)$, and under this condition, the bottom-hole flow rate Q_{bh} becomes identical to the well discharge Q, and therefore the dimensionless pressure P_d becomes :

$$P_d = \int_0^{t_{dp}+t_{d'}} Z(\tau) d\tau - \int_0^{t_{d'}} Z(\tau) d\tau \qquad (4.3.4)$$

where t_d' is the pressure buildup time.

If we define the dimensionless pressure recovery P_{dc} as $P_{dc} = P_{dp} - P_d$ where P_{dp} is the dimensionless pressure at shut-in time t_{dp} and P_d is the dimensionless pressure after recovery time t_d', then we obtain:

$$P_{dc} = \int_0^{t_d'} Z(\tau)d\tau - \left[\int_0^{t_{dp}+t_d'} Z(\tau)d\tau - \int_0^{t_{dp}} Z(\tau)d\tau\right] \tag{4.3.5}$$

the logarithmic derivative of P_{dc}, if expressed in field units $\Delta p'$, becomes:

$$\Delta p' = \frac{162.6B\mu Q}{h\sqrt{k_x k_y}} Z(t')t'[1 - \frac{Z(t+t')}{Z(t')}] = \frac{162.6\mu BQ}{h\sqrt{k_x k_y}} Z(t')t' R \tag{4.3.6}$$

where Z(t') is defined as in (4.3.2).

Equation (4.3.6) is composed of two terms. The first term Z(t')t' is equivalent to the derivative of a drawdown test, and the second term $R = 1 - Z(t_p + t')/Z(t')$ is the effect of the buildup superposition. We can call R the buildup reduction factor because the value of R is always less than 1, which therefore always reduces the derivative value of a buildup test if it is compared with a drawdown test. Obviously, the magnitude of the reduction factor will not only depend on the recovery time t_d', but most importantly, the buildup shut-in time t_p . If the magnitude of R is close to 1 then the derivative value as well as the flow regimes presented by the buildup test will be similar to those of a drawdown test. However, if $R << 1$, then the buildup test will be much different from the corresponding drawdown test. Because the value of R is usually close to 1 when t' is less than 10% of the shut-in time t_p, the flow regimes presented for early times are not affected significantly by the reduction factor, and therefore can usually be identified easily. On the other hand, if R decreases rapidly with increasing t_d' beyond the time point of $t' = t_p$, the flow regimes beyond this time will not be identifiable from the buildup test. Figure 4.14 shows an example using the buildup test reported by Sherrard et al., [1987].

To analyze the effect of the buildup reduction factor, we note that $t_p + t'$ is the only parameter which affects the value of R. In the following sections, we will give analysis for all the three possible cases for $t_p + t' > t_w$, $t_b < t_p + t' < t_w$, and $t_p + t' < t_b$ and obtain the corresponding segmentation solutions. Based on the segmentation solutions developed, an approximate method will be presented for restoration of the buildup flow

regimes masked by the buildup superposition.

4.3.2.2 The VLH complete - drawdown buildup test

The three flow regimes for a VLH flow sequence are: the early time vertical flow regime, the middle time linear flow regime and the late time horizontal radial flow regime. A complete drawdown-buildup test means that all three flow regimes were present before buildup shut-in, i.e. the shut-in time $t_p > t_w$. In a complete drawdown-buildup test, the derivative of P_{dc} at time $t_p + t'$ is $Z(t_p + t')t'$, which if expressed in field units, can be written as follows:

$$Z(t_p + t')t' = \frac{162.6\mu BQ}{h\sqrt{k_x k_y}} \frac{t'}{t_p + t'} \tag{4.3.7}$$

Therefore , the corresponding three segmentation solutions of the logarithmic derivatives can be obtained by obtaining the derivative of P_{dc} at time t', and then combining with equation (4.3.7), which leads to the following segmental solutions:

$$\Delta p_c' = \frac{162.6\mu BQ}{h\sqrt{k_x k_y}} \sqrt{\frac{t_b}{t_w}} \left[1 - \sqrt{\frac{t_w}{t_b}} \frac{t'}{t_p + t'} \right] \qquad t' < t_b \tag{4.3.8}$$

$$\Delta p_c' = \frac{162.6\mu BQ}{h\sqrt{k_x k_y}} \sqrt{\frac{t'}{t_w}} \left[1 - \frac{\sqrt{t_w t'}}{t_p + t'} \right] \qquad t_b < t' < t_w \tag{4.3.9}$$

$$\Delta p_c' = \frac{162.6\mu BQ}{h\sqrt{k_x k_y}} \left[1 - \frac{t'}{t_p + t'} \right] \qquad t' > t_w \tag{4.3.10}$$

Observe that the expressions of the buildup reduction factor R in the derivative equation (4.3.8) and (4.3.10) all decrease with increasing recovery time t', even though the reduction factors vary with different flow regimes. Numerical simulation shows that when the recovery time t' is less than 10% of the shut-in time t_p, the reduction factors in all three equations become very close to 1. The derivative of the buildup test for $t' < 0.1t_p$ is therefore similar to that of a drawdown test, and the flow regimes before this time can be identified in much the same way as a drawdown test. However, if the shut-in time t_p becomes larger than t_w, the reduction

factors will become smaller than 0.5, and will decrease further with increasing time t'. Flow regime characteristics beyond this point therefore will be significantly affected. To restore the flow regimes affected by these reduction factors, we write the horizontal radial flow reduction factor in equation (4.3.10) as :

$$R_h = 1 - \frac{t'}{t_p + t'} \tag{4.3.11}$$

We can obtain R_h modified derivatives by dividing the derivative solutions (4.3.8) - (4.3.10) by R_h . It becomes obvious that the R_h modified derivatives for the horizontal radial flow regime become identical to those of a drawdown test. On the other hand, the modification will also change the values of the derivatives in the vertical and linear flow regimes. However, based on the analysis above we may assume that this change will not significantly alter the flow regimes because both the reduction factors in the vertical and linear flow regimes will be close to 1, which is also true for R_h . The following inequalities in fact show that a consistent value slightly less than 1 is maintained for the R_h modifications.

For the VLH flow sequence, because $t_w > t_b$, if we carry out the division we find :

$$\left[1 - \sqrt{\frac{t_w}{t_b}} \frac{t'}{t_p + t'}\right] \div \left[1 - \frac{t'}{t_p + t'}\right] < 1 \qquad t' < t_b \tag{4.3.12}$$

and

$$\left[1 - \frac{\sqrt{t_w t'}}{t_p + t'}\right] \div \left[1 - \frac{t'}{t_p + t'}\right] < 1 \qquad t_b < t' < t_w \tag{4.3.13}$$

Equations (4.3.12) and (4.3.13) indicate that the R_h modified derivatives are always less than the equivalent drawdown test derivatives in the vertical and linear flow regimes. Therefore, the R_h modified derivatives (R_h curve) can be considered as the minimum derivative value of the equivalent drawdown in the vertical and linear flow regimes, and the identical equivalent drawdown derivative in the horizontal radial flow regime.

In the same way if we define the linear flow reduction factor R_l as:

$$R_I = 1 - \sqrt{\frac{t'}{t_p + t'}} \tag{4.3.14}$$

and obtain the R_I modifications by dividing R_I from equation (4.3.8) -(4.3.10), we have:

$$\left[1 - \sqrt{\frac{t_w t'}{t_b(t_p + t')}}\sqrt{\frac{t'}{t_p + t'}}\right] + \left[1 - \sqrt{\frac{t'}{t_p + t'}}\right] > 1 \qquad t' < t_b \tag{4.3.15}$$

$$\left[1 - \sqrt{\frac{t_w}{t_p + t'}}\sqrt{\frac{t'}{t_p + t'}}\right] + \left[1 - \sqrt{\frac{t'}{t_p + t'}}\right] > 1 \qquad t_b < t' < t_w \tag{4.3.16}$$

$$\left[1 - \frac{t'}{t_p + t'}\right] + \left[1 - \sqrt{\frac{t'}{t_p + t'}}\right] > 1 \qquad t' > t_w \tag{4.3.17}$$

which indicates that the R_I modified derivatives give the maximum derivative values of the equivalent drawdown in all three flow regimes. Clearly, if we can find some way to interpolate the equivalent derivative from the two modified derivative curves, the buildup test interpretation will become identical to a drawdown test interpretation. Because the two modified derivative curves are very close in the vertical and linear flow regimes as discussed above, a visual interpolation is often sufficient. Figure 4.15 shows such a simulated example for the case of $t_p > t_w$. From this figure we can see that the middle pattern between the two modified derivative curves give a good approximation for the vertical and linear flow regimes. The symbols (circles) are true drawdown derivatives which coincide with the R_h modified derivative in the horizontal radial flow regime. The B curve is the simulated buildup derivative curve.

4.3.2.3 The VLH non complete - drawdown buildup test

If the shut-in time t_p is less than the well length effect time t_w then a non-complete drawdown-buildup test is obtained. Two cases can be present in a non-complete drawdown-buildup test; $t_b < t_p + t' < t_w$ and $t_p + t' < t_b$.

In the first case, when $t_b < t_p + t' < t_w$, the superposition derivative becomes:

$$Z(t_p + t')t' = \frac{162.6\mu BQ}{h\sqrt{k_x k_y}} \frac{1}{\sqrt{t_w}} \frac{t'}{\sqrt{t_p + t'}} \tag{4.3.18}$$

Two segmentation solutions can be generated under this condition : $t' < t_b$ and $t_b < t' < t_w$:

$$\Delta p' = \frac{162.6\mu BQ}{h\sqrt{k_x k_y}} \sqrt{\frac{t_b}{t_w}} \left[1 - \frac{1}{\sqrt{t_b}} \frac{t'}{\sqrt{t_p + t'}} \right] \qquad t' < t_b \tag{4.3.19}$$

$$\Delta p_{c'} = \frac{162.6\mu BQ}{h\sqrt{k_x k_y}} \sqrt{\frac{t'}{t_w}} \left[1 - \sqrt{\frac{t'}{t_p + t'}} \right] \qquad t_b < t' < t_w \tag{4.3.20}$$

If we generate the R_h and R_l modifications to the derivatives of equations (4.3.19) and (4.3.20), we obtain the following inequalities for their reduction factors:

For the R_h modification:

$$\left[1 - \sqrt{\frac{t_p + t'}{t_b}} \frac{t'}{t_p + t'} \right] + \left[1 - \frac{t'}{t_p + t'} \right] < 1 \qquad t' < t_b \tag{4.3.21}$$

$$\left[1 - \sqrt{\frac{t'}{t_p + t'}} \right] + \left[1 - \frac{t'}{t_p + t'} \right] < 1 \qquad t_b < t' < t_w \tag{4.3.22}$$

and for the R_l modification:

$$\left[1 - \sqrt{\frac{t'}{t_b}} \sqrt{\frac{t'}{t_p + t'}} \right] + \left[1 - \sqrt{\frac{t'}{t_p + t'}} \right] > 1 \qquad t' < t_b \tag{4.3.23}$$

$$\left[1 - \sqrt{\frac{t'}{t_p + t'}} \right] + \left[1 - \sqrt{\frac{t'}{t_p + t'}} \right] = 1 \qquad t_b < t' < t_w \tag{4.3.24}$$

The inequalities of (4.3.21) - (4.3.24) indicate that the R_h modified derivatives also generate the minimum value of the equivalent drawdown in both flow regimes in the non-complete drawdown situation. The R_l modified derivatives generate a maximum equivalent derivative curve in the vertical flow regime, and an

identical equivalent drawdown in the linear flow regime. This also confirms the early definition of R_l, the linear flow reduction factor. For the same reason as in the complete drawdown test situation, both R_h and R_l modified derivative curves should be close to the equivalent drawdown in the early time vertical flow regime, therefore the identification of flow regimes from the two modified curves becomes the same as in the complete drawdown-buildup test discussed above. Figure 4.16 and 4.17 show such simulated examples for the case of $t_b < t_p < t_w$.

In the second case where $t_p + t' < t_b$, the superposition term becomes:

$$Z(t_p + t')t' = \frac{162.6\mu BQ}{h\sqrt{k_x k_y}}\sqrt{\frac{t_b}{t_w}}\frac{t'}{t_p + t'} \qquad (4.3.25)$$

There is only one possible segmentation solution for this case : $t' < t_b$. The buildup derivative for this case is :

$$\Delta p_c' = \frac{162.6\mu BQ}{h\sqrt{k_x k_y}}\sqrt{\frac{t_b}{t_w}}\left[1 - \frac{t'}{t_p + t'}\right] \qquad (4.3.26)$$

Obviously, the R_h modified derivative for solution (4.26) also gives the identical derivative to the equivalent drawdown test, and the R_l modified derivative curve gives its maximum value. This indicates that the drawdown derivative can be interpolated uniquely under any superposition effect, and this guarantees the applicability of the R_h - R_l method. Figure 4.18 shows a simulated example for the case of $t_p < t_b$. From this figure we can see good approximations of the R_h - R_l modification curves in various flow regimes, compared with the true drawdown derivative curve (symbols).

The R_h and R_l modified derivatives provide an approximate means to restore the masked buildup derivatives by the buildup reduction factors. In summary, if R_a stands for the average derivative between R_h and R_l (interpolated somehow between them), the following is the recommended procedures in interpreting a horizontal buildup test using the R_h and R_l method:

1. Plot the logarithmic derivative of a buildup test on a log-log graph.
2. Calculate and plot the R_h and R_l curves by dividing the reduction factors R_h and R_l from the derivative

data.

3. From the three derivative curves, estimate t_b and t_w and compare them with the shut-in time t_p.
4. If $t_p < t_b$: the equivalent drawdown derivative curve should be R_h - R_l - R_h
5. If $t_b < t_p < t_w$: the equivalent drawdown derivative curve should be R_s - R_l - R_h
6. If $t_p > t_w$: the equivalent drawdown derivative curve should be R_s - R_s - R_h .

4.3.2.4 Solutions for the VSH flow sequence

The boundary effect time t_b in the Vertical-Spherical-Horizontal (VSH) flow sequence becomes greater then the well length effect time t_w. Therefore, the order of the three flow regimes in the VSH sequence becomes : the early time vertical radial flow regime when $t' < t_w$, the middle transient spherical flow regime when $t_w < t' < t_b$ and, the late time horizontal radial flow regime when $t' > t_b$. The segmentation derivative of the pressure recovery can also be obtained from equation (4.3.5).

First let us consider the case when $t_p + t' > t_b$ which means that a complete drawdown-buildup test is obtained. The superposition term $Z(t_p + t')t'$ in such a situation is exactly the same as in equation (4.3.7) for the VLH sequence, which gives:

$$Z(t_p + t')t' = \frac{162.6\mu BQ}{h\sqrt{k_x k_y}} \frac{t'}{t_p + t'} \tag{4.3.27}$$

And the segmentation derivatives for the three flow regimes are :

$$\Delta p_c' = \frac{162.6\mu BQ}{h\sqrt{k_x k_y}} \sqrt{\frac{t_b}{t_w}} \left[1 - \sqrt{\frac{t_w}{t_b}} \frac{t'}{t_p + t'}\right] \qquad t' < t_w \tag{4.3.28}$$

$$\Delta p_c = \frac{162.6\mu BQ}{h\sqrt{k_x k_y}} \sqrt{\frac{t_b}{t'}} [1 - \sqrt{\frac{t'}{t_b}} \frac{t'}{t_p + t'}] \qquad t_w < t' < t_b \tag{4.3.29}$$

$$\Delta p_c = \frac{162.6\mu BQ}{h\sqrt{k_x k_y}} \left[1 - \frac{t'}{t_p + t'}\right] \qquad t' > t_w \tag{4.3.30}$$

We still can use R_h defined in equation (4.3.11) as the horizontal radial flow buildup reduction factor because the derivative in this flow regime is the same as in the VLH sequence. However, the transient spherical flow buildup reduction factor R_s is different from R_l because of the differences between the two middle transient flow regimes. The spherical flow reduction factor has the following form:

$$R_s = 1 - \sqrt{\left[\frac{t'}{t_p + t'}\right]^3} \tag{4.3.31}$$

If we apply the R_h and R_s modifications to equations (4.3.28) - (4.3.30), the following inequalities are generated:

for the R_h modification we have:

$$\left[1 - \sqrt{\frac{t_w}{t_b}}\frac{t'}{t_p + t'}\right] + \left[1 - \frac{t'}{t_p + t'}\right] > 1 \qquad t' < t_w \tag{4.3.32}$$

$$\left[1 - \sqrt{\frac{t'}{t_b}}\frac{t'}{t_p + t'}\right] + \left[1 - \frac{t'}{t_p + t'}\right] > 1 \qquad t_w < t' < t_b \tag{4.3.33}$$

$$\left[1 - \frac{t}{t_p + t}\right] + \left[1 - \frac{t'}{t_p + t'}\right] = 1 \qquad t' > t_b \tag{4.3.34}$$

and for the R_s modification we have:

$$\left[1 - \sqrt{\frac{t_w}{t_b}}\frac{t'}{t_p + t'}\right] + \left[1 - \sqrt{\left[\frac{t'}{t_p + t'}\right]^3}\right] < 1 \qquad t' < t_w \tag{4.3.35}$$

$$\left[1-\sqrt{\frac{t_p+t'}{t_b}}\sqrt{[\frac{t'}{t_p+t'}]^3}\right]+\left[1-\sqrt{[\frac{t'}{t_p+t'}]^3}\right]<1 \qquad t_w < t' < t_b \qquad (4.3.36)$$

$$\left[1-\frac{t'}{t_p+t'}\right]+\left[1-\sqrt{[\frac{t'}{t_p+t'}]^3}\right] < 1 \qquad t' > t_b \qquad (4.3.37)$$

These inequalities indicate that the maximum and minimum derivatives conditions are also satisfied for the R_h - R_s modifications for VSH sequence. However, different from the VLH flow sequence, the R_h modified derivatives give the maximum derivative to the equivalent drawdown test instead of the minimum in the vertical and spherical flow regimes. But, similar to the VLH sequence, the modified curve becomes identical in the horizontal radial flow regime. The R_s modified derivatives, on the other hand, give the minimum values in all three flow regimes.

The non complete - drawdown buildup test of the VSH flow sequence can also be similarly obtained as follows:

If $t_w < t_p + t' < t_b$ then $Z(t_b + t')t'$ is:

$$Z(t_p+t')t' = \frac{162.6\mu BQ}{h\sqrt{k_x k_y}}\frac{\sqrt{t_b}\,t'}{\sqrt{(t_p+t')^3}} \qquad (4.3.38)$$

The two derivative segmentations for this case are:

$$\Delta p_c' = \frac{162.6\mu BQ}{h\sqrt{k_x k_y}}\sqrt{\frac{t_b}{t_w}}\left[1-\frac{\sqrt{t_w}t'}{\sqrt{(t_p+t')^3}}\right] \qquad t' < t_w \qquad (4.3.39)$$

$$\Delta p_c = \frac{162.6\mu BQ}{h\sqrt{k_x k_y}}\sqrt{\frac{t_b}{t'}}\left[1-\sqrt{[\frac{t'}{t_p+t'}]^3}\right] \qquad t_w < t' < t_b \qquad (4.3.40)$$

We obtain the following inequalities for the R_h and R_s modification of equation (4.3.39) and (4.3.40) :

for the R_h modification we have:

$$\left[1-\sqrt{\frac{t_w}{t_p+t'}\frac{t'}{t_p+t'}}\right]+\left[1-\frac{t'}{t_p+t'}\right] > 1 \qquad t' < t_w \qquad (4.3.41)$$

$$\left[1-\sqrt{\left[\frac{t'}{t_p+t'}\right]^3}\right]+\left[1-\frac{t'}{t_p+t'}\right] > 1 \qquad t_w < t' < t_b \qquad (4.3.42)$$

and for R_s modification we have:

$$\left[1-\sqrt{\frac{t_w}{t_p+t'}\frac{t'}{t_p+t'}}\right]+\left[1-\sqrt{\frac{t'}{t_p+t'}\frac{t'}{t_p+t'}}\right] < 1 \qquad t' < t_w \qquad (4.3.43)$$

$$\left[1-\sqrt{\left[\frac{t'}{t_p+t'}\right]^3}\right]+\left[1-\sqrt{\left[\frac{t'}{t_p+t'}\right]^3}\right] = 1 \qquad t_w < t' < t_b \qquad (4.3.44)$$

Equations (4.3.41) - (4.3.44) indicate that the R_h and R_s modification also possess the maximum and minimum derivative properties to the equivalent drawdown derivative. Besides, we find that the R_s modified derivative curve also generates the identical value to the equivalent drawdown derivative from equation (4.4.44) , as expected. Figure 4.19 shows the simulated example of a complete drawdown-buildup test for the VSH flow sequence and the modified derivatives compared with the true drawdown derivative.

For the case of $t_p + t' > t_b$, an identical derivative solution is obtained as equation (4.3.24) which means that the R_h modified derivative also gives identical values to the equivalent derivative, and that the R_s modified derivatives give the minimum value. Therefore, the same strategy can be used for the VSH sequence in buildup test interpretation. The following procedure is similar to the VLH sequence, and can be applied in a horizontal buildup test interpretation for the vertical - spherical - horizontal flow sequence:

1. Plot the logarithmic derivative of a buildup test on a log-log graph.
2. Calculate and plot the R_h and R_s curves by dividing the reduction factors R_h and R_s into the derivative data.
3. From the three derivative curves, estimate t_b and t_w and compare them with the shut-in time t_p.
4. If $t_p < t_b$: the equivalent drawdown derivative curve should be R_h - R_s - R_h
5. If $t_b < t_p < t_w$: the equivalent drawdown derivative curve should be R_a - R_s - R_h
6. If $t_p > t_w$: the equivalent drawdown derivative curve should be R_a - R_a - R_h .

TABLE 1 lists the various reduction factors in different flow regimes.

4.3.3 Field Examples of Buildup Test Interpretation

Example 1: Figure 4.20 shows the buildup test interpretation using the R_h - R_s modification method. This buildup test is a multi-rate test, but the discussion we presented above is only for a single rate test. However, for a multi-rate test, only some additional terms need to be added in the buildup superposition to account for the muti-rate effect.

If a multi-rate test with Q_1 at (t_0 - t_1), Q_2 at (t_1 - t_2)...., and Q_n at (t_{n-1} - ∞), then dimensionless pressure drop P_d becomes:

$$P_d = \sum_{i=1}^{n} \int_{0}^{t_d - t_{i-1}} (Q_i - Q_{i-1}) Z(\tau) d\tau \qquad (4.3.45)$$

where $t_0 = 0$ is the start time of the drawdown .

If the test is shut-in at time $t_p = t_{n-1}$, then $Q_n = 0$, and the buildup recovery pressure P_{dc} becomes:

$$P_{dc} = \int_{0}^{t_d} Q_{n-1} Z(\tau) d\tau - \sum_{i=1}^{n-1} \int_{0}^{t_d - t_{i-1} + t_d} (Q_i - Q_{i-1}) Z(\tau) d\tau - \int_{0}^{t_d - t_{i-1}} (Q_i - Q_{i-1}) Z(\tau) d\tau \qquad (4.3.46)$$

The logarithmic derivative of equation (4.3.36) becomes:

$$\Delta p' = Q_{n-1}Z(t')t'\left[1 - \frac{\sum_{i=1}^{n-1}[Q_i - Q_{i-1}]Z(t_p - t_{i-1} + t')}{Q_{n-1}Z(t')t'}\right] \quad (4.3.47)$$

Therefore, the only difference between the single rate and multi-rate tests is the reduction term. If we still apply the procedures discussed for the single rate test but use the reduction factor presented in solution (4.3.37), the multi-rate test can also be interpreted by the same method.

Figure 4.20 is the interpretation result using the reduction factor in (4.3.37). The three flow regimes identified by the R_h - R_s modification method are shown in the figure by the segmentation lines.

Example 2: Figure 4.21 shows the field buildup test reported by Mattar and Santo [1995]. The authors declared that the horizontal radial flow regime has just been reached at the end of the buildup. Obviously this conclusion is based on the horizontal trend of the buildup derivative at the end. However, after we calculated the R_h and R_l modified derivatives, it becomes clear that the horizontal trend of the buildup derivative curve does not give any information about the horizontal radial flow regime, but is the result of the effect of the buildup reduction.

Example 3: Figure 4.22 shows the buildup test example of figure 4.14 from Sherard et al., [1987]. The special characteristics of the test make the test interpretation difficult, particularly the flow pattern identifications, i.e the VLH or VSH. We applied all three modifications, R_h, R_l and R_s. All three modified curves show more or less the dual pattern property, but a VLH flow sequence seems more likely to be present. This is because, as discussed in the previous sections, the R_l modified derivative gives the maximum and the R_s modified derivative gives the minimum derivative in the vertical flow regime, and the R_h modified derivative gives the identical value in this regime. If we observe the position of all these three modifications, we may say that the HV = 1 case is present in this example, which means that the boundary effect time becomes identical to the well length effect time.

4.3.4 Discussions and Conclusion

We have discussed an approximate method in buildup test interpretation. This method can interpolate a drawdown equivalent derivative from the R_h - R_l (R_h - R_s for the VSH flow sequence) modifications of the

buildup derivative.

The R_h - R_l modification method can restore the altered flow regimes by the superposition effect . This method is more useful for buildup tests which have longer recovery times than drawdown times. This also implies the possibility that a short drawdown and longer buildup test can be used in reservoir characterization if the method discussed in this paper is used.

The method is developed based on the inequalities derived from the theoretical analysis of the segmentation solution for various flow regimes. Even though the drawdown equivalent derivative needs to be interpolated from the two modified derivatives, both simulation and field examples indicate that the difference between them is small and can be interpolated visually with good accuracy.

Table 1 Reduction factors in the pressure derivatives

VLH VSH	$\frac{162.6\mu BQ}{h\sqrt{k_x k_y}}\sqrt{\frac{t_b}{t_w}}\left[1-\frac{t'}{t_p+t'}\right]$ same		
VLH	$\frac{162.6\mu BQ}{h\sqrt{k_x k_y}}\sqrt{\frac{t_b}{t_w}}\left[1-\frac{1}{\sqrt{t_b}}\frac{t'}{\sqrt{t_p+t'}}\right]$	$\frac{162.6\mu BQ}{h\sqrt{k_x k_y}}\sqrt{\frac{t'}{t_w}}\left[1-\sqrt{\frac{t'}{t_p+t'}}\right]$	
VSH	$\frac{162.6\mu BQ}{h\sqrt{k_x k_y}}\sqrt{\frac{t_b}{t_w}}\left[1-\frac{t'\sqrt{t_w}}{\sqrt{(t_p+t')^3}}\right]$	$\frac{162.6\mu BQ}{h\sqrt{k_x k_y}}\sqrt{\frac{t_b}{t'}}\left[1-\sqrt{(\frac{t'}{t_p+t'})^3}\right]$	
VLH	$\frac{162.6\mu BQ}{h\sqrt{k_x k_y}}\sqrt{\frac{t_b}{t_w}}\left[1-\sqrt{\frac{t_{dw}}{t_{db}}}\frac{t'}{t_p+t'}\right]$	$\frac{162.6\mu BQ}{h\sqrt{k_x k_y}}\sqrt{\frac{t'}{t_w}}\left[1-\frac{\sqrt{t_w t'}}{t_p+t'}\right]$	$\frac{162.6\mu BQ}{h\sqrt{k_x k_y}}\left[1-\frac{t'}{t_p+t'}\right]$
VSH	same	$\frac{162.6\mu BQ}{h\sqrt{k_x k_y}}\sqrt{\frac{t_b}{t'}}\left[1-\sqrt{\frac{t'}{t_b}}\frac{t'}{t_p+t'}\right]$	same

4.4 Reservoir Anisotropy Determination

4.4.1 Anisotropic permeability ellipse and ellipsoid

Segmentation solutions developed in the drawdown and buildup test sections have often been used in well test interpretation. However, if we substitute t_b and t_w of equation (4.2.51) into these solutions, it becomes apparent that, except for the horizontal radial flow regime (equation (4.2.54) and (4.3.57)) where the horizontal average permeability $k_h = \sqrt{k_x k_y}$ is obtained , the permeability determined by other regimes is orientation-dependent. For example, the permeability determined from the vertical radial flow regime is $\sqrt{k_\alpha / k_x k_y k_z}$ and from the transient flow regime (linear or spherical) is $\sqrt{k_\alpha / k_x k_y}$.

If all flow regimes are clearly identifiable in a test, then the permeabilities we can determine are well direction permeability k_α, the vertical permeability k_z and the horizontal average permeability k_h, but the true anisotropy of the reservoir can not be uniquely determined.

To determine the principal permeabilities and their directions, the permeability ellipse in the horizontal plane must be determined. From Figure 4.2 we find that there are four possible directions in which the permeability has the same magnitude. If two directional permeabilities k_1 and k_2 have been determined from two horizontal wells in different location but separated by an angle of β degrees measured counter-clockwise from k_1 to k_2, then the permeability ellipse can be uniquely determined. Therefore, two well test data sets from two differently orientated wells are required in order to determine the permeability ellipse. Several methods can be used in determining the permeability ellipse, and we will discuss two of them in the following section.

4.4.2 A graphical method in anisotropy determination

If we rewrite the equation of directional permeability (4.2.19) in the following form :

$$\frac{k_h^2}{k_\alpha} = \frac{1}{2}(k_x + k_y) - \frac{1}{2}(k_x - k_y)\cos(2\alpha) \qquad (4.4.1)$$

and define variables $P_m = (k_x + k_y)/2$, $Q_m = (k_x - k_y)/2$ and the modified permeability $k_m = k_h^2/k_\alpha$ then equation (4.4.1) becomes:

$$\begin{aligned} k_m &= P_m - Q_m \cos(2\alpha) \\ P_m^2 - Q_m^2 &= k_h^2 \end{aligned} \qquad (4.4.2)$$

Two circles can be generated from the two equations in (4.4.2), the k_h circle and the k_m circle. The k_h circle is a circle centred at (0, 0) and with radius k_h. The k_m circle is centred at (P_m, 0) with radius Q_m (Figure 4.23). Two important properties can be generated from these two circles:

1) The centre of the k_m circle is outside of the k_h circle i.e. $P >= k_h$;
2) The two circles have at least one intersection i.e $P <= Q + k_h$.

Both properties can be proved from the second equation of (4.4.2).

The modified directional permeability k_m in any direction α can be determined by finding the point on the k_m circle which forms $2\alpha + \pi$ degrees from the k_x point, which is the right intersection of k_m circle with the k_m axis (Figure 4.23).

If two directional modified permeabilities k_{m1} and k_{m2} are known, then the k_m circle must satisfy the following conditions:

1) The angle from k_{m1} to k_{m2} is 2β;
2) At least one of the k_m circle radial lines is tangential to the k_h circle.

In order to determine these two properties, a measuring tool such as a compass net is required. The net should be composed of concentric circles which can be used to identify the k_m circle, and radial lines which can be used to find the tangential line to the k_h circle. At the same time, it must permit one to measure the angles between the two modified permeability points. Figure 4.24 shows an example of such a net.

To determine the permeability ellipse by using the net of Figure 4.24, the following steps are recommended:

1 Obtain the two directional and horizontal average permeabilities $k_{\alpha 1}$, $k_{\alpha 2}$ and k_h from two well tests in different azimuths using curve matching or segmental methods. Transform $k_{\alpha 1}$ and $k_{\alpha 2}$ into the modified permeability k_{m1} and k_{m2} by the following relationships:

$$k_{m1} = \frac{k_h^2}{k_{\alpha 1}} \qquad k_{m2} = \frac{k_h^2}{k_{\alpha 2}} \tag{4.4.3}$$

and write down the orientation angle β measured from $k_{\alpha 1}$ to $k_{\alpha 2}$.

2 Draw the k_h circle with its centre at (0,0) and radius k_h on a transparency. Make the positive k_m axis 3-4 times longer than k_h.

3 Mark out k_{m1} and k_{m2} on the k_m-axis and draw vertical lines through these two points.

4 Put the paper on top of the compass net (Figure 4.24) and, move the transparency horizontally with the k_m axis coinciding with the 0°-180° line of the net.

5 The k_m circle is the one which intersects the k_h circle and the two vertical lines of k_{m1} and k_{m2}. The azimuth angle between the two intersection of k_m circle with k_{m1} and k_{m2} is 2β.

6 Now, k_x and k_y can be measured directly from the graph. We also can obtain the P_m and Q_m values from the graph and the primary permeability k_x is $P_m + Q_m$ and k_y is $P_m - Q_m$. The angle measured from k_x to k_{m1} is $2\alpha + \pi$, where α is the direction of k_1 measured from the k_x direction.

4.4.3 Numerical method in anisotropy determination

If two directional permeabilities $k_{\alpha 1}$ and $k_{\alpha 2}$ with directions α_1 and $\alpha_1 + \beta$ have been determined from two well tests, then from equation (4.4.1) we know that they satisfy the following two equations:

$$\frac{2k_h^2}{k_{\alpha 1}}=(k_x+k_y)-(k_x-k_y)\cos(2\alpha) \tag{4.4.4}$$

$$\frac{2k_h^2}{k_{\alpha 2}}=(k_x+k_y)-(k_x-k_y)\cos(2\alpha+2\beta) \tag{4.4.5}$$

where β is the angle from the first well ($k_{\alpha 1}$) to the second ($k_{\alpha 2}$) measured counter-clockwise.

An analytical solution for (4.4.4) and (4.4.5) has evaded us, therefore numerical techniques may be required to solve for k_x and k_y. To make the numerical calculation easier, we would like to simplify the two equations by first subtracting equation (4.4.5) from equation (4.4.4) to obtain:

$$k_x-k_y=\frac{2k_h^2(k_{\alpha 2}-k_{\alpha 1})}{k_{\alpha 1}k_{\alpha 2}[\cos(2\alpha+2\beta)-\cos(2\alpha)]} \tag{4.4.6}$$

and then if we substitute (4.4.6) into (4.4.4) we obtain:

$$k_x+k_y=\frac{2k_h^2[k_{\alpha 2}\cos(2\alpha+2\beta)-k_{\alpha 1}\cos(2\alpha)]}{k_{\alpha 1}k_{\alpha 2}[\cos(2\alpha+2\beta)-\cos(2\alpha)]} \tag{4.4.7}$$

If we add equation (4.4.6) to (4.4.7) we obtain an expression for k_x:

$$k_x = \frac{2k_h^2 \quad k_{\alpha 2}\cos^2(\alpha+\beta) - k_{\alpha 1}\cos^2(\alpha)}{k_{\alpha 1}k_{\alpha 2} \quad \cos(2\alpha+2\beta) - \cos(2\alpha)} \tag{4.4.8}$$

and if we subtract (4.4.7) from (4.4.6) we obtain another expression for k_x by using the relationship of $k_h^2 = k_x k_y$:

$$k_x = \frac{k_{\alpha 1}k_{\alpha 2} \quad \cos(2\alpha+2\beta) - \cos(2\alpha)}{2 \quad k_{\alpha 1}\sin^2(\alpha) - k_{\alpha 2}\sin^2(\alpha+\beta)} \tag{4.4.9}$$

Equations (4.4.8) and (4.4.9) represent two independent relationships between k_x and α. The

variations of k_x with α (0° to 180°) for both equations can be drawn by any commercial spread-sheet software, such as Excel or Qpro, and the intersections between the two curves give the k_x and k_y value. However, one drawback for equations (4.4.8) and (4.4.9) is that four singular points can be present, which complicates the identification of these intersections. To overcome this difficulty, it may be a good idea to calculate the ratio R between the two equations which is:

$$R = k_h^2 \left[\frac{4\sin^2(\beta) - \left[\sqrt{\frac{k_{\alpha 2}}{k_{\alpha 1}}} \sin(2\alpha+2\beta) - \sqrt{\frac{k_{\alpha 1}}{k_{\alpha 2}}} \sin(2\alpha) \right]^2}{k_{\alpha 1} k_{\alpha 2} [\cos(2\alpha+2\beta) - \cos(2\alpha)]^2} \right] \qquad (4.4.10)$$

If the k_x values of equation (4.4.8) and the R values of (4.4.10) are plotted by varying α from 0° to 180°, then the four singular points are reduced to two which are located at $\alpha = 90° - \beta/2$ and $\alpha = 180° - \beta/2$ respectively. Moreover, because the two curves share the same singularities, this makes their identification obvious. Also, the point of R = 1 gives the α value which is the direction of k_x relative to the $k_{\alpha 1}$ direction. The k_x value can be determined from the k_x curve at the determined α value.

Sometimes the k_x values may be much larger than 1, which can make the two curves (R and k_x) very incompatible in their magnitude from a same scale graph. It may be a good idea to multiply R with a known constant of the same order of magnitude as permeability, such as k_h, to make the two curves compatible. The orientation of k_x under this condition can be obtained at the point of $R = k_h$. Also, two such points are obtained, one gives the k_x value (the one with large value), and the other gives the k_y value (smaller one). Figure 4.28 shows an example of the numerical method in permeability ellipse determination.

The two methods discussed above each have advantages and disadvantages. The numerical method is more accurate than the graphical method but the equations need to be input to a program. Also, we need to figure out and eliminate the singularities. The graphical method is easy to use but less accurate, and a measuring net is required. In practical applications, if all three permeabilities $k_{\alpha 1}$, $k_{\alpha 2}$ and k_h are very close in their magnitude, then it is possible that the reservoir is an isotropic reservoir; if $k_{\alpha 1}$ and $k_{\alpha 2}$ are close in magnitude but differ from k_h, then the spread sheet method might be preferable; if $k_{\alpha 1}$ and $k_{\alpha 2}$ differ significantly, then the graphical method is convenient.

4.4.4 A field example

Figure 4.25 and 4.26 are two horizontal well tests reported by Karakas et al., [1991]. The wells were drilled from a old vertical well in directions 195° apart in two adjacent layers with thickness 44 ft and 22 ft respectively. If we assume the primary permeability directions in both layers are the same (very likely because of a similar deposition environment) and have similar magnitude, then the permeability ellipse can be determined by the well tests conducted. From the two figures we find that only the middle linear flow regimes are observable. However, if we utilize the horizontal average permeability determined from the previous vertical well test, the horizontal permeability ellipse can be obtained. Karakas et al., [1991] lists the permeabilities estimated by those well tests (including the vertical well). If we assume the permeabilities were estimated by the conventional method from Figure 4.25 and 4.26, then the following permeability values are pertinent to the new solution:

k_h = 134.1 md $\quad$ $k_{\alpha 1}$ = 205.5 md $\quad$ $k_{\alpha 2}$ = 242.4 md
β = 15° (195°)

We now use both the graphical and numerical (spreadsheet) methods to determine the permeability ellipse for this example.

The modified permeabilities for k_1 and k_2 are k_{m1} = 87.5 md and k_{m2} = 74.18 md. The k_{θ_1} and k_{θ_2} circles determined using the measuring net of Figure 4.24 for these values are shown in Figure 4.27. The following values are obtained from the figure:

$2\alpha + 180 = 150$, $\alpha = -15$
k_x = 240 md
k_y = 74.0 md

The example is also evaluated numerically by drawing the R curve of equation 4.4.10 and the k_x curve of equation (4.4.8). using Excel (Figure 4.28). The corresponding values for k_x, k_y and α obtained from Figure 4.28 are:

$\alpha = -16.3$
k_x = 242.6 md
k_y = 74.1 md

Comparing these two sets of results we find that if an accurate measuring net is used, the graphical

method can be quite satisfactory. Figure 29 shows the permeability ellipse determined for this example. From this figure we find that the minimum permeability direction in this area is almost perpendicular to the HD2 well. Therefore, we might obtain optimum productivity if wells are drilled in the northwest direction, i.e along the minimum permeability direction.

4.5 Conclusions and Discussions

The effect of well orientation on horizontal well test interpretation has been analyzed in this paper. For a horizontally isotropic reservoir, or if the horizontal well is in the primary permeability (k_x) direction, then the new solutions for the VLH flow pattern are the same as those developed by Goode et al.[1987]. However, the orientation effect can be significant in highly anisotropic reservoirs.

In an anisotropic reservoir, the parameters estimated from the early vertical and middle transitional flow regimes are orientation-dependent. We presented and discussed two methods to determine the permeability ellipse, a graphical method and a numerical method. The graphical method is easy to use but less accurate and a measuring net is required. The numerical (spreadsheet) method usually gives more accurate results, but is inconvenient to use because of the requirement of invalid solution elimination.

If the vertical permeability is very small compared with the well direction permeability, then the commonly observed Vertical-Linear-Horizontal flow pattern (VLH) can be replaced by the Vertical-Spherical-Horizontal flow pattern (VSH), but linear and spherical flow can not co-exist. The linear flow regime is identified by a slope of 0.5 in the log-log derivative graph and the spherical flow is identified by a negative slope of 0.5.

We also have attempted to eliminate the test-dependent features of the segmental solutions derived by Goode by identifying two critical time criteria, the boundary effect time t_b and the well length effect time t_w [Goode et al., 1987]. The segmentation approximation solutions are obtained by integration using these criteria, which eliminates the requirement of measuring the test curve slope discussed by Goode et al., [1987]. The relative error caused by using t_b in the integration is less than 0.1%. Even though slightly larger errors can be introduced by using t_w without correction, if it is corrected the error also becomes less than 0.1%, except in the range of two logarithmic cycles around t_w. Even though it is extremely rare, if most of the well test data fall into the two log-cycles around t_w, then the segmental solutions can not be used for test interpretation.

Two field case examples are used to demonstrate the application of the methods introduced in this paper. One shows the spherical flow regime and its derivative in a log-log graph, and the other demonstrates the application of permeability ellipse determination. If the permeability ellipse is determined for a reservoir or part of a reservoir, then optimum productivity wells can be designed along the minimum permeability (k_y) direction [Zhang et al., 1994].

Appendix 4.1

Error Analysis by t_w Approximation

Because the error function term changes gradually, the criterion t_w used in determining the pressure drops can lead to errors during and after the time of t_w.

The error caused by t_w can be evaluated from comparing the true pressure drops obtained by (4.2.22) and (4.2.27) with those obtained by (4.2.45)-(4.2.49) at the period around t_{dw}. We can assign the integration range as $t_{dw}/m < t_d < mt_{dw}$, where m is a constant.

For the VLH flow system, the integral in this period can be approximated as:

$$\begin{aligned} M_t &= \int_{1/(m\pi)}^{m/\pi} \frac{\sqrt{\pi}}{2}\frac{1}{\sqrt{t_d}}\left[erf\left(\frac{(1-\delta)}{\sqrt{t_d}}\right) + erf\left(\frac{\delta}{\sqrt{t_d}}\right)\right]dt_d \\ &= \int_{\sqrt{\pi/m}}^{\sqrt{m\pi}} \frac{\sqrt{\pi}}{\gamma^2}\left[erf[(1-\delta)\gamma] + erf[\delta\gamma]\right]d\gamma \end{aligned} \tag{A1}$$

and the segmentation solution gives:

$$\begin{aligned} M_s &= 2\sqrt{\frac{\pi}{\pi}}\left[1 - \sqrt{\frac{1}{m}}\right] + \ln\left(\frac{m\pi}{\pi}\right) - \ln\left(\frac{\pi}{\pi}\right) \\ &= 2\left[1 - \sqrt{\frac{1}{m}}\right] + \ln(m) \end{aligned} \tag{A2}$$

If we evaluate the difference between (A1) and (A2) by increasing the value of m, we obtain the steady value of E_f :

$$E_f = M_t - M_s = -0.93 \tag{A3}$$

For the VSH system the system integral is:

$$\begin{aligned} N_t &= \int_{1/(m\pi)}^{m/\pi} \frac{h}{2L}\sqrt{\frac{k_a}{k_z}}\frac{1}{t_d}\left[erf\left(\frac{(1-\delta)}{\sqrt{t_d}}\right) + erf\left(\frac{\delta}{\sqrt{t_d}}\right)\right]dt_d \\ &= \frac{h}{L}\sqrt{\frac{k_a}{k_z}}\int_{\sqrt{\pi/m}}^{\sqrt{m\pi}}\frac{1}{\gamma}\left[erf[(1-\delta)\gamma] + erf(\delta\gamma)\right]d\gamma \end{aligned} \tag{A4}$$

and the segmentation solution is:

$$\begin{aligned} N_s &= \frac{h}{L}\sqrt{\frac{k_a}{k_z}}\left[\ln\left(\frac{A^2}{C\pi}\right) - \ln\left(\frac{A^2}{m\pi C}\right) + 2\sqrt{\frac{1}{m}} - 2\right] \\ &= \frac{h}{L}\sqrt{\frac{k_a}{k_z}}\left[\ln(m) + 2\sqrt{\frac{1}{m}} - 2\right] \end{aligned} \tag{A5}$$

and evaluation of E_g gives:

$$E_g = N_t - N_s = -0.56\frac{h}{L}\sqrt{\frac{k_a}{k_z}} \tag{A6}$$

In the evaluation we found that a value of m = 10 gives a good approximation of the segmentation solution.

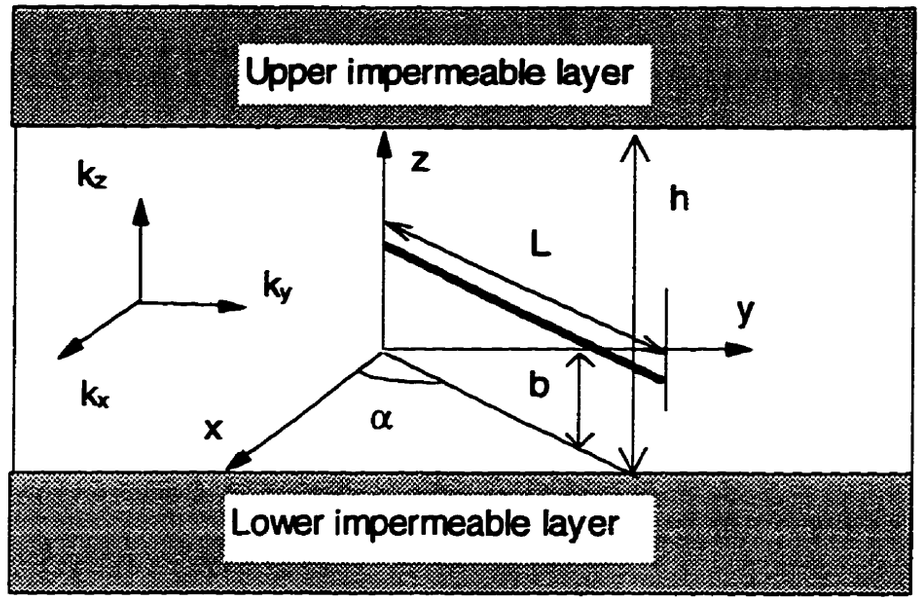

Figure 4.1 An arbitrarily oriented horizontal well in an anisotropic reservoir.

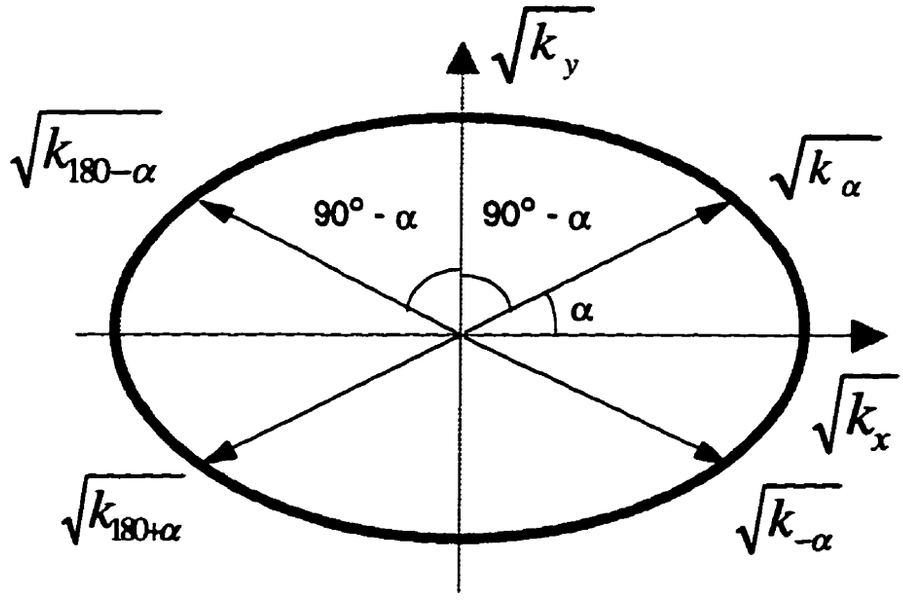

Figure 4. 2 There are four directions in a permeability ellipse where the directional permeability k_α has the same magnitude.

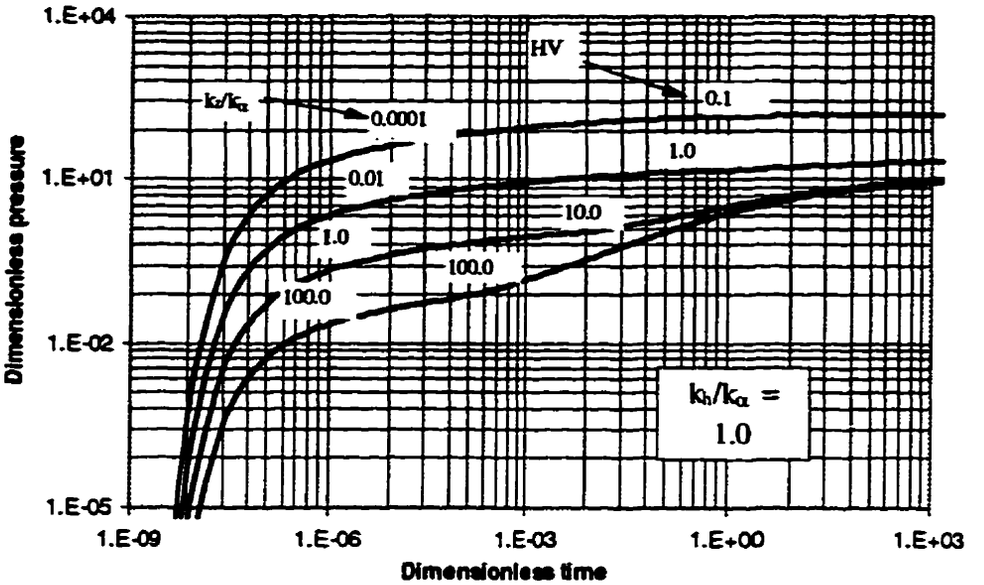

Figure 4.3 Horizontal well test type curves with different β_z values. If HV <1 then the middle flow regime is spherical instead of linear (storage neglected).

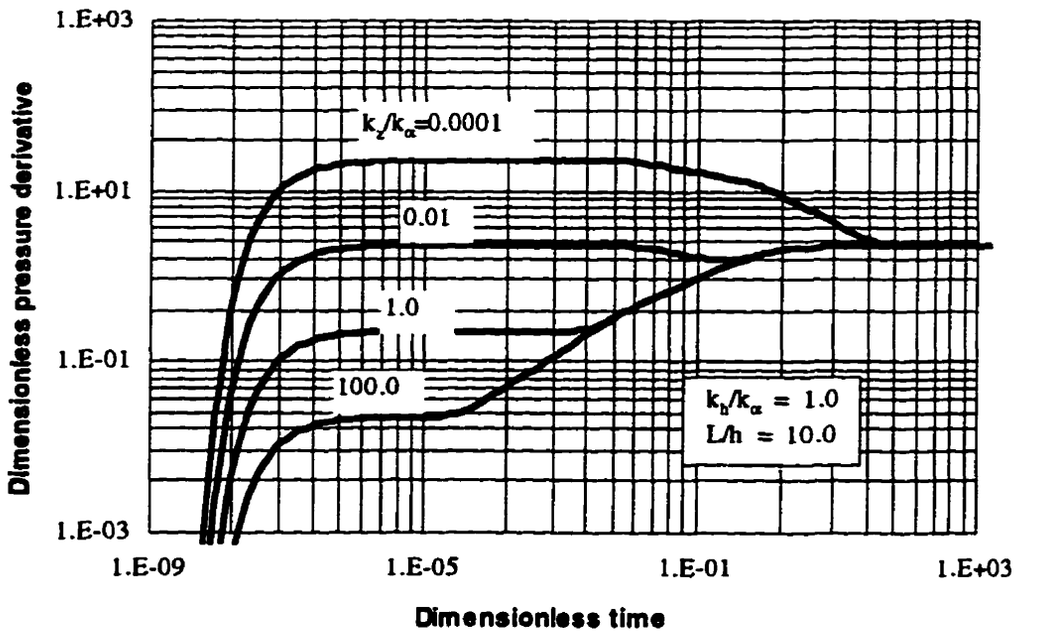

Figure 4.4 Flow regimes can be identified from a horizontal well test using a logarithmic derivative graph.

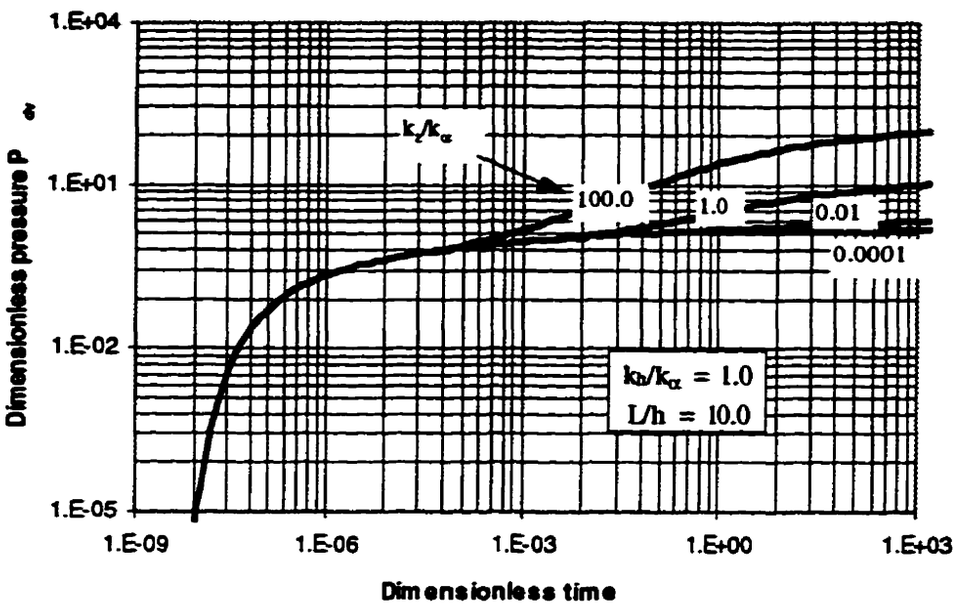

Figure 4.5 Horizontal well test type curves of P_{dv} versus t_d with different β_z values (wellbore storage not considered).

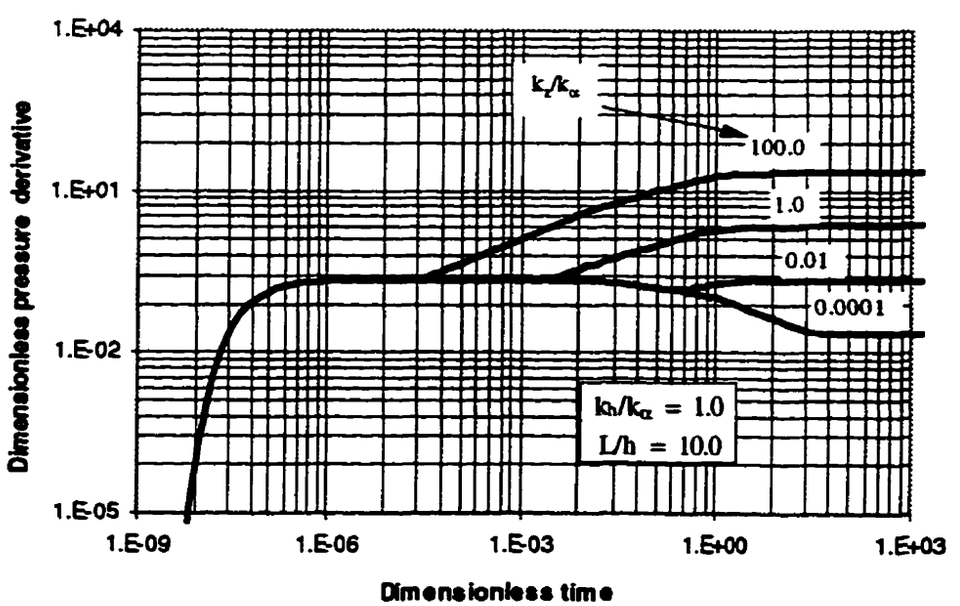

Figure 4.6 Horizontal well test derivative curves with different β_z values (wellbore storage not considered).

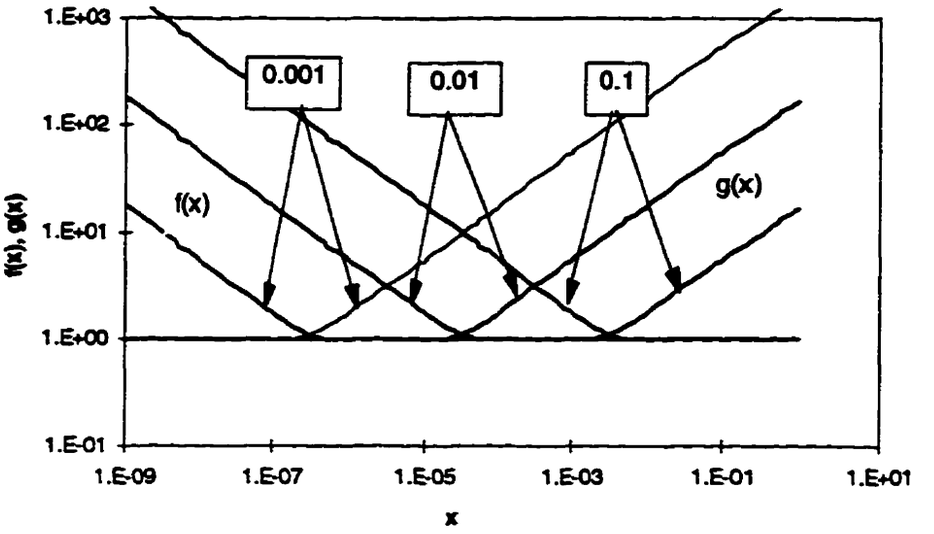

Figure 4.7 Variations of the series term in the form of f(x) and g(x). The intersections mark the transient points from vertical to transient flow regimes.

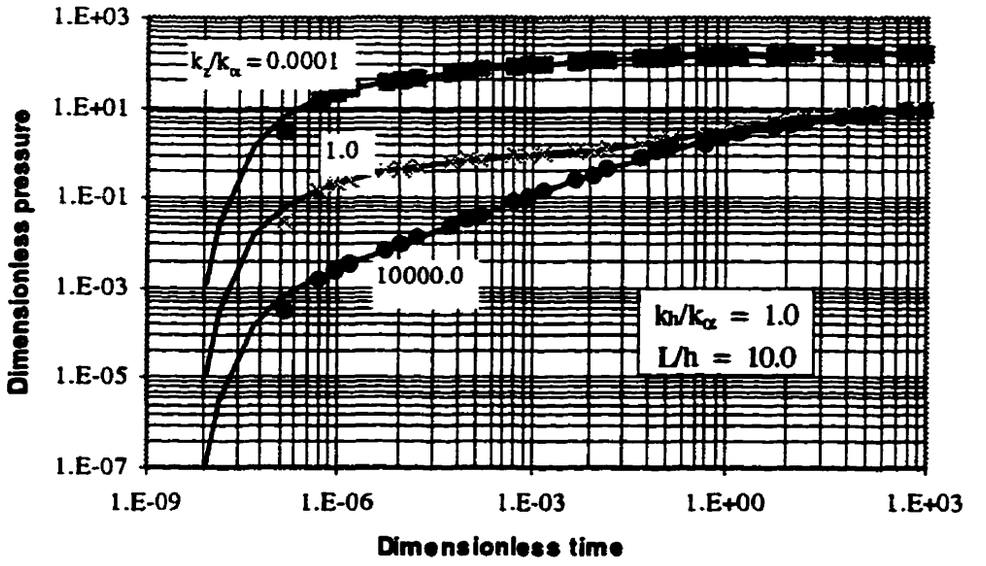

Figure 4.8 Comparison between the approximate segmentation solutions (symbols) and the system solution (lines).

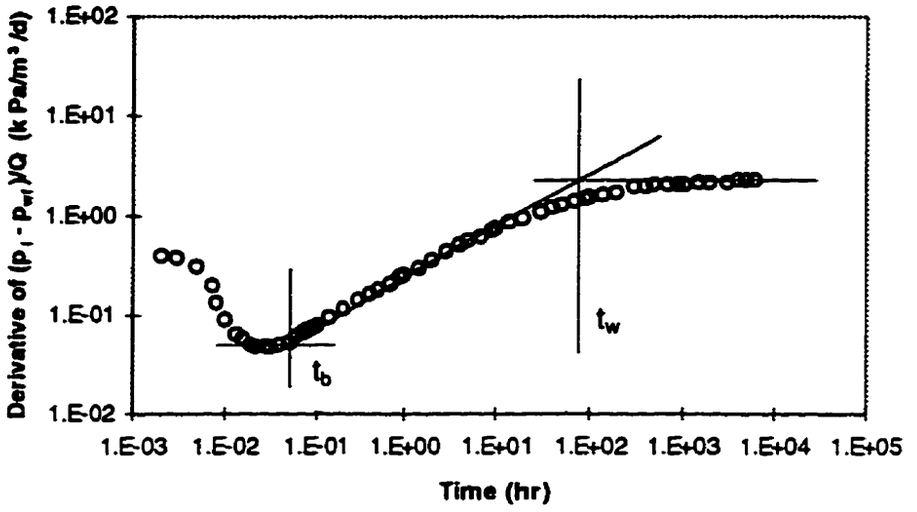

Figure 4.9 A horizontal well test usually presents the Vertical-Linear-Horizontal (VLH) flow pattern (after Mattar and Santo, 1995).

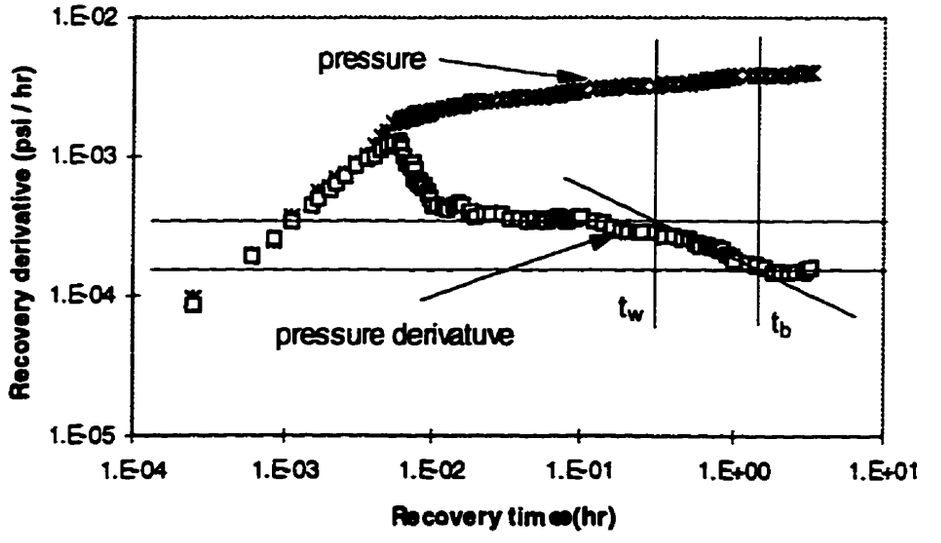

Figure 4.10 A horizontal well test can also present the Vertical-Spherical-Horizontal (VSH) flow pattern (after Domzalski and Yuer, 1992).

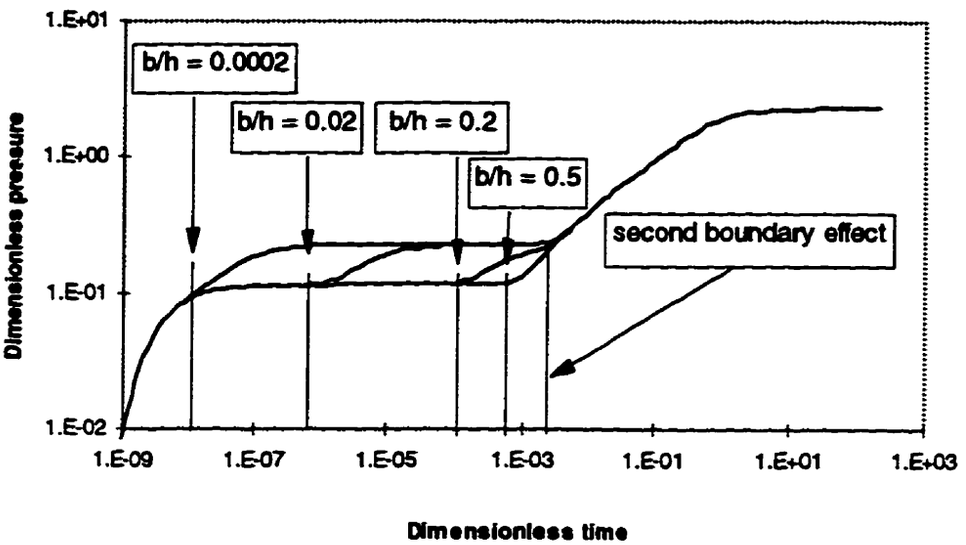

Figure 4.11 Two boundary effect times can be observed if the well is not located at the center of the reservoir, each reflects one boundary's effect.

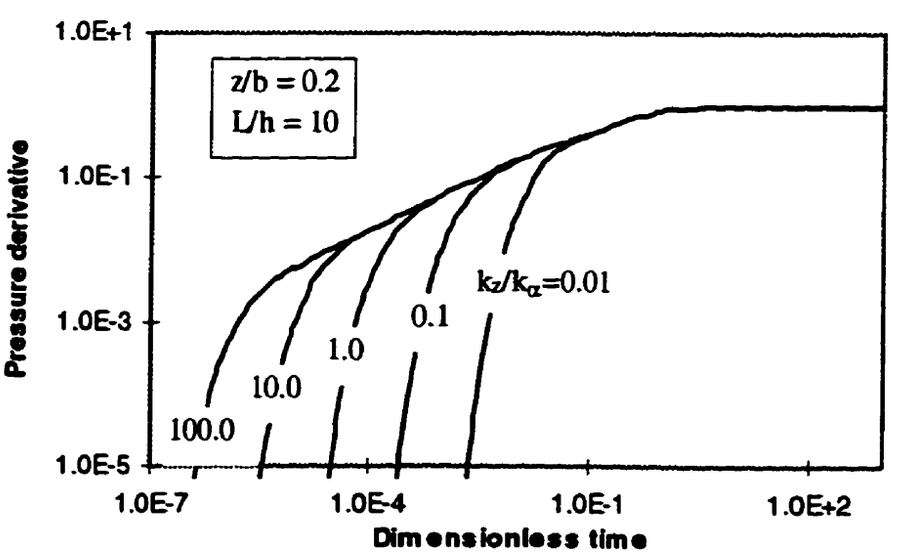

Figure 4.12 Pressure derivatives from an observation well located close to the lower impermeable boundary.

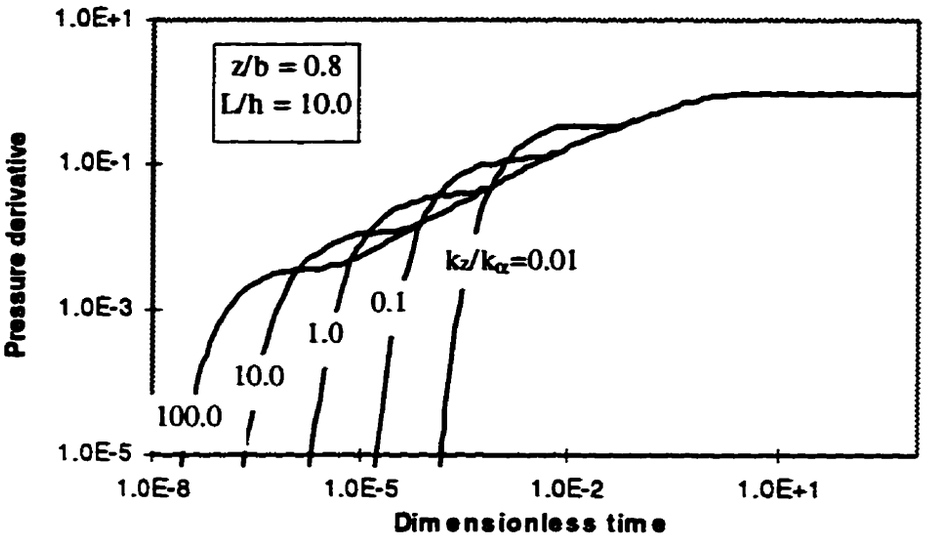

Figure 4.13 Pressure derivatives from an observation well located close to the wellbore.

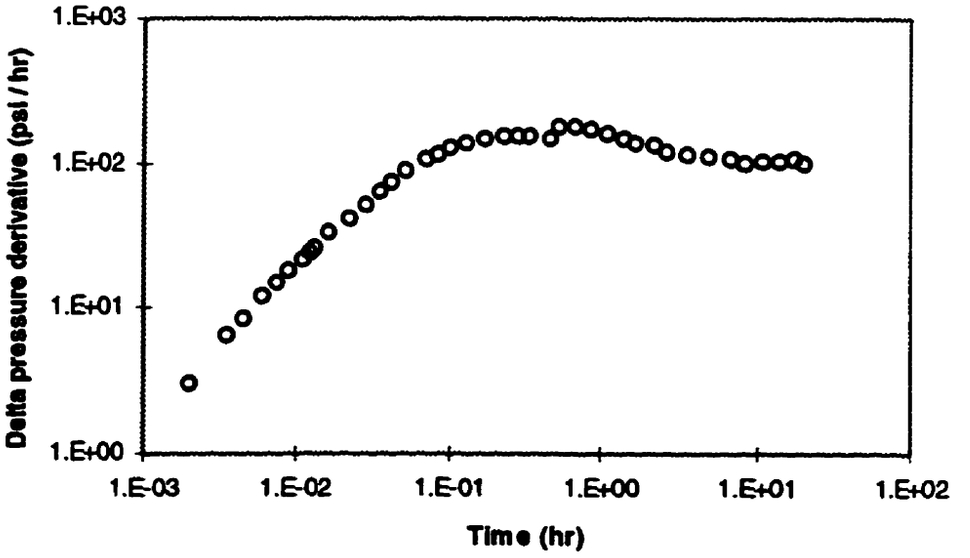

Figure 4.14 Decreases of the buildup test derivative value because of the buildup reduction effect (Sherrard et al., 1987)

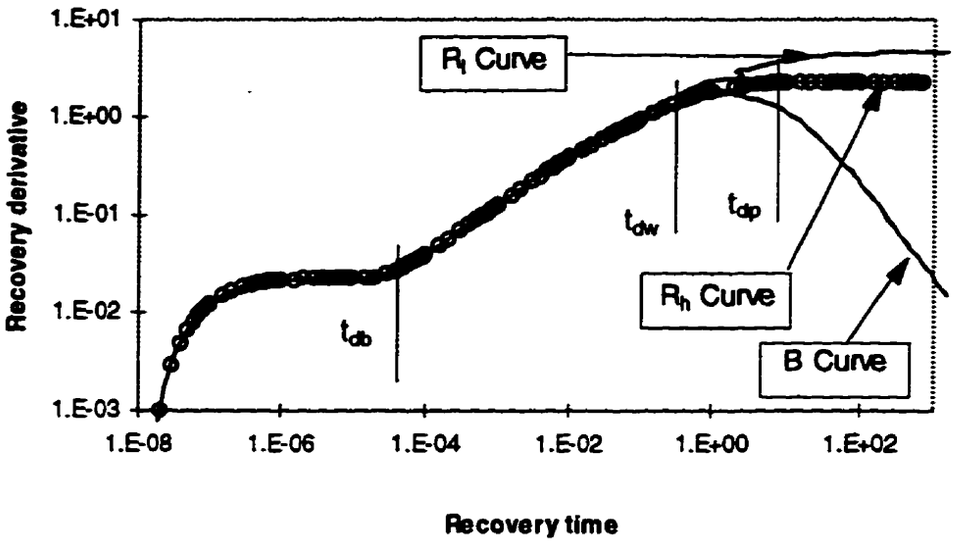

Figure 4.15 Horizontal well buildup test simulation and the application of R_h and R_i curves in test interpretation (case $t_{dp} > t_{dw} > t_{db}$) .

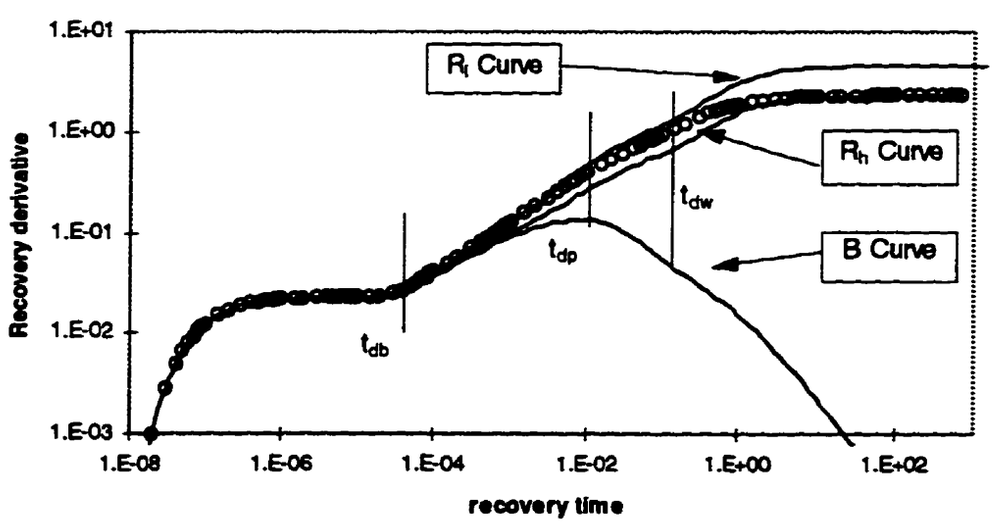

Figure 4.16 Horizontal well buildup test simulation and the application of R_h and R_i curves in test interpretation (case $t_{db} < t_{dp} < t_{dw}$) .

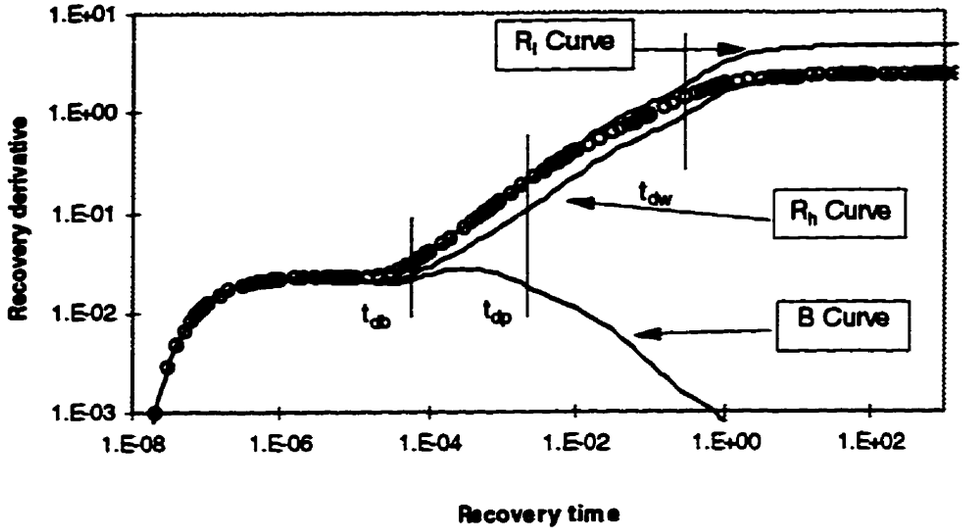

Figure 4.17 Horizontal well buildup test simulation and the application of R_h and R_i curves in test interpretation (case $t_{db} < t_{dp} < t_{dw}$) .

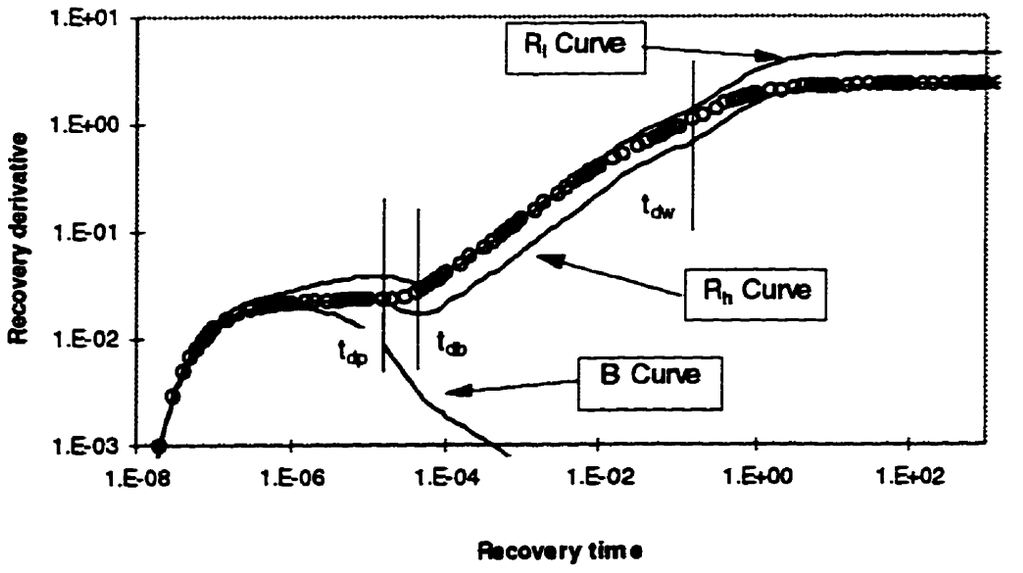

Figure 4.18 Horizontal well buildup test simulation and the application of R_h and R_i curves in test interpretation (case $t_{dp} < t_{db} < t_{dw}$) .

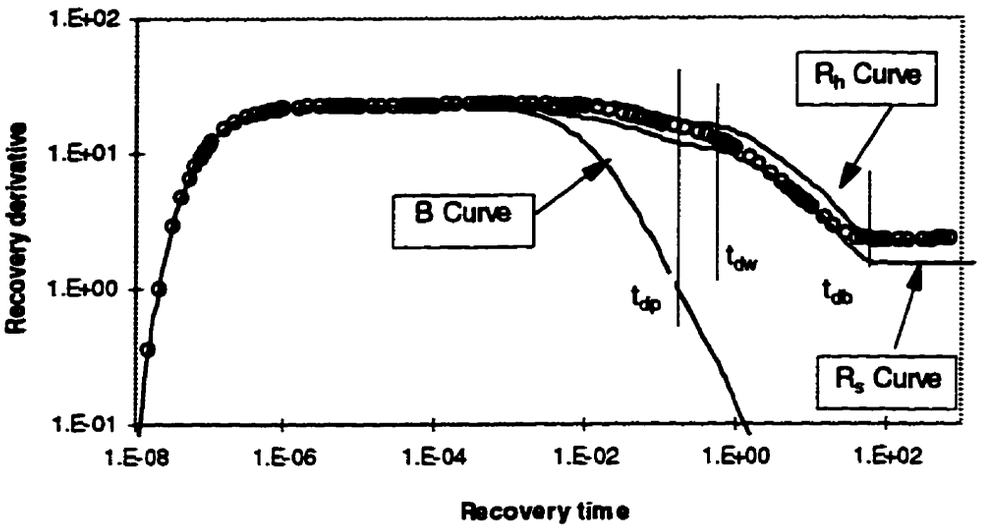

Figure 4.19 Horizontal VSH flow sequence test buildup simulation and its R_h and $R_s$curves in test interpretation.

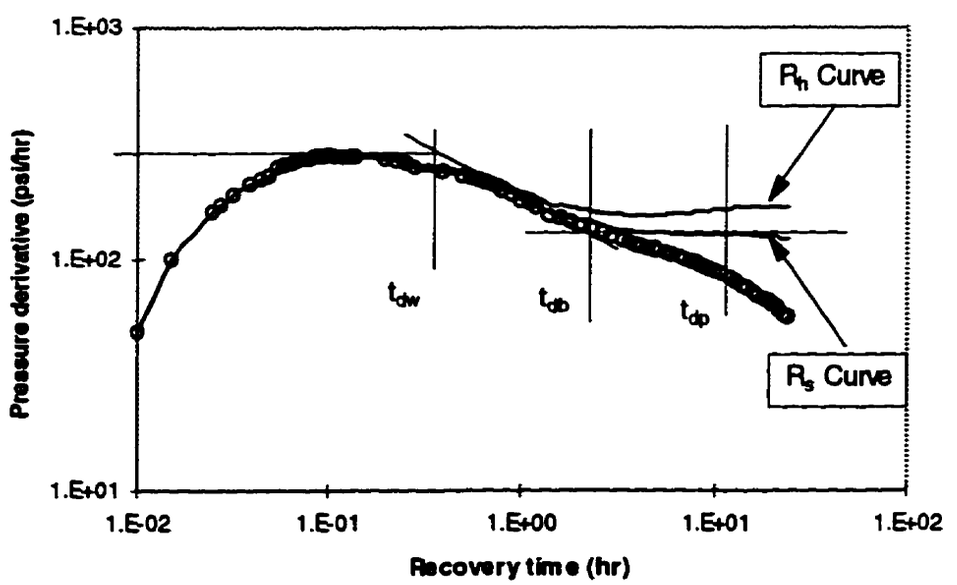

Figure 4.20 Buildup test interpretation of case example 2 by applying R_h and R_s curves (after Sherrard et al., 1987).

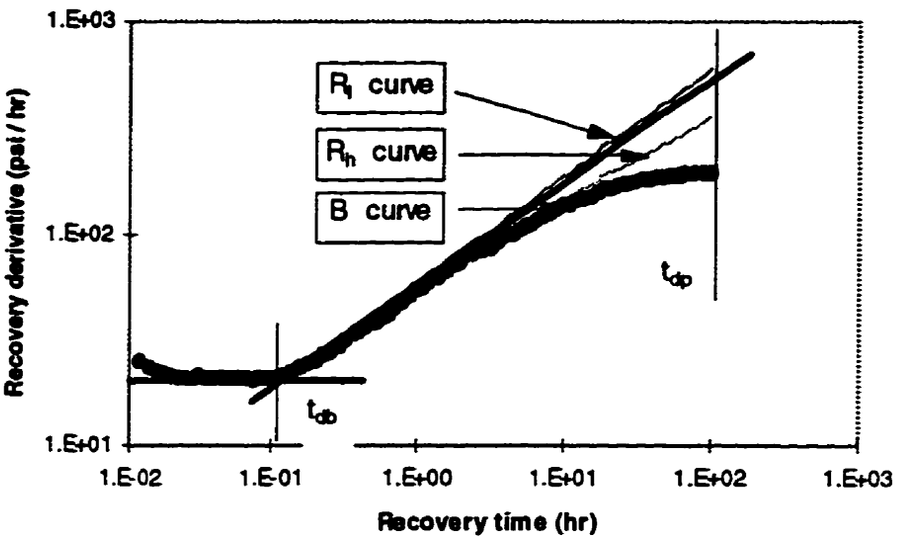

Figure 4.21 By applying the R_h and R_i curves, it becomes obvious that we can not determine the horizontal radial flow regime from this field test (Mattar and Santo, 1995).

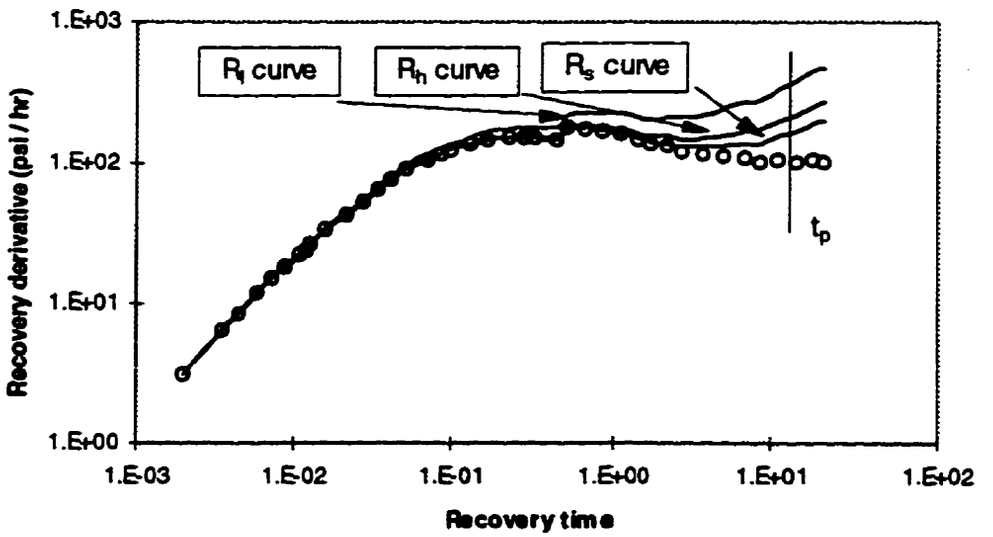

Figure 4.22 Identification of flow regimes where the flow sequence pattern becomes difficult to identify (after Sherrard et al., 1987)

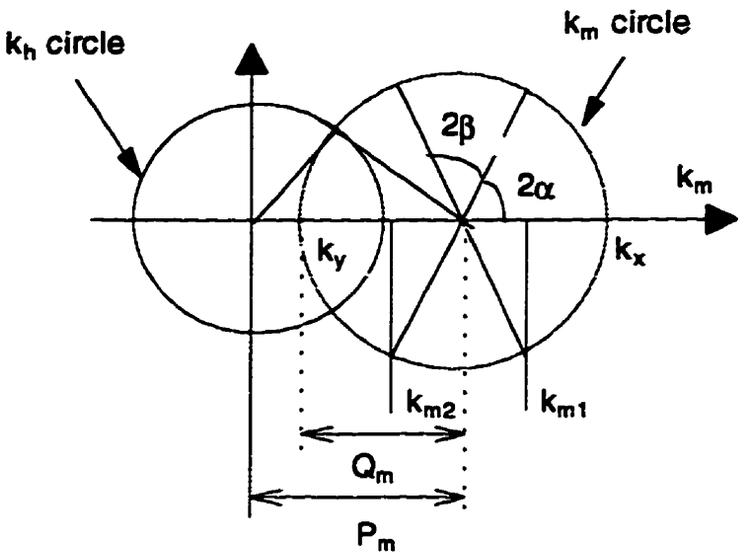

Figure 4.23 The k_h and k_m circles used in the graphical method in permeability ellipse determination.

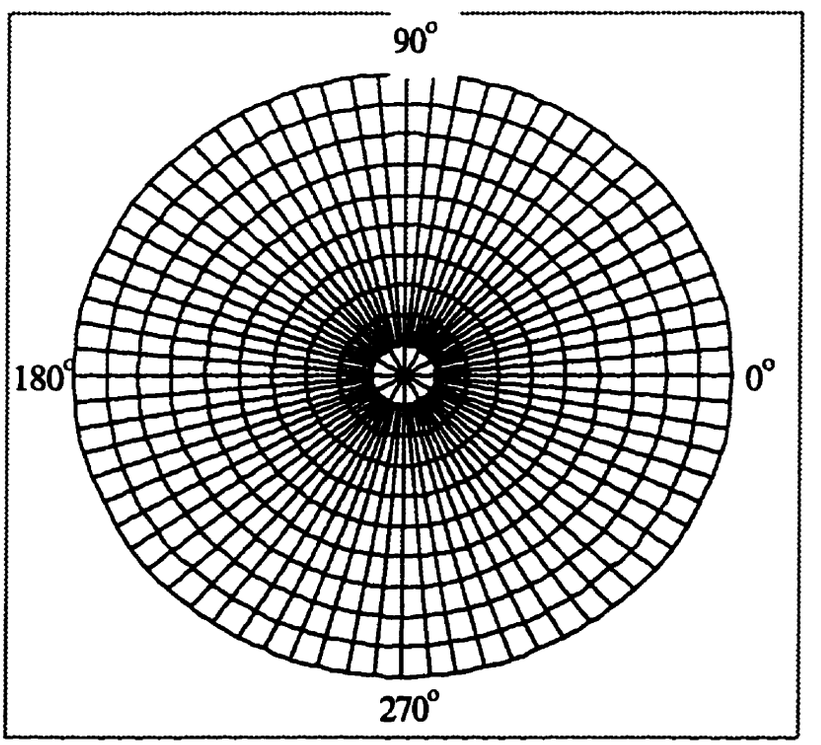

Figure 4.24 A measuring net to determine the anisotropic permeability ellipse from two horizontal well tests.

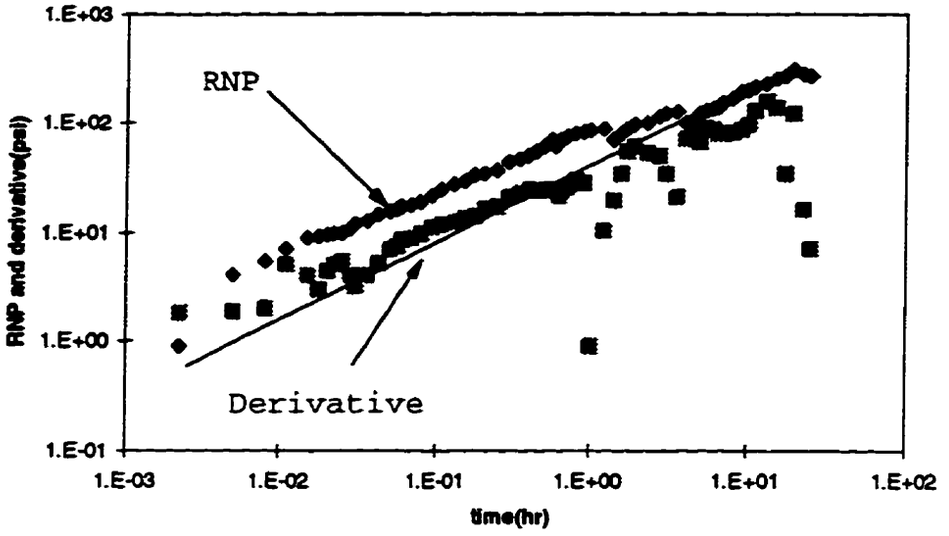

Figure 4.25 Rate Normalized Pressure (RNP) of the HD1 horizontal well test and derivative data from Karakas et al., (1991).

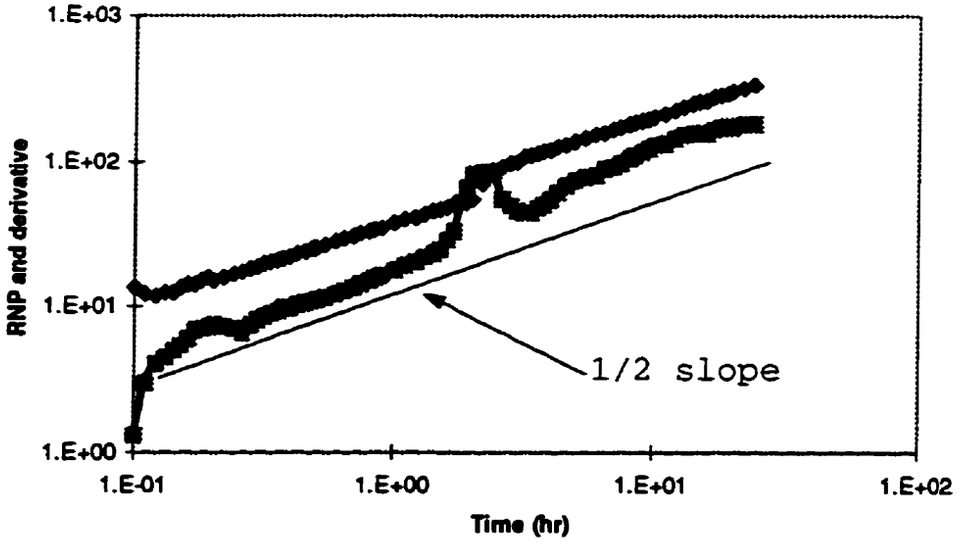

Figure 4.26 Rate Normalized Pressure (RNP) of the HD2 horizontal well test data from Karakas et al., (1991).

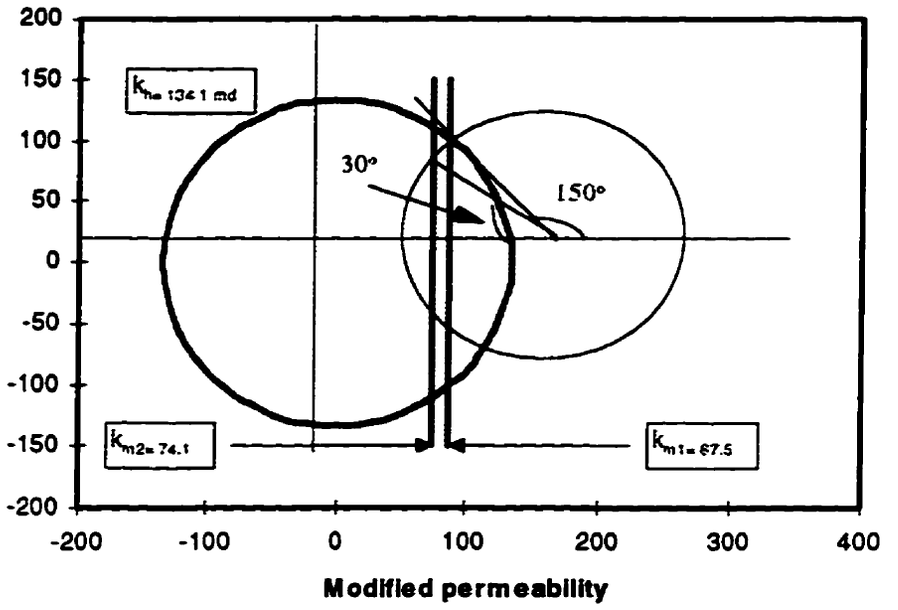

Figure 4.27 The k_h and k_m circles and permeability ellipse determination from well tests data of Karakas et al., (1991)

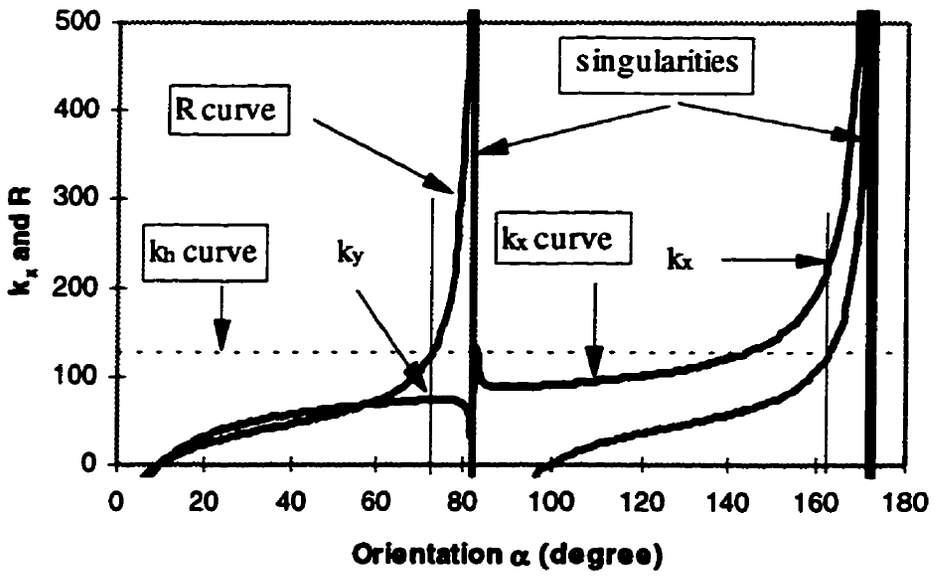

Figure 28 Permeability ellipse determination by numerical (spread sheet) method for the test data of Karakas et al., (1991)

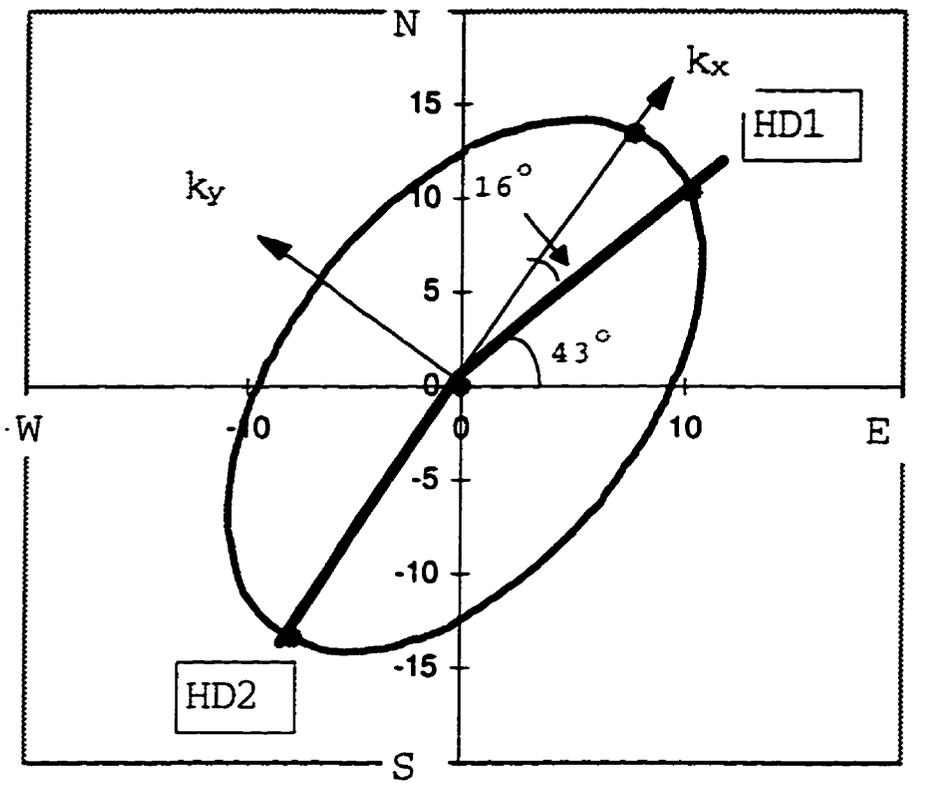

Figure 4.29 The permeability ellipse obtained from the well test discussed by Karakas et al., (1991)

Chapter Five

Wellbore Storage Effect

5.1 Wellbore Storage Effect in a Drawdown Test

The horizontal well test solutions developed in Chapter 4 assume that wellbore storage can be minimized to such a small value that no obvious effects can be observed from a well test. This is possible through use of carefully chosen measuring tools such as a downhole pressure gauge or a flow meter. However, sometimes the wellbore effect can be very large and becomes non-negligible. In such situations, the wellbore storage must be considered in interpreting a well test.

Wellbore storage in a horizontal well can come from two sections, the vertical section and the horizontal section. Obviously, the vertical section is more important than the horizontal section because it contributes immediately after a test starts. The horizontal section only applies when the pressure has declined to the elevation of the horizontal section. In such cases, the drawdown cone usually has become very large, and the flow regimes could have reached the middle transient or the horizontal radial flow regime. Because of the huge recharge area at this stage, the wellbore pressure drawdown rate in such periods will be very small and, the percentage of wellbore discharge in the total flow rate becomes very small. Therefore, it is most likely that the wellbore storage effect in such stages of a test can be safely neglected. Because of this, we will only discuss the wellbore storage effect of the vertical section in this chapter.

Wellbore storage comes into effect by contributing the fluid stored in the wellbore to the whole well discharge rate. The solutions obtained in Chapter 4 assume that the discharge totally comes from the reservoir through sand face flow (no storage) $Q_{sf}(t)$. If the total well discharge rate is a constant Q, then it is composed of two parts, the sand face discharge $Q_{sf}(t)$, and the wellbore discharge Q_w. The sand face discharge satisfies the mass conservation equation:

$$Q_{sf}(t) = Q - Q_w(t) = Q - C_c\frac{\partial \Delta p_w}{\partial t} \tag{5.1.1}$$

where Δp_w is the pressure drawdown at the wellbore and C_c is the wellbore storage coefficient which is the volume of wellbore discharge per unit of pressure changes and can be approximately calculated as $C_c = \pi r_c^2$ for a vertical section with wellbore radius r_c. If the wellbore is inclined with θ degrees from the vertical, then $C_c = \pi r_c^2/\cos(\theta)$.

If we use the following dimensionless variables of t_d and P_d defined in Chapter 4 in equation (5.1.1):

$$P_d = \frac{4\pi h\sqrt{k_x k_y}}{\mu Q}\Delta p \qquad t_d = \frac{4k_\alpha t}{L^2 c_m \phi \mu} \tag{5.1.2}$$

we have:

$$Q_{sf}(t_d) = Q - \frac{QC_c k_\alpha}{\pi h L^2 c_m \phi k_h}\frac{\partial P_{dw}}{\partial t_d} = Q(1 - C_d\frac{\partial P_{dw}}{\partial t_d}) \tag{5.1.3}$$

where

$$C_d = \frac{C_c}{\pi L^2 h c_m \phi \beta_h} \qquad \beta_h = \frac{k_h}{k_\alpha} \tag{5.1.4}$$

and C_d is the dimensionless storage coefficient.

Take Laplace transforms of (5.1.3) with respect to t_d to obtain:

$$\bar{Q}_{sf}(s) = Q(\frac{1}{s} - C_d s\bar{P}_{dw}) \tag{5.1.5}$$

For a non-constant sandface flow rate $Q_{sf}(t)$, the general horizontal solution of (4.2.22) of Chapter 4

can be written as:

$$P_d = \int_0^{t_d} \frac{Q_{sd}(t_d - \tau)}{Q} Z(\tau) d\tau \qquad (5.1.6)$$

If we take Laplace transforms of solution (5.1.6) by applying the result of (5.1.5) we have:

$$\bar{P}_d = L\left[\int_0^{t_d} \frac{Q(t_d-\tau)}{Q} Z(\tau) d\tau\right] = \bar{Z}(s)[\frac{1}{s} - C_d s \bar{P}_{dw}] \qquad (5.1.7)$$

Take the drawdown at the wellbore in equation (5.1.7) and solve for P_{dw} :

$$\bar{P}_{dw} = \frac{\bar{Z}_w(s)}{s[1 + C_d s \bar{Z}_w(s)]} \qquad (5.1.8)$$

and if we substitute (5.1.8) into (5.1.7), we obtain:

$$\bar{P}_d = \frac{\bar{Z}(s)}{s[1 + C_d s \bar{Z}_w(s)]} \qquad (5.1.9)$$

where the Laplace transform of $Z(\tau)$ is:

$$\bar{Z}(s) = \int_0^{\infty} e^{-s\tau} Z(\tau) d\tau \qquad (5.1.10)$$

The Laplace transformed logarithmic derivative of P_d is:

$$L\left[\frac{\partial P_{dw}}{\partial[\log_{10}(t_d)]}\right] = \frac{\partial[-2.3 s \bar{P}_{dw}(s)]}{\partial s} = \frac{2.3[C_d \bar{Z}_w^2(s) - \bar{Z}_w'(s)]}{[1 + C_d s \bar{Z}_w(s)]^2} \qquad (5.1.11)$$

where $Z_w'(s)$ is the derivative of $Z_w(s)$ with respect to s and which can be written as:

$$\bar{Z}'_w(s) = -\int_0^{\infty} e^{-st_d} Z(t_d) t_d \, dt_d \tag{5.1.12}$$

Therefore by inverting solution (5.1.9), the dimensionless pressure under the storage effect can be obtained. In the same manner, by inverting solution (5.1.11), the dimensionless pressure derivative can also be obtained. Analytical inversions of solutions (5.1.9) and (5.1.11) are not realistic, therefore a numerical scheme has to be applied.

5.2 Wellbore Storage Effect in a Buildup Test

The buildup test can be simulated by superposition of two sectional drawdown tests with different well production rates. The sand face flow rate in such superpositions can be written as follows, with consideration of the wellbore storage:

$$Q_{sf}(t_d) = \begin{bmatrix} Q[1 - C_d \dfrac{\partial P_{dw}}{\partial t_d}] & (t_d < t_{dp}) \\ -QC_d \dfrac{\partial P_{dw}}{\partial t_d} & (t_d \geq t_{dp}) \end{bmatrix} \tag{5.2.1}$$

where $t_{dp} = 4k_a t_p/(L^2 c_m \phi \mu)$ and Q is the well discharge.

By applying the Laplace transformation to both equations (5.1.1) and (5.2.1) in the same way as in the last section, the pressure transient equation can be obtained in Laplace space as :

$$\bar{P}_d = \frac{[1 - e^{-st_{dp}}]\bar{Z}(s)}{s[1 + C_d s \bar{Z}_w(s)]} \tag{5.2.2}$$

where $Z_w(s)$ is the value of Z(s) at the wellbore.

As we can see when t_{dp} tends to infinity, solution (5.2.2) becomes identical to the solution (5.1.9) developed above.

If we denote the Laplace transformed dimensionless pressure drawdown P_{dw} of equation (5.1.8) at wellbore as $P_{dwd}(s)$, and its logarithmic derivative of equation (5.1.11) as $P'_{dwd}(s)$ with :

$$\bar{P}_{dwd}(s) = \frac{\bar{Z}_w(s)}{s[1 + C_d s\bar{Z}_w(s)]} \tag{5.2.3}$$

and

$$\bar{P}'_{dwd}(s) = \frac{2.3[C_d\bar{Z}_w^2(s) - \bar{Z}'_w(s)]}{[1 + C_d s\bar{Z}_w(s)]^2} \tag{5.2.4}$$

then the buildup dimensionless pressure of solution (5.2.2) at the wellbore can be written as:

$$\bar{P}_{dw} = P_{dwd}(s) - e^{-st_{dp}}P_{dwd}(s) \tag{5.2.5}$$

and the logarithmic derivative of the buildup solution (5.2.5) becomes:

$$\begin{aligned}\frac{\partial P_{dw}}{\partial \log_{10}(t_d)} &= \bar{P}'_{dwd}(s) - [2.3t_{dp}e^{-st_{dp}}s\bar{P}_{dwd}(s) + e^{-st_{dp}}P'_{dwd}(s)] \\ &= P'_{dwd}(s)[1 - e^{-st_{dp}}] - \frac{2.3t_{dp}e^{-st_{dp}}\bar{Z}_w(s)}{1+C_d s\bar{Z}_w(s)}\end{aligned} \tag{5.2.6}$$

or in the expanded form:

$$\frac{\partial P_{dw}}{\partial \log_{10}(t_d)} = \frac{2.3[1-e^{-st_{dp}}][C_d Z_w^2(s) - Z'_w(s)]}{[1 + C_d s Z_w(s)]} - \frac{2.3t_{dp}Z_w(s)e^{-st_{dp}}}{1 + C_d s Z_w(s)} \tag{5.2.7}$$

Therefore, the dimensionless pressure of a buildup test and its logarithmic derivatives including the wellbore storage effect can also be obtained from solution (5.2.5) and (5.2.7).

5.3 The Effect of Wellbore Storage Masking

When solutions (5.1.9) or (5.1.11) are evaluated, we find that the effect of wellbore storage for a horizontal well test is very similar to that of a vertical well test. At very early times the dimensionless pressure and its logarithmic derivatives are masked by wellbore storage (Figure 5.1). Larger values of storage (larger C_d) generate proportionally longer times of masking.

From solution (5.1.9) for very small times we have :

$$L^{-1}\left[s\bar{P}_d\right]\Big|_{s\to\infty} = L^{-1}\left[\frac{1}{C_d s}\right] = \frac{t_d}{C_d} \tag{5.3.1}$$

which shows that the dimensionless pressure and its derivative at very small dimensionless times has a linear function with t_d and C_d:

$$P_d(t_d) = \frac{t_d}{C_d} \qquad \frac{\partial P_d}{\partial[\log(t_d)]} = \frac{t_d}{C_d} \tag{5.3.2}$$

This is exactly the same as for the vertical well.

To determine the wellbore storage coefficient we can extend the straight line to intersect with the vertical line at $t_d = 1.0$, and the corresponding P_d value gives for the coefficient C_d in the following relationship:

$$C_d = \frac{1}{P_d} \tag{5.3.3}$$

Solution (5.3.3) indicates that at the very beginning of a test, wellbore storage dominates the well discharge and the reservoir discharge is negligible. With increasing time, the reservoir discharge

gradually increases, and the wellbore storage dominance diminishes. When the reservoir discharge becomes dominant, the wellbore storage effect vanishes. The end point of the wellbore storage period can be considered as the point where the wellbore storage straight line intersects with the type curve (Figure 5.1). This point is presented in the logarithmic derivative curve as the peak value at the end of the $\log(t_d/C_d)$ straight line, as shown in Figure 5.2.

5.4 Wellbore Storage Effect Analysis

Figure 5.3 and Figure 5.4 show the wellbore storage effect on the type and logarithmic derivative curves of an isotropic reservoir. Because of the flow regimes in a horizontal well test, the storage effect termination time varies not only with the storage coefficient C_d, but also with well and reservoir parameters such as reservoir thickness h and well length L. Depending on the magnitude of C_d, one or more flow regimes of a horizontal well test can be masked.

In the anisotropic permeability situation, the wellbore storage effect termination time clearly depends also on the degree of anisotropy. Figure 5.5 and Figure 5.6 are the type and derivative curves for $k_z/k_\alpha = 0.01$, the situation where the vertical permeability is much less than the horizontal permeability. Figure 5.7 and Figure 5.8 are for $k_z/k_\alpha = 100$, the situation where the vertical permeability is much greater than the horizontal permeability.

Comparing the derivative curves of different anisotropy cases in Figures 5.4, 5.6 and 5.8, we find that the storage effect is more obvious in reservoirs with higher vertical permeability than in lower vertical permeability situations.

The wellbore storage effect in a buildup test is very similar to the drawdown test, as can be seen from Figures 5.9 and 5.10. If the storage effect becomes negligible at the shut-in time, then the R_h -R_i (R_s) reduction factor method is also effective. However, if the storage effect is non-negligible at the shut-in time, then the R_h -R_i (R_s) method will not work before the storage effect becomes very small.

The wellbore storage effect on a VSH flow sequence is shown in Figure 5.11 and its derivative in Figure 5.12. The same effect is also observed in the VSH flow sequence as in the VLH flow sequence. The only difference is that the storage effect time will be longer for the VSH sequence than for the VLH sequence under the same conditions because of the higher pressure (derivative) required in such a flow sequence.

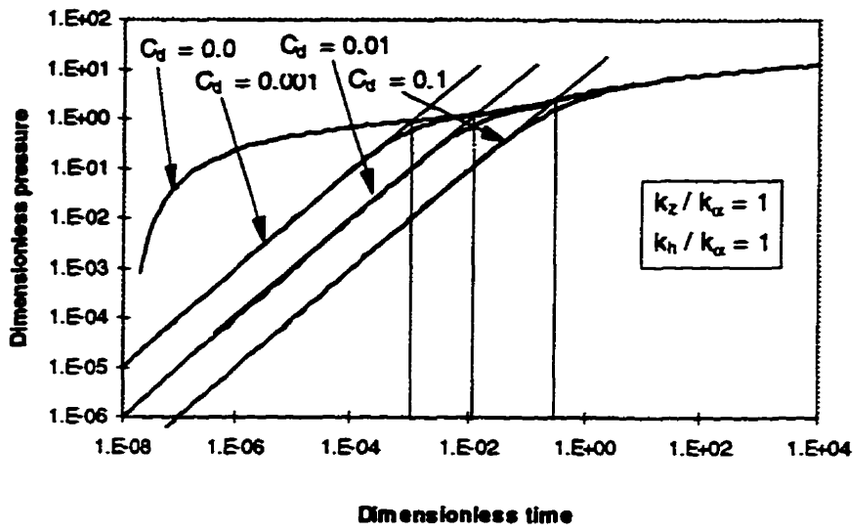

Figure 5.1 Determination of the wellbore storage effect termination time from a horizontal well test pressure curve.

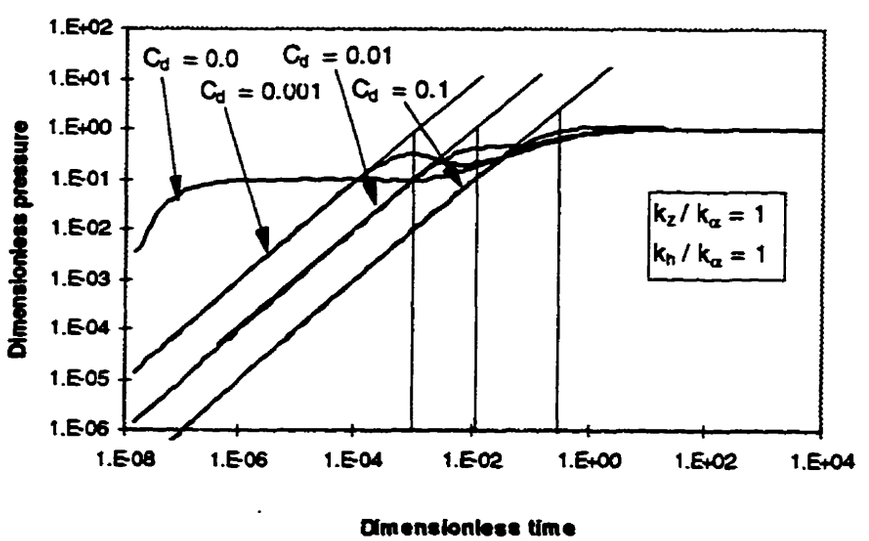

Figure 5.2 Wellbore storage effect terminates at the time where a peak derivative value is obtained.

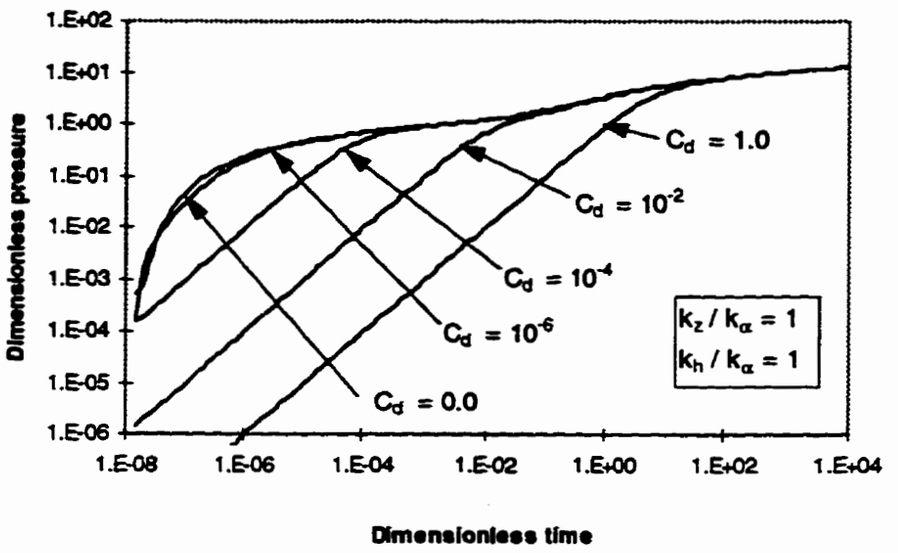

Figure 5.3 Wellbore storage effect on a horizontal well test in an isotropic permeability

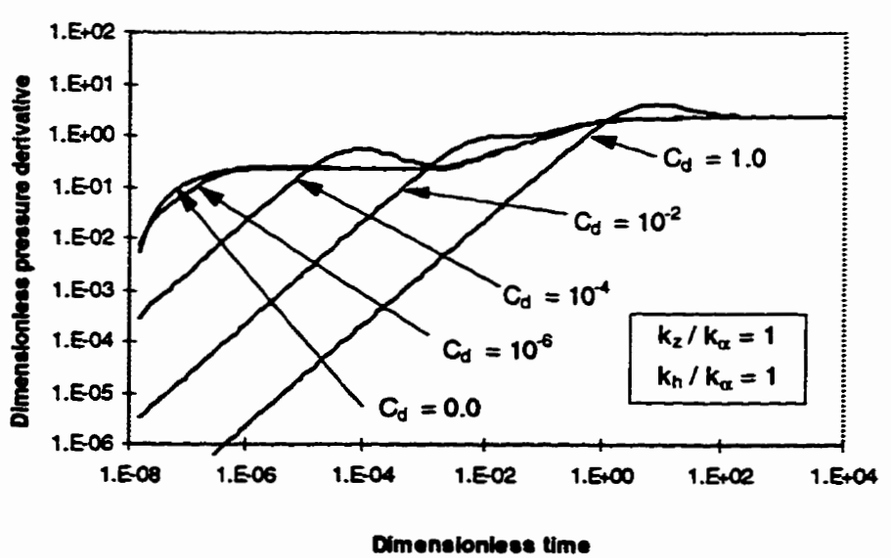

Figure 5.4 Wellbore storage effect on a horizontal well test in an isotropic reservoir presented in a logarithmic derivative graph.

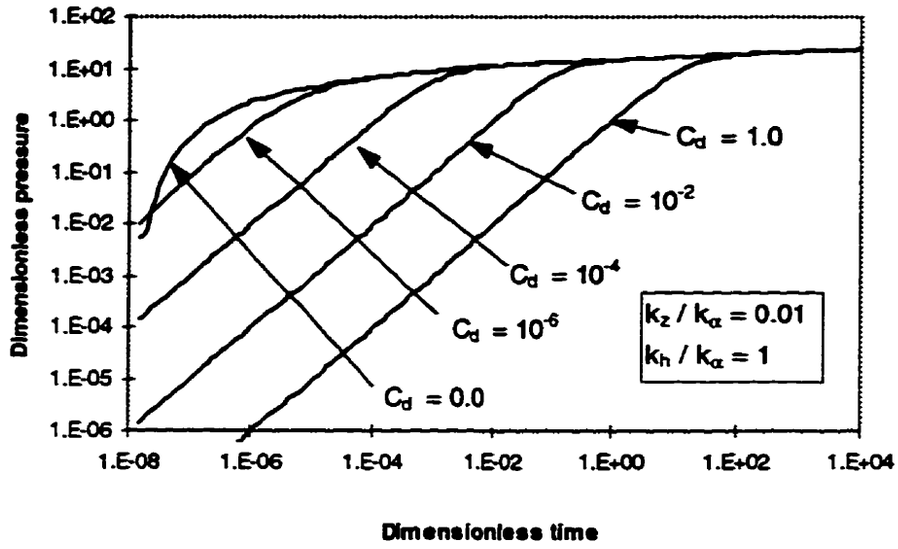

Figure 5.5 Wellbore storage effect of a horizontal well test in an anisotropic reservoir with $k_z < k_\alpha$.

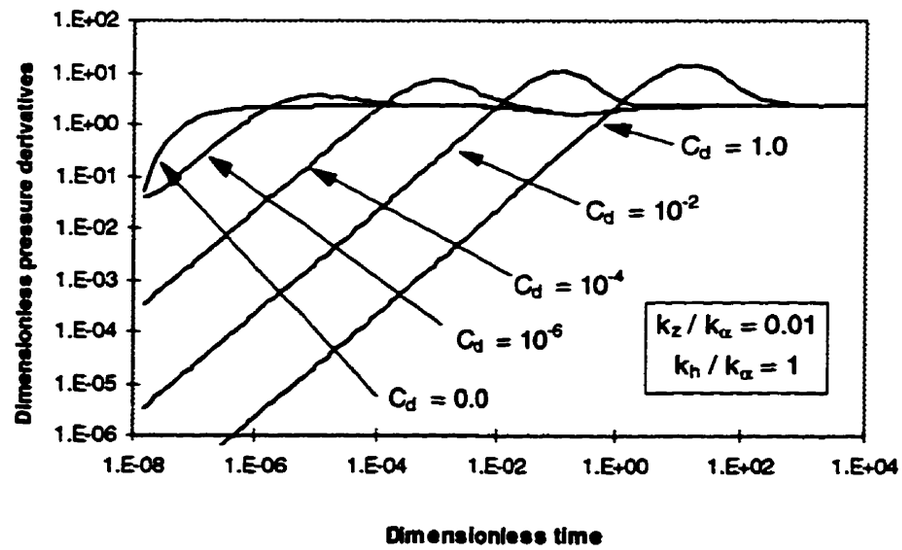

Figure 5.6 Logarithmic derivatives of the wellbore storage effect on a horizontal well test in an anisotropic permeability reservoir with $k_z < k_\alpha$.

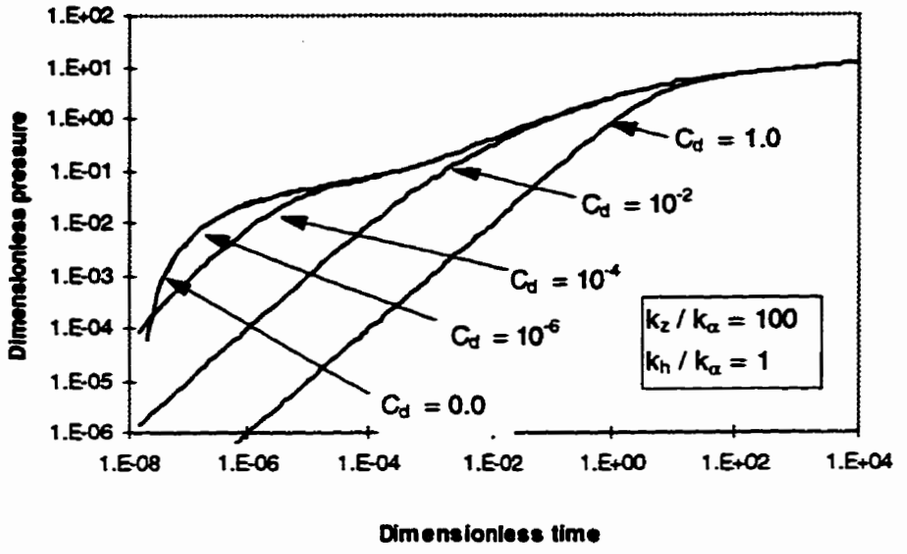

Figure 5.7 Wellbore storage effect of a horizontal well test in an anisotropic permeability reservoir with $k_z > k_\alpha$.

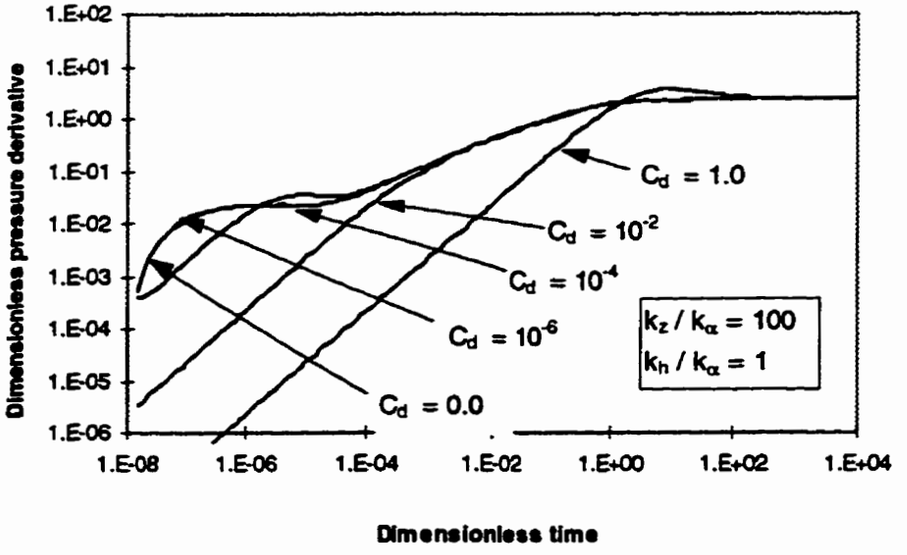

Figure 5.8 Logarithmic derivatives of the wellbore storage effect of a horizontal well test in an anisotropic permeability reservoir with $k_z > k_\alpha$.

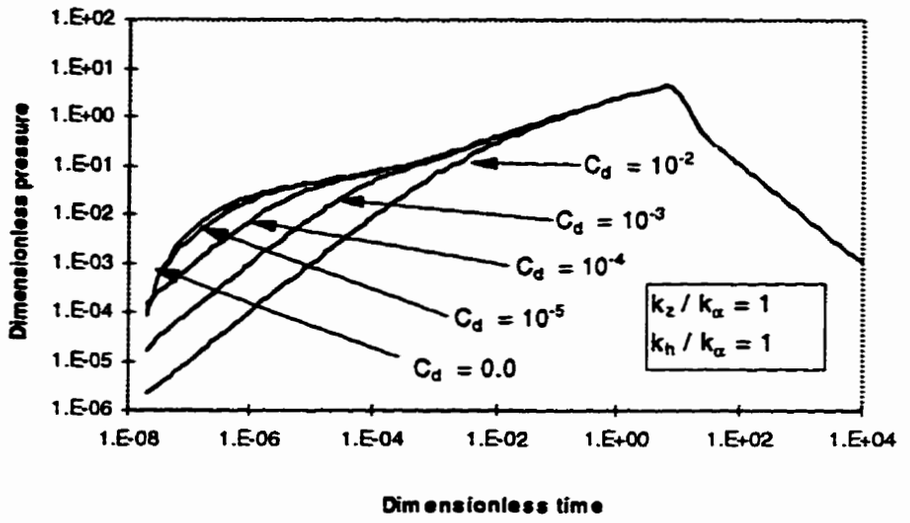

Figure 5.9 Wellbore storage effect on a horizontal well buildup test with the shut - in time $t_{dp} = 10.0$.

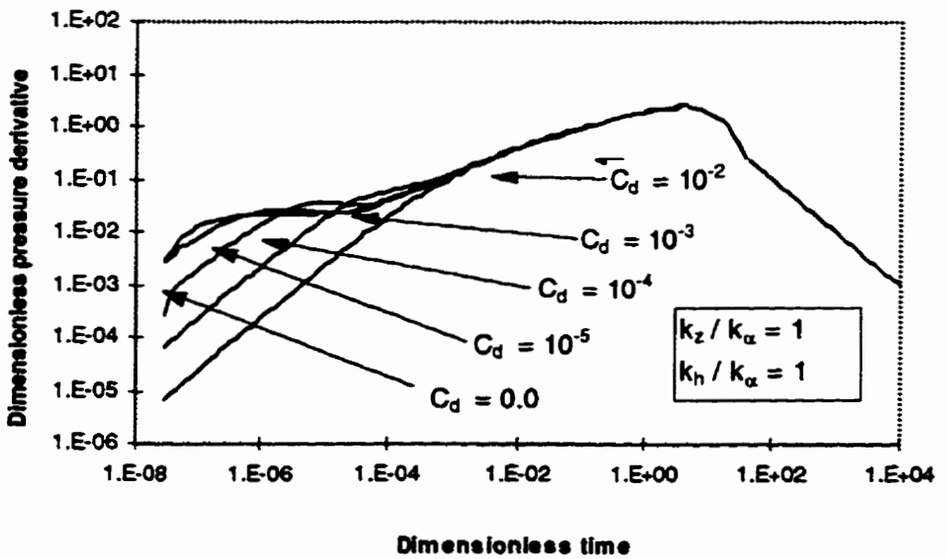

Figure 5.10 Wellbore storage effect on a horizontal well buildup test with the shut - in time $t_{dp} = 10.0$ presented in the derivative graph.

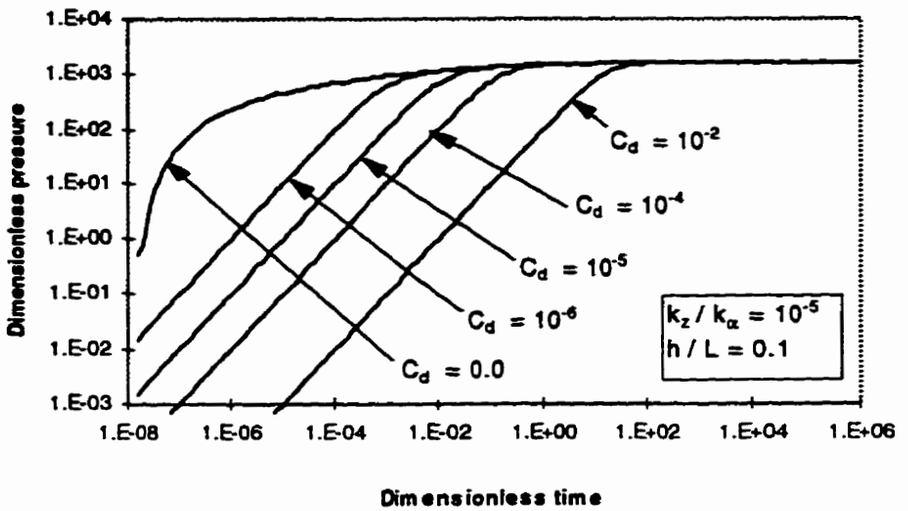

Figure 5.11 Wellbore storage effect on a VSH flow sequence horizontal well test.

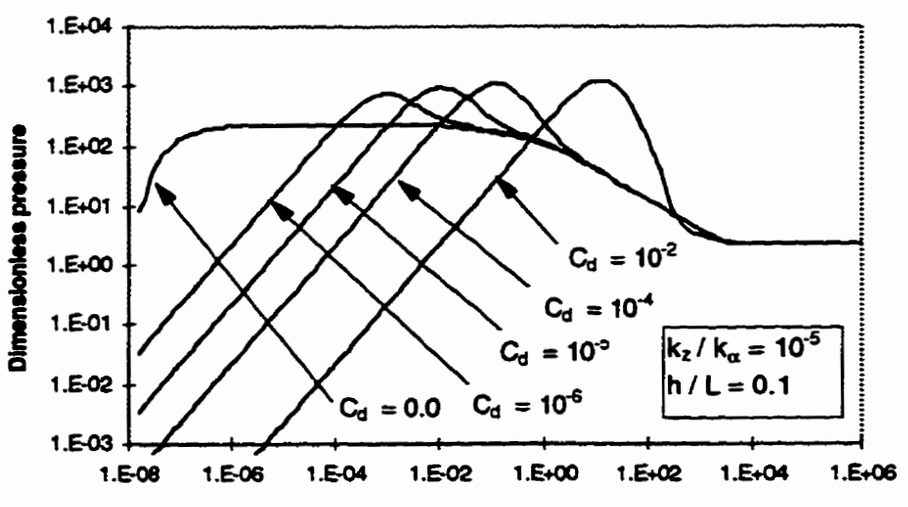

Figure 5.12 Wellbore storage effect on a VSH flow sequence horizontal well test presented in terms of logarithmic derivative.

Chapter Six

Effect of Formation Alteration Around a Well

6.1 Formation Alteration

6.1.1 Artificial stimulation

6.1.1.1 Hydraulic fracturing

Hydraulic fracturing, a method for increasing well productivity by fracturing the producing formation and thus increasing the formation permeability, was originally conceived and patented by R. F. Farris [Howard and Fast,1970]. The effectiveness of hydraulically created fractures is governed by the orientation, areal extent, and conductivity of the fracture system, and is evaluated by post-treatment production rate tests, compared to pretreatment transient well testing.

The effect of fracturing on both short and long term well productivity has been studied by many investigators, most of whom concluded that, regardless of the kind of treatment, four basic patterns of production behaviour have been observed:

Type - A: Sustained increase in well production accompanied by a flattening of the production decline curve following the treatment.

Type - B: Sustained increase in production with the higher production rate of the well after treatment declining essentially at the same rate which had been established before treatment.

Type - C: Transitory increase in production lasting from a few weeks to several months, after which the well continues to follow the production decline trend that was observed prior to treatment.

Type - D: No increase in production after treatment, with the well continuing to follow its established, normal production history.

As an example of the application of these concepts, Ghauri [1960] gave several well production histories after hydraulic fracturing treatment and analyzed them in terms of the four "type cases' outlined above.

The search for appropriate flow solutions for well evaluation after hydraulic fracturing has been extensive. The goal is to be able to conduct a relatively short-term well test on a hydraulically fractured well after clean-up, and to analyze that information in such a way that the long-term productivity (sustained-rate production) can be reliably predicted. One early approach to this goal was to modify existing solutions by considering the hydraulic fracturing treatment as adding a negative skin factor to the flow equation. However, this does not always work satisfactorily, particularly for short times; one study clearly shows that a negative skin effect was not sufficient to define short time well behaviour [Agarwal et al., 1970].

To consider the individual fracture as a boundary possessing infinite-conductivity or constant flow rate is an alternative method to analyze this problem quantitatively. Several solutions have been developed [Van Everdingen and Meyer, 1971; Russell and Truitt, 1964; Gringarten et al., 1974]. However, these solutions are generally too complicated to be used systematically by field engineers evaluating actual cases unless they are coded into a computer program, and there are always concerns about the suitability of the assumptions in particular cases.

6.1.1.2 Formation acidizing

The Pure Oil Co. in cooperation with Dow Chemical Co. performed the first acidizing of a oil well in 1932. By 1934 acidizing had become an accepted practice for well simulation in areas where the producing formation was limestone. Acidizing increases the diameter of the flow channels (pore throats, fracture apertures) in the limestone, and therefore increases the permeability in the near wellbore environment. Conventionally, these enhancements have been analyzed in a manner similar to hydraulic fractures, with modified flow equations incorporating a negative skin factor, or with a radially symmetric step-permeability flow model. In some cases, particularly those in vuggy dolomites or jointed limestones, the acidizing may have a more concentrated effect on channels, and instead of opening up and helping to unblock pore throats generally, a network of flow-enhanced tubes is created. These effects must be considered by the appropriate models, and it is not evident that a simple step-

permeability radial flow model is applicable to these cases. It would seem more appropriate to develop tools which provide transient or steady-state flow analyses based on a physically more realistic interpretation of the near-wellbore flow situation.

6.1.2 Non-artificial alteration

Formation improvement or damage refers to the process of changing formation parameters by other operating processes, either deliberate or natural. For example, particularly in a reservoir dominated by fissure flow, permeability may change because of stress redistribution after the well has been drilled, and this is a "natural" effect. Depending on the magnitudes of the stress field and the nature of the reservoir, the change of stress around a well can compress or dilate the formation and decrease or increase formation flow parameters. A similar effect could occur during injection of hot or cold fluids, which would cause fractures to close or open.

The formation also can be altered during the drilling operation. On the one hand, drill bit and drill pipe action can break or damage the formation near the wellbore to increase the permeability through microfissure generation or general shearing and extensional circumferential fracturing; on the other hand, drilling muds can invade the formation through the wellbore and thereby clog pore throats, change saturations, affect chemistry, and in general decrease the formation permeability. Other changes which occur during the production phase include fine-grained material migration, solids co-production, asphaltene or carbonate precipitation, all of which serve to contribute to the parameter alteration in the wellbore region, or even for a large region around the wellbore in the case of wells which have produced large amounts of sand.

6.2 Formation Alteration Analysis in the Literature

6.2.1 Alteration analysis around a horizontal well

Formation alteration around a horizontal well has been recognized as early as the horizontal well was considered for use by hydrogeologists and petroleum engineers. Formation parameters may change with radial distance from the wellbore because of stress redistribution, drilling damage, fine-grained material migration, solids co-production, asphaltene or carbonate precipitation, drilling mud invasion or some combination of these processes. The solutions for well test interpretation presented in Chapter 4, as

well as all other solutions reported in the literature, do not consider the true effect of these alterations on well test interpretation, but instead utilize the skin term concept in their development.

Some mechanisms in formation alteration around a horizontal are the same as in a vertical well situation, such as drilling damage and solids co-production. However, others may be more complicated than a vertical well, such as drilling mud infiltration. This is because a horizontal well is generally much longer than a vertical well, and therefore the infiltration time is longer near the heel (start section) than the toe (end section). This time difference can make the shape of the damaged zone like a cone along the well. The shape and distribution of damage around a horizontal well would also reflect the vertical-horizontal permeability anisotropy. During production, the large pressure gradient near the vertical section would result in a similar shape of production induced damage. During drilling, it is obvious that drilling mud penetration would generate a truncated cone with a large base near the vertical section of the well. The base of this cone would be radial if the reservoir is isotropic, and elliptical if it is anisotropic. If the vertical permeability is much smaller than the horizontal permeability (typical anisotropy), then the cone will be elliptical with the large axis of the ellipse being horizontal. In the case when the vertical permeability may be larger, then the large axis of the ellipse will be vertical.

Frick and Economides [1993] established an analytical expression for the skin term in such an elliptical shape damage zone using the following form:

$$s_{eq} = \left(\frac{k}{k_s}-1\right)\ln\left(\frac{1}{(I_{ani}+1)}\sqrt{\frac{4}{3}\left(\frac{a^2_{sH,\max}}{r_w^2} + \frac{a_{sH,\max}}{r_w}+1\right)}\right) \qquad (6.1.1)$$

However, the actual size of the damage ellipse zone will depend on the magnitude of the permeability around the well and the time of drilling. Generally, the size difference caused by fluid penetration will not be very large, and taking the average size to make a cylindrical shape assumption will be sufficient.

Therefore, the vertical well solution in most cases will be applicable for a horizontal well, particularly in the early vertical flow period. In the following sections we will develop a semi-analytical solution to simulate a well test in an altered reservoir. Obviously, this solution can also be used in horizontal well test interpretations.

6.2.2 Alteration analysis around a vertical well

Pumping or injection tests performed in vertical wells have traditionally been the standard methods used to evaluate the permeability and storage coefficient of aquifers for water supply purposes or in oil reservoir evaluation. The Theis [1935] solution, which assumes a fully penetrating well in a homogeneous, isotropic, infinite confined aquifer, is the most popular solution used by hydrogeologists, and its modifications by Muskat are the basis of petroleum reservoir evaluation. Formation alteration around a vertical well has also been recognized by hydrogeologists and petroleum engineers, but it is not considered in the basic solutions. Formation parameters may change with radius for the same reasons, as discussed above, around a horizontal well. To consider the influence of this altered permeability on productivity and well behaviour, several models have been proposed in the literature. One of the earliest models, which has also been adapted to the horizontal well solution, is the "skin term" model [Hawkins, 1956], in which an small thin skin close to the well was assumed, and an increase (or decrease) of permeability can cause a finite hydraulic head rise (drop) equivalent to the effect of the aquifer improvement or damage resulting from this skin. This model has been repeatedly used by petroleum engineers [Robert, 1977] and groundwater scientists [Moench, 1985]. The model assumes a zero thickness and storativity for the skin, and the hydraulic head drop across the skin is presumed to occur under steady flow conditions [Novakowski, 1989]. Because of the reality that the skin region must be finite in nature and have some storativity, many composite models have also been proposed [Olarewaju and Lee, 1987; Butler, 1988; Novakowski, 1989]. All these models assume a axisymmetric two-annulus aquifer around the wellbore, with permeability being constant within each zone, and an abrupt jump at the interface. Because permeability changes in the form of a step function with radius in these models, we will refer to them as "step permeability" models. However, both experiments and theoretical analysis show that most of the permeability changes because of formation alterations are continuous, rather than abrupt [Bennion and Thomas, 1994].

The step permeability model is probably a good approximation only when the altered zone has a small thickness. If the altered zone is very large, as arises in the case of massive sand production in a oil well [Geilikman et al., 1994], the two-zone step permeability model will likely be invalid. To more closely consider realistic cases, a multi-zonal composite model has been proposed [Kamal et al., 1992]. In this model, the altered zone is divided into many subzones with the average permeability in each subzone expressed as a constant. They also presented a relationship among the permeabilities which is expressed as: $k_i = a \cdot k_{i+1}^{\,b} + d$, where i stands for the i^{th} subzone, and a,b,d are constants. In two field examples to which the model was applied they found that $d = 0$ and $b = 1$, thus a linear relationship was obtained. Two difficulties arise in this model: first, it is often difficult to find the boundaries for many subzones; and second, the solution becomes more complicated with the increase

of the number of subzones. To develop a more realistic composite model, a continuously varying permeability which can be simply expressed and can also approximate the real permeability variation is desired; ideally, this solution would be semi-analytic instead of numerical to allow more easy inversions.

A new analytical solution has been developed for a two-zone composite model. The permeability in the first zone is assumed to change continuously in a power relationship with radius, and the permeability in the second zone is a constant and equals the original permeability. The permeability can change smoothly at the interface, or jump in a discontinuous manner, depending on the parameters considered most appropriate. The solution is obtained in the Laplace space, and numerical inversions are needed to evaluate the solution and to generate type curves for general well test interpretations.

6.3 A New Model for Alteration Analysis

6.3.1 Parameter variation because of formation alteration

Several reservoir parameters can be altered because of formation alteration, such as formation permeability, porosity, compressibility, Young's modulus and so on. Among those, the first three: the permeability, formation compressibility and porosity, are the most important ones in flow analysis. In order to consider the true effect of these altered parameters on well test interpretation, instead of using a simple skin term, the variation of the parameters with space and time are required. Unfortunately, such quantitative relationships are extremely rare, particularly when they are required in both the space and time domain. To simplify the problem, we would like only to consider the situation where the formation has already experienced the alteration. This assumption is reasonable in most practical problems because most of the formation alteration mechanisms are largely time independent, such as drilling damage or stress redistribution because of drilling. Other mechanisms can be time dependent, such as production induced alteration, sand production and fluid injection. We deal only with the first category in this chapter. We also assume the compressibility and porosity change because of formation alteration can be expressed by a step function; two constant values in both the alteration and unaltered zones. The continuous permeability variation model will be discussed in the following section.

6.3.2 Post alteration variation model in permeability

Permeability in an aquifer can be increased or decreased because of formation alteration. It is called formation improvement if the permeability is increased and formation damage if it is decreased. Formation alteration can be caused by several factors. Drilling damage can induce mechanical breakage of the wellbore (improvement) or mud invasion (damage). The former is of considerable interest to borehole stability in shales [Dusseault, 1994]; the latter is commonly found in drilling sandstone reservoirs and aquifers, and is usually deliberately cleaned up during completion to guarantee good productivity. Stress-induced alterations involve the compaction or dilation of the aquifer because of stress redistribution around the well, and effects may be expected to be the largest in those reservoirs dominated by fracture flow, as fracture permeability is most susceptible to effective stress changes. Large-scale solids production, usually found in uncemented heavy oil reservoirs, can alter the permeability in zones that may approach several tens of meters, particularly if hundreds of cubic metres of sand are produced over prolonged time periods [Geilikman et al., 1994]. Accompanying the permeability change in this case are large-scale porosity and compressibility alterations. In the case of fine-grained material migration, the permeability can be massively altered as well, but for a smaller zone, perhaps a meter or two, and the porosity and compressibility alterations are far more moderate than in the case of massive solids production. In heavy oil production, asphaltenes precipitating near the wellbore can also impair permeability, and similar effects can be envisioned in cases of aquifer production.

Exactly how the permeability is altered by these processes remains a challenging topic, exacerbated by the lack of suitable models and the difficulty of careful sampling of the near-wellbore environment. The relationship used by Kamal et al., [1992], for example, is one approximation available in the literature for formation damage. An experiment concerning formation damage is presented by Bennion and Thomas [1994], where continuous permeability-radius data were published. Real cases concerning explicit measurements of permeability increases caused by solids production are rare. One theoretical derivation of the porosity-radius relationship in the altered zone was proposed by Geilikman et al., [1994]. The model suggests that the porosity increases caused by solids production are in a power relationship with radius at any moment, and can be expressed as $\phi = \phi_0 - Mr^{\alpha}$, where ϕ_0, α are constants and M is a function of formation properties, well radius, and time.

Relationships between porosity and permeability have been well tabulated in the literature; most of these are linear or power-law approximations. The former includes the capillary tube model based on the Hagen-Poisseuille law [Scheidegger, 1960], and the fissure model [Irmay, 1955]. The latter

includes the hydraulic radius model and the resistance flow model [Rumer, 1969].

It therefore seems reasonable to express the permeability variation with radius as a power relationship in the form $k = k_2 + k_0 r^{\alpha}$; however, some difficulties arise in applying this relationship. First, it does not show any "composite" properties, i.e. the permeability changes within a limited area around the well and becomes the constant original permeability outside the altered zone. Second, it becomes more complicated to solve the resulting boundary value problem analytically. To make it simple, a two-part relationship is suggested: it is assumed that in the altered zone the permeability can be expressed as $k = k_0 r^{\alpha}$, and outside the altered zone it is a constant $k = k_2$. These relationships are mathematically written as:

$$\begin{aligned} k(r) &= k_0 r^{\alpha} && r_w \le r < r_s \\ k(r) &= k_2 && r \ge r_s \end{aligned} \qquad (6.3.1)$$

where k_0, α and k_2 are constants, r_s is the radius of the altered zone and r_w is the well radius.

Using the dimensionless variable $r_d = r/r_w$ instead of r, equation (6.3.1) can be written as:

$$\begin{aligned} k(r_d) &= k_1 r_d^{\alpha} && 1 < r_d < r_{ds} \\ k(r_d) &= k_2 && r_d \ge r_{ds} \end{aligned} \qquad (6.3.2)$$

where $k_1 = k_0 r_w^{\alpha}$ is the permeability at the wellbore, k_2 is the original formation permeability in the un-altered zone, and $r_{ds} = r_s/r_w$ is the radius of the altered zone in dimensionless form.

Using equation (6.3.2), if $\alpha > 0$, then k increases with radius, and this represents formation damage (i.e., reduced k near the wellbore, rising to the original k away from the wellbore). If $\alpha < 0$, then k decreases with radius to the virgin state, which represents formation improvement. If $\alpha = 0$, the relationship may be used to represent the two-zone, single-step permeability model. Figure 6.1 graphically shows these relationships for various values of the power law parameters. The model is therefore highly general compared to either the single-step or the multi-step permeability model.

It may be stated from observing the figure that if the permeability is maintained continuous across the interface, α may be interpreted as the "degree" of improvement or damage of the formation if the size of the altered zone r_{ds} is fixed. Alternatively, it represents the "extent" of the alteration in the

formation if the permeability at the wellbore k_1 is fixed. The boundary value problems solved here are based on these permeability relationships and will be referred to as the "power permeability" model.

Figure 6.2 shows experimental data (symbols) on permeability variation reported by Marx and Rahman [1987], and the lines are permeability variations simulated with the power permeability model (6.3.2). The power permeability model simulation curves agree with the experimental data quite well.

6.3.3 Pressure analysis in an altered reservoir

The mathematical description of the composite model for a fully penetrating well with permeabilities defined above can be described as:

$$\frac{1}{r}\frac{\partial}{\partial r}[T_1 r_d^{\alpha} r\frac{\partial s_1}{\partial r}] = S_1\frac{\partial s_1}{\partial t} \qquad (r_w \le r < r_s) \tag{6.3.3}$$

$$\frac{1}{r}\frac{\partial}{\partial r}[T_2 r\frac{\partial s_2}{\partial r}] = S_2\frac{\partial s_2}{\partial t} \qquad (r \ge r_s) \tag{6.3.4}$$

where, $T_1 = k_1 h\rho g/\mu$, $T_2 = k_2 h\rho g/\mu$ are transmissivities with subscripts 1 and 2 denoting the altered and unaltered regions, respectively, s is hydraulic head drawdown, S_1 and S_2 are storativities, r_d is the dimensionless radial distance from the well, and r_s is the radius of the altered zone.

The initial condition is:

$$s_1(r,t)|_{t=0} = s_2(r,t)|_{t=0} = 0 \tag{6.3.5}$$

and the boundary conditions at the infinite far-field and wellbore are:

$$s_2(r,t)|_{r\to\infty}=0 \tag{6.3.6}$$

$$2\pi T_1 r_w \frac{\partial s_1}{\partial r}|_{r=r_w} - C_w \frac{\partial s_1}{\partial t}|_{r=r_w} = -Q \tag{6.3.7}$$

where C_w is a constant describing wellbore storage capacity and is equal to πr_c^2 for an open pumping well with standpipe radius r_c.

The boundary conditions at the interface r_s of the two regions must satisfy the continuity conditions:

$$s_1(r_s,t) = s_2(r_s,t) \tag{6.3.8}$$

$$T_1 r_{ds}^{\alpha} \frac{\partial s_1}{\partial r}|_{r=r_s} = T_2 \frac{\partial s_2}{\partial r}|_{r=r_s} \tag{6.3.9}$$

If we define and substitute the following dimensionless variables:

$$t_d = \frac{T_2}{S_2 r_w^2} t \qquad s_d = \frac{2\pi T_2}{Q} s, \qquad \theta = \frac{T_2}{T_1} \tag{6.3.10}$$

into equations (6.3.3) and (6.3.4), then apply the Laplace transform (considering the initial condition (6.3.5)) to equations (6.3.3) and (6.3.4), the following equations are obtained:

$$\frac{1}{r_d}\frac{\partial}{\partial r_d}[r_d^{\alpha+1}\frac{\partial \bar{s}_{d1}}{\partial r_d}] = A_m^2 \bar{s}_{d1} \tag{6.3.11}$$

$$\frac{1}{r_d}\frac{\partial}{\partial r_d}[r_d\frac{\partial \bar{s}_{d2}}{\partial r_d}] = B_m^2 \bar{s}_{d2} \tag{6.3.12}$$

where $A_m = \sqrt{p\theta\beta}$, $B_m = \sqrt{p}$, $\beta = S_1/S_2$ is the storativity ratio of the two zones, and p is the Laplace transform variable.

The Laplace transformed boundary conditions of (6.3.6) and (6.3.7) are:

$$\bar{s}_{d2}(r_d,p)|_{r_d\to\infty} = 0 \tag{6.3.13}$$

$$\frac{\partial \bar{s}_{d1}}{\partial r_d}|_{r_d=1} - C_d\, p\theta \bar{s}_{d1}|_{r_d=1} = -\frac{\theta}{p}|_{r_d=1} \tag{6.3.14}$$

where $C_d = C_w/(2\pi r_w^2 S_2)$ and the internal boundary conditions (6.3.8) and (6.3.9) become:

$$\bar{s}_{d1}(r_{ds},p) = \bar{s}_{d2}(r_{ds},p) \tag{6.3.15}$$

$$\frac{\partial \bar{s}_{d1}}{\partial r_d}|_{r_d=r_{ds}} = \frac{\theta}{r_{ds}^{\alpha}} \frac{\partial \bar{s}_{d2}}{\partial r_d}|_{r_d=r_{ds}} \tag{6.3.16}$$

The governing equation for the unaltered region (6.3.12) together with its far-field boundary condition (6.3.13) can be solved in the Laplace space to produce an expression of the following form [Carslaw and Jaeger,1959]:

$$\bar{s}_{d2} = CK_0(B_m r_d) \tag{6.3.17}$$

where $K_0(z)$ is the modified Bessel function of the second kind and order zero, and C is a constant which is to be determined by the internal boundary conditions (6.3.15) and (6.3.16).

To solve the equation of the altered zone (6.3.11), we define a new variable ξ as:

$$r_d = \xi^m , \quad i.e. \quad dr_d = m\xi^{m-1}d\xi \tag{6.3.18}$$

and if we substitute the relationships of (6.3.18) into (6.3.11), we obtain:

$$\frac{\partial^2 \bar{s}_{dl}}{\partial \xi^2} + \frac{m\alpha+1}{\xi}\frac{\partial \bar{s}_{dl}}{\partial \xi} = m^2 A_m^2 \xi^{m(2-\alpha)} \bar{s}_{dl} \qquad \textbf{(6.3.19)}$$

Obviously if m is defined as:

$$m(2-\alpha) - 2 = 0\ , \qquad i.e. \qquad m = \frac{2}{2-\alpha} \qquad \textbf{(6.3.20)}$$

where $\alpha \neq 2$, then equation (6.3.19) can be simplified to:

$$\frac{\partial^2 \bar{s}_{dl}}{\partial \xi^2} + \frac{2+\alpha}{2-\alpha}\frac{1}{\xi}\frac{\partial \bar{s}_{dl}}{\partial \xi} = m^2 A_m^2 \bar{s}_{dl} \qquad \textbf{(6.3.21)}$$

The wellbore boundary condition of (6.3.14) at $\xi = r_d^{1/m} = 1$ becomes:

$$\frac{\partial \bar{s}_{dl}}{\partial \xi} - C_d \theta m p\ \bar{s}_{dl}|_{\xi=1} = -\frac{m\theta}{p} \qquad \textbf{(6.3.22)}$$

and the internal boundary conditions (6.3.15) and (6.3.16) at $\xi_s = r_{ds}^{1/m}$ become:

$$\bar{s}_{dl}(\xi_s, p) = \bar{s}_{d2}(r_{ds}, p) \qquad \textbf{(6.3.23)}$$

$$\frac{\partial \bar{s}_{dl}}{\partial \xi}|_{\xi=\xi_s} = m\theta \xi_s^{\gamma} \frac{\partial \bar{s}_{d2}}{\partial r_d}|_{r_d=r_{ds}} \qquad \textbf{(6.3.24)}$$

where $\gamma = -\alpha/(2-\alpha) = 1 - m$.

Equation (6.3.21) can be further simplified by defining another new variable X as: $s_{dl} = \xi^{\nu} X$, and by applying its first and second order derivatives:

$$\frac{\partial \bar{s}_{dl}}{\partial \xi} = \gamma \xi^{\gamma-1} X + \xi^{\gamma} \frac{\partial X}{\partial \xi} \tag{6.3.25}$$

$$\frac{\partial^2 \bar{s}_{dl}}{\partial \xi^2} = \gamma(\gamma-1)\xi^{\gamma-2} X + 2\gamma \xi^{\gamma-1} \frac{\partial X}{\partial \xi} + \xi^{\gamma} \frac{\partial^2 X}{\partial \xi^2} \tag{6.3.26}$$

equation (6.3.21) becomes the standard modified Bessel partial differential equation :

and its solution has the following form:

$$X = A I_{\gamma}(mA_m \xi) + B K_{\gamma}(mA_m \xi) \tag{6.3.28}$$

Substituting s_{dl} back into (6.3.28), we obtain:

$$\bar{s}_{dl} = \xi^{\gamma}\left[A I_{\gamma}(\lambda\xi) + B K_{\gamma}(\lambda\xi)\right] \tag{6.3.29}$$

where $\lambda = mA_m$ and, the two constants A and B are to be determined by the boundary conditions of in (6.3.22), (6.3.23) and (6.3.24).

By using the derivative properties of modified Bessel's functions (A3) of Appendix 6.1, the wellbore boundary condition (6.3.22) can be written in terms of solution (6.3.29) as:

$$\begin{aligned} -\frac{m\theta}{p} &= \lambda[A I_{\gamma-1}(\lambda) - B K_{\gamma-1}(\lambda)] \\ &- C_d \theta m p [A I_{\gamma}(\lambda) + B K_{\gamma}(\lambda)] \end{aligned} \tag{6.3.30}$$

If constant A is expressed as $A = R_1 - B R_2$ where:

$$R_1 = \frac{\theta}{p[C_d \theta p I_{\gamma}(\lambda) - A_m I_{\gamma-1}(\lambda)]} \tag{6.3.31}$$

$$R_2 = \frac{A_m K_{\gamma-1}(\lambda) + C_d \theta p K_\gamma(\lambda)}{C_d \theta p I_\gamma(\lambda) - A_m I_{\gamma-1}(\lambda)} \tag{6.3.32}$$

then solution (6.3.29) becomes:

$$\bar{s}_{dI} = \xi^\gamma \left[R_1 I_\gamma(\lambda\xi) + B[K_\gamma(\lambda\xi) - R_2 I_\gamma(\lambda\xi)] \right] \tag{6.3.33}$$

If we apply the identical drawdown condition at the interface (6.3.23) to solutions (6.3.17) and (6.3.29) we have:

$$CK_0(B_m r_{ds}) - R_1 \xi_s^\gamma I_\gamma(\lambda\xi_s) = B\xi_s^\gamma [K_\gamma(\lambda\xi_s) - R_2 I_\gamma(\lambda\xi_s)] \tag{6.3.34}$$

and if we apply the identical cross flow condition (6.3.24) at the interface to solutions (6.3.17) and (6.3.29) we have:

$$Cm\theta B_m K_1(B_m r_{ds}) + \lambda R_1 I_{\gamma-1}(\lambda\xi_s) = \lambda B \left[K_{\gamma-1}(\lambda\xi_s) + R_2 I_{\gamma-1}(\lambda\xi_s) \right] \tag{6.3.35}$$

Solve equations (6.3.34) and (6.3.35) simultaneously to obtain:

$$\frac{CK_0(B_m r_{ds}) - R_1 \xi_s^\gamma I_\gamma(\lambda\xi_s)}{Cm\theta B_m K_1(B_m r_{ds}) + \lambda R_1 I_{\gamma-1}(\lambda\xi_s)} = \frac{\phi_1}{\phi_2} \tag{6.3.36}$$

where:

$$\begin{aligned} \phi_1 &= \xi_s^\gamma [K_\gamma(\lambda\xi_s) - R_2 I_\gamma(\lambda\xi_s)] \\ \phi_2 &= \lambda [K_{\gamma-1}(\lambda\xi_s) + R_2 I_{\gamma-1}(\lambda\xi_s)] \end{aligned} \tag{6.3.37}$$

By applying the property (A3) of Appendix 6.1, we obtain the following relationship:

$$R_1 \xi_s^{\gamma} I_{\gamma}(\lambda \xi_s)\phi_2 + \lambda R_1 I_{\gamma-1}(\lambda \xi_s)\phi_1 = \frac{R_1}{r_{ds}} \tag{6.3.38}$$

and constant C is obtained from equations (6.3.36), (6.3.37) and (6.3.38):

$$C = \frac{R_1}{r_{ds}\left[\lambda K_0(B_m r_{ds})[K_{\gamma-1}(\lambda \xi_s)+R_2 I_{\gamma-1}(\lambda \xi_s)] - m\theta B_m \xi_s^{\gamma} K_1(B_m r_{ds})[K_{\gamma}(\lambda \xi_s)-R_2 I_{\gamma}(\lambda \xi_s)]\right]} \tag{6.3.39}$$

Constants B and A are therefore obtained as:

$$B = \frac{CK_0(B_m r_{ds}) - R_1 \xi_s^{\gamma} I_{\gamma}(\lambda \xi_s)}{\xi_s^{\gamma}[K_{\gamma}(\lambda \xi_s) - R_2 I_{\gamma}(\lambda \xi_s)]}, \quad A = \frac{R_1 \xi_s^{\gamma} K_{\gamma}(\lambda \xi_s) - R_2 CK_0(B_m r_{ds})}{\xi_s^{\gamma}[K_{\gamma}(\lambda \xi_s) - R_2 I_{\gamma}(\lambda \xi_s)} \tag{6.3.40}$$

If we substitute the constants A, B and C into solutions (6.3.29) and (6.3.17), we obtain the altered zone solution:

$$\bar{S}_{d1} = \xi_{\gamma}\left[\frac{R_1[K_{\gamma}(\lambda \xi_s)I_{\gamma}(\lambda \xi) - I_{\gamma}(\lambda \xi_s)K_{\gamma}(\lambda \xi)]}{K_{\gamma}(\lambda \xi_s) - R_2 I_{\gamma}(\lambda \xi_s)} + \frac{CK_0(B_m r_{ds})[K_{\gamma}(\lambda \xi) - R_2 I_{\gamma}(\lambda \xi)]}{\xi_s^{\gamma}[K_{\gamma}(\lambda \xi_s) - R_2 I_{\gamma}(\lambda \xi_s)]}\right] \tag{6.3.41}$$

and the unaltered zone solution :

$$\bar{S}_{d2} = CK_0(B_m r_d) \tag{6.3.42}$$

6.3.4 Solution verification

Verification of the solutions (6.3.41) and (6.3.42) can be performed by comparing to existing solutions for special cases that appear in the literature. If $\alpha = 0$ and $\theta \neq 1$, then $m = 1$, $\gamma = 0$, and $\xi = r_d$. The

solutions lead directly to the solutions derived by Novakowski [1989].

If we assume $\alpha = 0$, $\theta = 1$ and $\beta = 1$, i.e. the permeability and storativity are the same in both zones, then we have $A_m = B_m$. By using the properties of (A1) and (A3) (Appendix 6.1), the constant C of (6.3.39) becomes:

$$C = \frac{R_1}{r_{ds}A_m R_2[K_0(A_m r_{ds})I_1(A_m r_{ds}) + I_0(A_m r_{ds})K_1(A_m r_{ds})]} = \frac{R_1}{R_2} = \frac{1}{p[C_d p K_0(B_m) + B_m K_1(B_m)]} \tag{6.3.43}$$

Constants B and A become:

$$B = \frac{R_1[K_0(B_m r_{ds}) - R_2 I_0(B_m r_{ds})]}{R_2[K_0(B_m r_{ds}) - R_2 I_0(B_m r_{ds})]} = C$$

$$A = \frac{R_1[K_0(B_m r_{ds}) - K_0(B_m r_{ds})]}{K_0(B_m r_{ds}) - R_2 I_0(B_m r_{ds})]} = 0 \tag{6.3.44}$$

and the solution simplifies to:

$$\bar{s}_1 = \bar{s}_2 = \frac{K_0(\sqrt{p}\, r_d)}{p[C_d p K_0(\sqrt{p}) + \sqrt{p}\, K_1(\sqrt{p})]} \tag{6.3.45}$$

This is the well flow solution in an homogeneous isotropic aquifer considering the wellbore storage effect given by Papadopulos and Cooper [1967].

If $r_{ds} = 1$, which also means no altered zone exists, then $\xi_s = 1$ equations (6.3.41) and (6.3.42) also give the identical solution to (6.3.45). Therefore, the new solution corresponds precisely to well-known existing solutions in the limiting cases, giving confidence in the use of the new results for general cases.

6.3.5 Production analysis in an altered reservoir

The evaluation of well production in the transient flow period is usually obtained by evaluating the production variation with time when the wellbore pressure (hydraulic head) is fixed as a constant. The pressure solution obtained in the above section can not be used in production evaluation because a constant flow rate is assumed as the wellbore condition.

To analyze the production in such an altered reservoir, the wellbore condition of (6.3.7) must be changed into the following constant pressure (hydraulic head) condition:

$$s_1(r, t)|_{r=r_w} = s_w \tag{6.3.46}$$

If we redefine the dimensionless pressure s_d as:

$$s_d = \frac{s}{s_w} \tag{6.3.47}$$

and maintain other dimensionless variables the same as defined in (6.3.10) then we obtain the same governing equation as equations (6.3.11) and (6.3.12) for flow in the two zones. The boundary condition of (6.3.14) becomes:

$$\bar{s}_{d1}(r_d, p)|_{r_d=1} = \frac{1}{p} \tag{6.3.48}$$

and the interface boundary is still the same as in (6.3.15) and (6.3.16).

The procedure in solving the constant wellbore pressure condition is the same as in the constant wellbore flow condition, and if we use the relationship of $\xi^m = r_d$ to $r_{dw} = 1$, we have $\xi_w = 1$. The constant wellbore pressure condition, however, gives the following relationship which corresponds to equation (6.3.30) of the constant flow condition:

$$\frac{1}{p} = AI_\gamma(\lambda) + BK_\gamma(\lambda) \tag{6.3.49}$$

Therefore, parameters R_1 and R_2 in equations (6.3.31) and (6.3.32) change to:

$$R_1 = \frac{1}{pI_\gamma(\lambda)}, \qquad R_2 = \frac{K_\gamma(\lambda)}{I_\gamma(\lambda)} \tag{6.3.50}$$

Because other conditions are the same as in the constant wellbore flow analysis, the only difference between them is the different R_1 and R_2 formulations in equation (6.3.50).

The wellbore production can be obtained by using Darcy's law:

$$Q = -2\pi T_1 r_d^{\alpha} r_w \frac{\partial s_1}{\partial r} \tag{6.3.51}$$

where C_w is the wellbore storage coefficient.

If we substitute the dimensional variables s_d, t_d and $r_d = \xi^m$ into equation (6.3.51) we obtain:

$$Q = -\frac{2\pi T_1 s_w}{m\xi^\gamma} \frac{\partial s_{d1}}{\partial \xi} \tag{6.3.52}$$

and the Laplace transformed Q becomes:

$$\bar{Q} = -\frac{2\pi T_1 s_w}{m} \frac{\partial \bar{s}_{d1}}{\partial \xi} \tag{6.3.53}$$

The derivative of s_{d1} with respect to ξ can be obtained from solution (6.3.41), which gives:

$$\frac{\partial \bar{s}_{d1}}{\partial \xi} = \lambda\xi^\gamma [AI_{\gamma-1}(\lambda\xi) - BK_{\gamma-1}(\lambda\xi)] \tag{6.3.54}$$

and the well production rate in the Laplace space (6.3.53) becomes:

$$\bar{Q} = -2\pi T_1 s_w A_m [A I_{\gamma-1}(\lambda) - B K_{\gamma-1}(\lambda)] \tag{6.3.55}$$

If we define the dimensionless wellbore storage coefficient $C_d = C_w/(2\pi r_w^2 S_2)$, and the dimensionless well production rate $Q_d = Q/(2\pi T_2 s_w)$, the dimensionless production rate gives the following solution:

$$\bar{Q}_d = \frac{A_m}{\theta} [B K_{\gamma-1}(\lambda) - A I_{\gamma-1}(\lambda)] \tag{6.3.56}$$

Obviously, the well production rate Q_d must be inverted numerically.

6.4 Well test interpretation in an altered formation

6.4.1 Pressure variation in an altered formation

Heterogeneity of aquifers directly affects hydraulic head distribution with space and time in the transient period. The hydraulic head (drawdown) distributions under the proposed power permeability models can be evaluated by numerically inverting the solutions obtained. Stehfest's Laplace inversion algorithm has been used in the evaluation in this paper [Stehfest, 1970].

Figure 6.3 shows hydraulic head (drawdown) variation with radial distance in an altered formation obtained by this power permeability model. From this figure we find that the effect of permeability alteration on pressure distribution is only observable in the altered zone. The drawdown-radius curves of altered permeability fall into the homogeneous one ($\alpha = 0$) at a point within the altered zone. An increment of the altered permeability (negative α) reduces the drawdown, and a decrease (formation damage) of the altered permeability increases the drawdown, compared to the homogeneous case ($\alpha = 0$).

The type curves of drawdown with time generated under this power permeability model show similar properties, as shown in Figure 6.4. The magnitude of drawdown of these type curves increases with increasing value of the power parameter α, because larger α values mean more damage to the aquifer. Because of the difference in drawdown values presented from the type curves in Figure 6.4, the curve matching method is a possible means to identify formation alterations by estimating the power

parameter of a field well test.

The type curves generated in Figure 6.4 neglect the effect of wellbore storage. If this effect is considered, then typical type curves are shown in Figure 6.5, where the storage parameter $C_d = 1000$ is used. The effect of wellbore storage on type curves of an altered formation is similar to the homogeneous cases discussed in the literature. A linear relationship is presented in the early times where wellbore storage is the dominant factor controlling the drawdown rate. After the storage dominant period, the effect gradually vanishes. Type curves with different degrees of formation alteration still possesses the differences caused by the magnitude of α in the wellbore storage situations considered.

6.4.2 Logarithmic pressure derivatives in an altered formation

The effect of formation alteration can be more clearly observed in a logarithmic derivative graph as shown in Figure 6.6, because the logarithmic derivative of pressure drawdown gives a horizontal line in a log-log graph after a very short period at the beginning of a test. The effect of different α values is clearly presented in Figure 6.6. From Figure 6.6 we find that the type curves under formation enhancement (negative α) are below the homogeneous formation type curve, and type curves under formation damage are above the homogeneous one. Therefore, from this figure it is possible to determine the degree of formation alteration if a test derivative curve is matched to the type curves generated, such as in Figure 6.6.

The size of the altered zone can also be determined if a test curve is compared with the type curves generated under different alteration radii, such as the one shown in Figure 6.7, where a formation enhancement is assumed (α = -0.5). Different sizes of alteration are represented by approximately parallel line segments at early times, and the segments intersect the late time horizontal line at different times. Because these intersection times are independent of the alteration degree (Figure 6.6), therefore they directly reflect the size of the alteration. For a damaged formation (positive α), similar results are obtained, as shown in Figure 6.8. From a theoretical analysis, we find that the alteration size has the following approximate relationship with the dimensionless time:

$$t_d = r_{ds}^n \tag{6.4.1}$$

where n is a constant which takes values between 2 and 3.

If the wellbore storage effect is considered, the derivative curves are as shown in Figure 6.9. Because wellbore storage is the dominant factor in the early time period of a test, the alteration effect in this time period is most likely to be masked by the wellbore storage. However, if the alteration effect time is longer than the wellbore storage effect time, then it is still possible to identify the degree of alteration from the unmasked part of the derivative curves (Figure 6.9). Figure 6.10 shows the alteration size effects presented in derivative type curves considering the wellbore storage effect. One obvious effect of the wellbore storage is that equation (6.4.1) may become invalid for small alteration sizes, such as $r_{ds} = 50$ in Figure 6.10.

6.4.3 Comparisons between the power and step permeability model

Figure 6.11 and Figure 6.12 compare the power permeability model (solid lines) with the step permeability model (dotted lines). The case of $\alpha = 0$ corresponds to the homogeneous aquifer case obtained from the power permeability model. The step permeability model also requires setting $\alpha = 0$, but the constant altered permeability k_1 is a steady-sate equivalent average obtained by assuming the same flow rate and pressure drawdown between the wellbore and altered boundary and which has the following form:

$$k = \frac{k_2 \alpha \ln(r_{ds})}{r_{ds}^{\alpha} - 1} \tag{6.4.2}$$

The drawdown difference between the step permeability model and power permeability model is shown in Figure 6.11 and 6.12. The step permeability by using the equivalent permeability k obtained form (6.4.2) has a similar effect as decreasing the α value of the power permeability model (Figure 6.11). However, in Figure 6.12 we find that besides the magnitude difference of drawdown, the shape of the type curves can be different between the step and power permeability models. This shape deviation becomes more obvious for heavily improved aquifer (increased permeability) situations (Figure 6.12).

6.4.5 Production evaluation

Well productivity in the transient flow period can be evaluated by using the constant wellbore pressure (hydraulic head) solution of (6.3.56). Under the constant wellbore pressure condition, well production

rate Q will vary with time. Figure 6.13 shows the production variation with time in an permeability enhanced reservoir (negative α values). Generally, the production rate will decrease with time regardless if the reservoir is altered or not, and the production increase caused by the improvement of permeability near the well is only beneficial in the early production times. As the production time becomes longer, the production rate gradually decreases to the non-alterted rate, as has been observed in the field.

However, if the reservoir is damaged instead of improved, the production decreases not only at the early production times, but also at late times. The damaged (positive α) reservoir production is shown in Figure 6.14. This indicates that if a reservoir is damaged, then use of reservoir stimulation approaches to overcome the damage can improve a production well significantly.

Figures 6.13 and 6.14 also imply that artificial reservoir stimulation, such as hydraulic fracturing or reservoir acidizing are only beneficial economically for damaged reservoirs. For non-damaged reservoir, such methods can only be beneficial at early times, provided that the production reservoir is very large (laterally infinite condition). Because most of production patterns limit the production area of each well to a finite size, an increase of the permeability near the well may not be beneficial in the long term.

6.5 Model Application to Horizontal Wells

Formation alteration mechanisms for horizontal wells will yield similar characteristics as for the vertical well discussed above. The mechanism of alteration for a horizontal well can also result in an increase or decrease in permeability around the wellbore. If the alteration radius around the horizontal well is less than the distance from the well to the upper or lower boundary, then it has exactly the same effects as the vertical well, because both vertical and horizontal wells have the permeability near the entry area altered. However, horizontal wells are usually drilled in thin reservoirs with the well length much larger than the reservoir thickness. It is quite possible that the alteration will reach the upper and lower boundaries. If this is the case, then the early vertical radial flow period actually takes place in the altered zone, and will obviously show the same behaviour as the vertical well. The early time horizontal line of the logarithmic derivative, therefore, will have the same characteristics as those presented in Figure 6.6 - Figure 6.10. The identification of such characteristics will also be the same, as discussed in the last section. In such situations, the whole vertical flow regime may be affected and this makes the identification of the early flow regime difficult.

If the alteration radius is greater than the upper and lower boundaries, then both the early and middle linear flow regimes will also be affected by the alteration effects. On the other hand, if the alteration also appears beyond the well length, then the middle time spherical and the late time horizontal flow regimes will also be affected by the alteration. Such alterations will affect the appearance of the straight lines of the middle, as well as of the late time segmental lines in a derivative graph. However, identification of the size and degree of the alteration is still possible.

APPENDIX 6.1 Some Properties of Modified Bessel Functions

1. Modified Bessel functions of negative order satisfy:

$$I_{-\gamma}(z) = I_{\gamma}(z) + \frac{2\sin(\gamma\pi)K_{\gamma}(z)}{\pi}$$
$$K_{-\gamma}(z) = K_{\gamma}(z) \tag{A1}$$

and if of integer order n, (A1) becomes:

$$I_{-n}(z) = I_{n}(z), \quad K_{-n}(z) = K_{n}(z) \tag{A2}$$

2. Derivatives of Modified Bessel functions

$$\frac{d}{dz}[z^{\gamma}I_{\gamma}(\beta z)] = \beta z^{\gamma}I_{\gamma-1}(\beta z)$$
$$\frac{d}{dz}[z^{-\gamma}K_{\gamma}(\beta z)] = -\beta z^{-\gamma}K_{\gamma-1}(\beta z) \tag{A3}$$

and if $\gamma = 0$ then

$$I_0'(z) = I_1(z), \quad K_0'(z) = -K_1(z) \tag{A4}$$

3. Some relationships of Modified Bessel functions

$$I_{\gamma}(z)K_{\gamma+1}(z) + K_{\gamma}(z)I_{\gamma+1}(z) = \frac{1}{z}$$
$$I_{\gamma}(z)K_{\gamma}'(z) - K_{\gamma}(z)I_{\gamma}'(z) = -\frac{1}{z} \tag{A5}$$

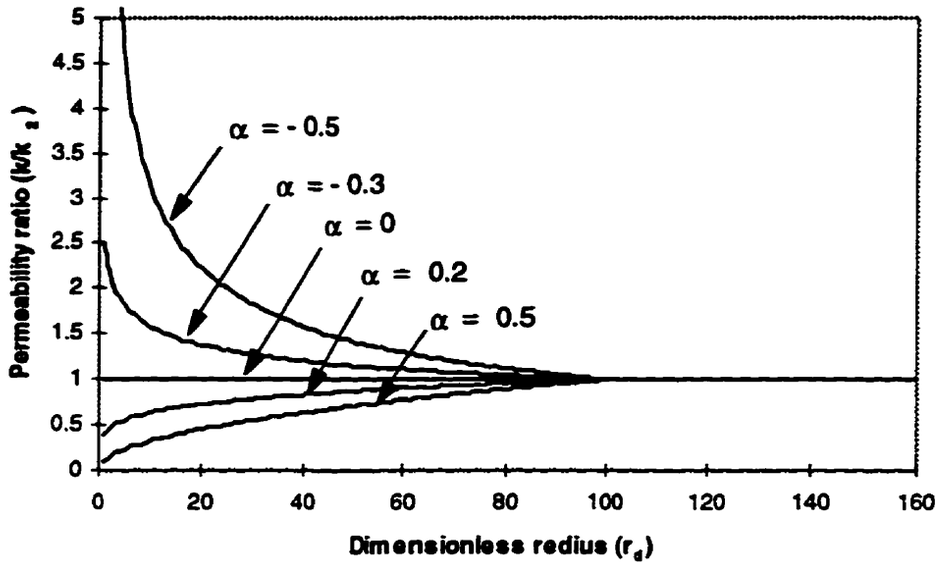

Figure 6.1 Permeability variations along radius using the power permeability model with different power parameter values.

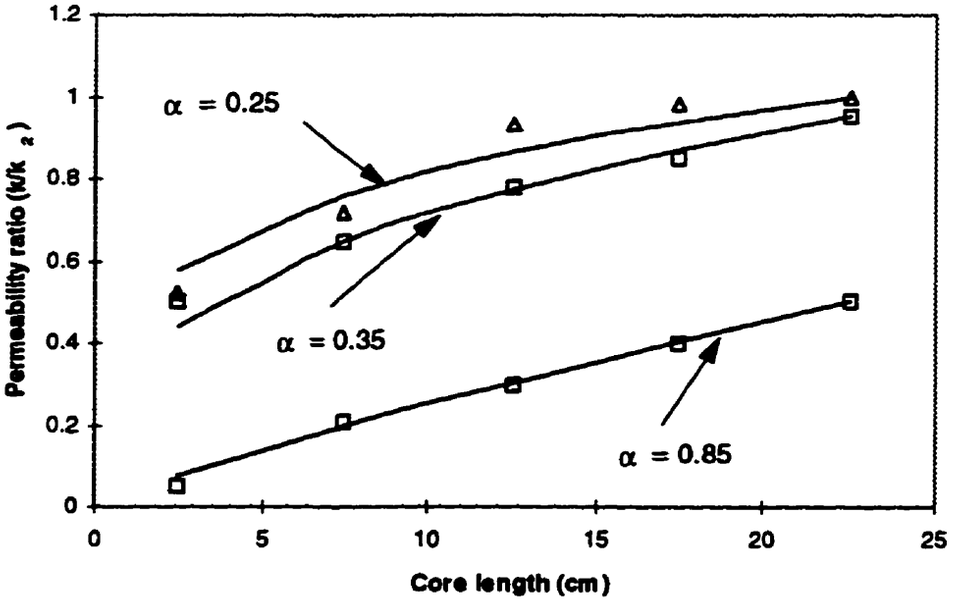

Figure 6.2 Comparison between the power permeability model predicted permeability variation with experimental data (after Claus, 1987).

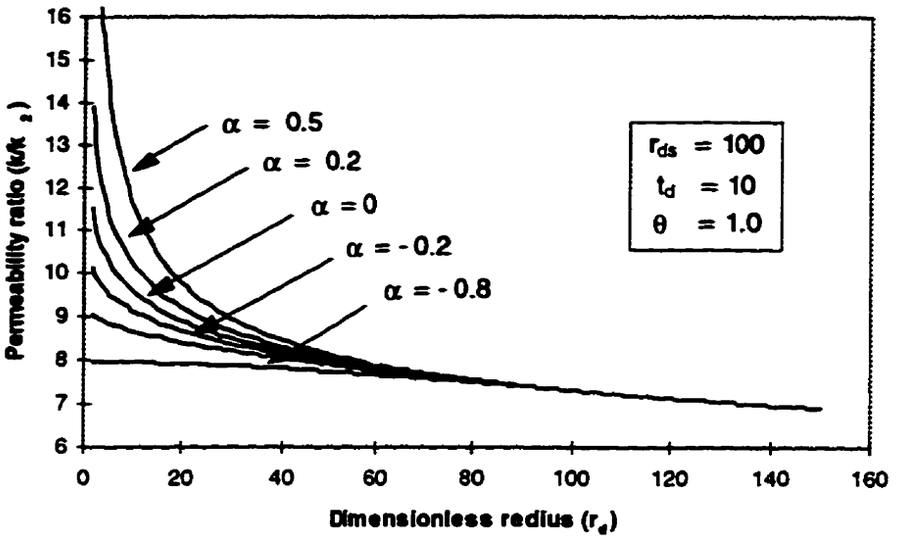

Figure 6.3 Hydraulic head (drawdown) variations along radius using different power parameter values.

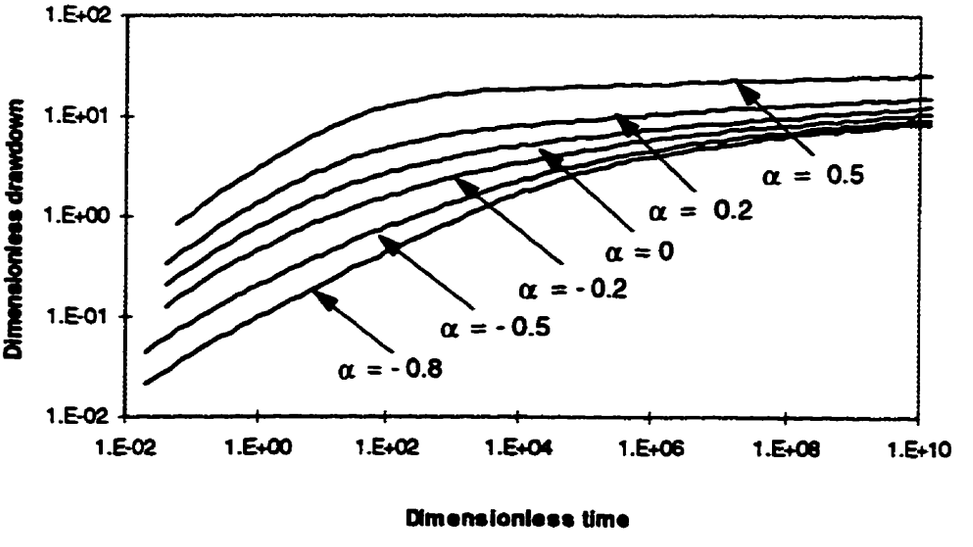

Figure 6.4 Hydraulic head (drawdown) variations with time using different power parameter values.

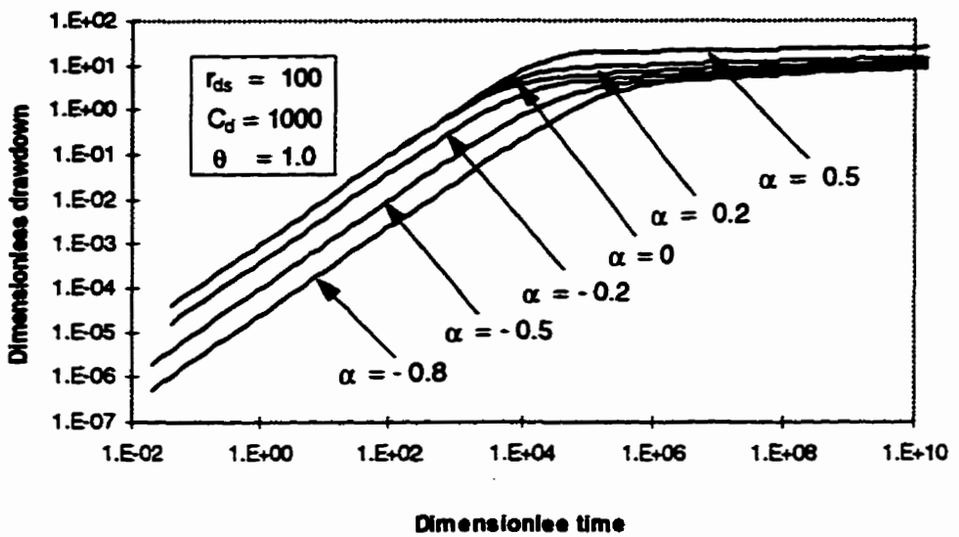

Figure 6.5 Effect of wellbore storage on drawdown-time relationships using different power parametr values.

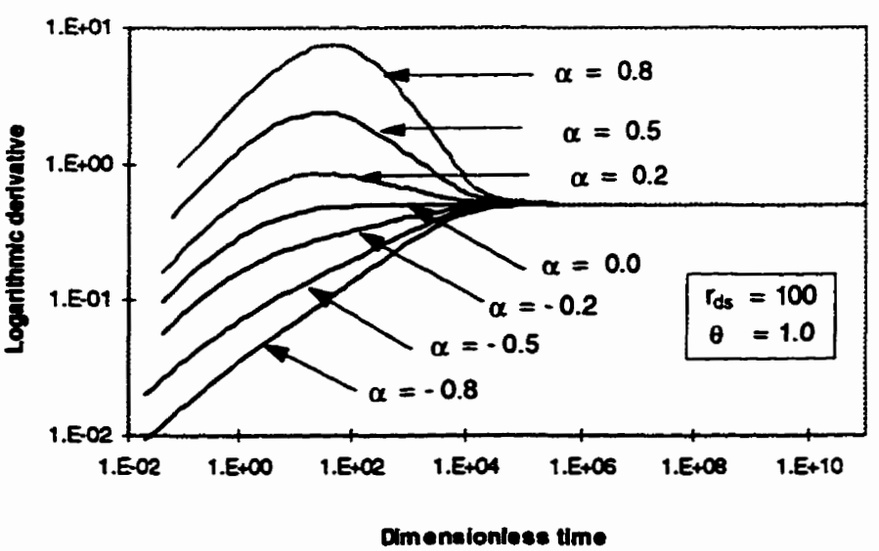

Figure 6.6 Logarithmic derivatives of hydraulic head (drawdown) using different power parameters values (neglect wellbore storage effect).

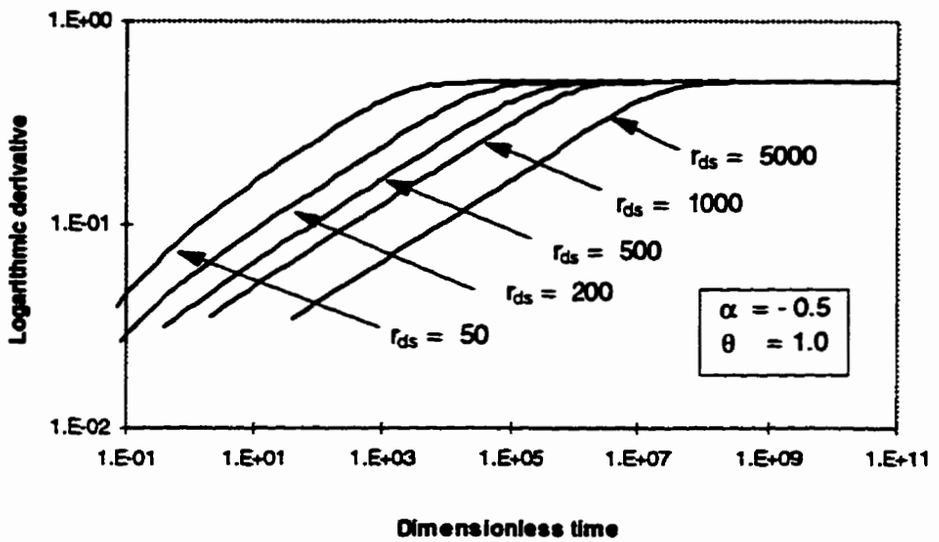

Figure 6.7 Logarithmic derivatives of hydraulic head (drawdown) with different size of alteration (neglect wellbore storage effect).

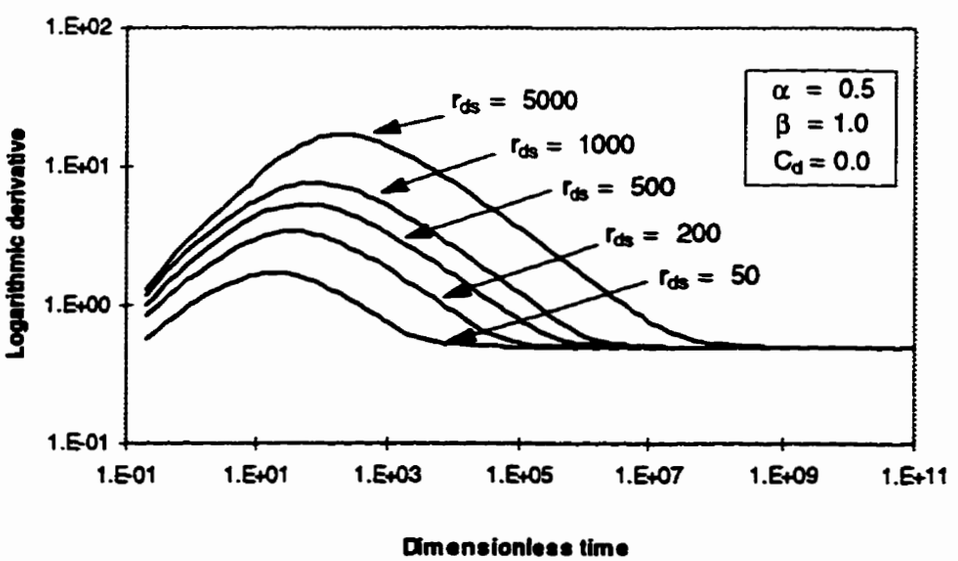

Figure 6.8 Logarithmic derivatives of hydraulic head (drawdown) with different size of alteration.

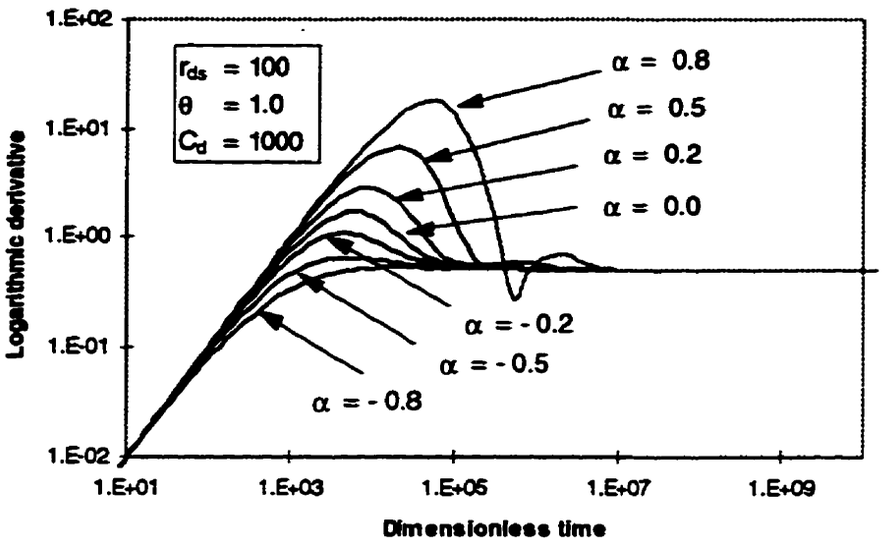

Figure 6.9 Logarithmic derivatives of hydraulic head drawdown using different power parameter values with wellbore storage considered.

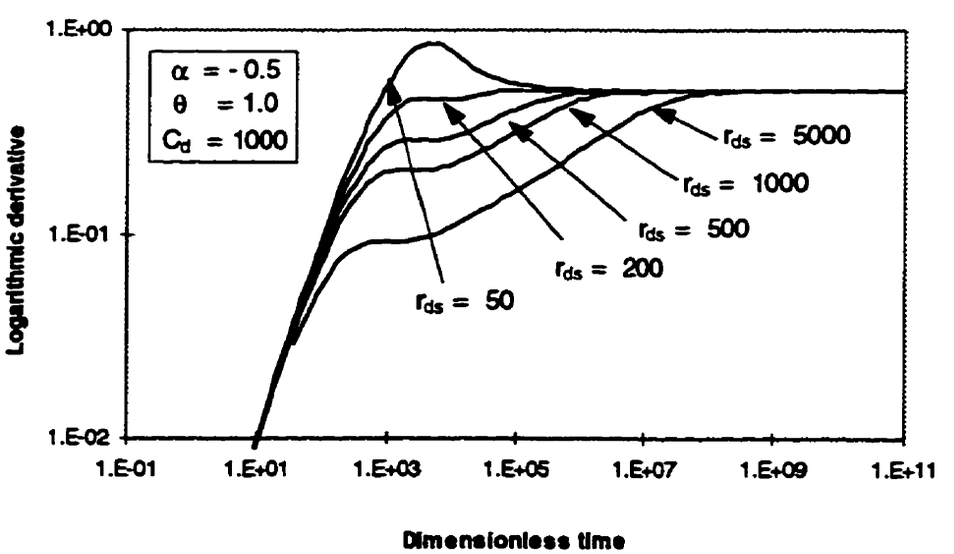

Figure 6.10 Logarithmic derivatives of hydraulic head (drawdown) with different size of alteration with wellbore storage considered.

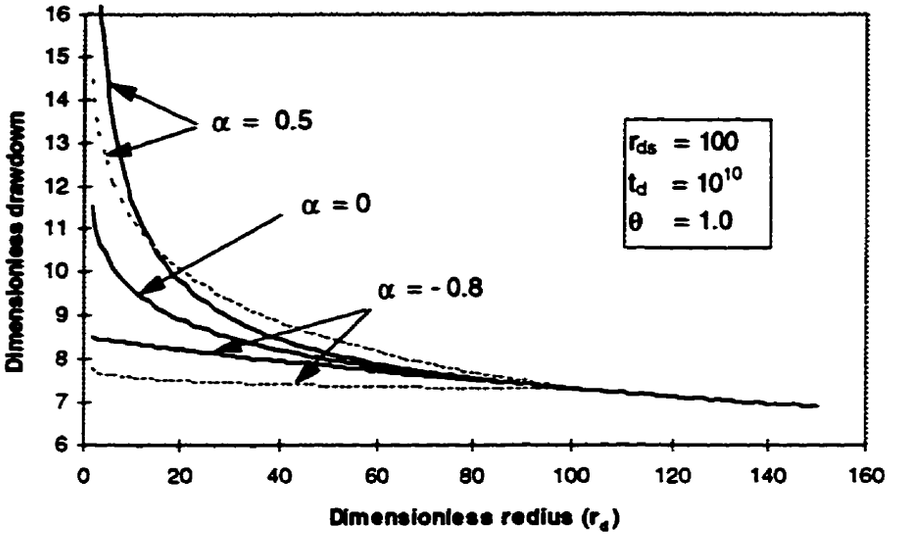

Figure 6.11 Comparisons of hydraulic head (drawdown) variations along radius between step permeability and power permeability models.

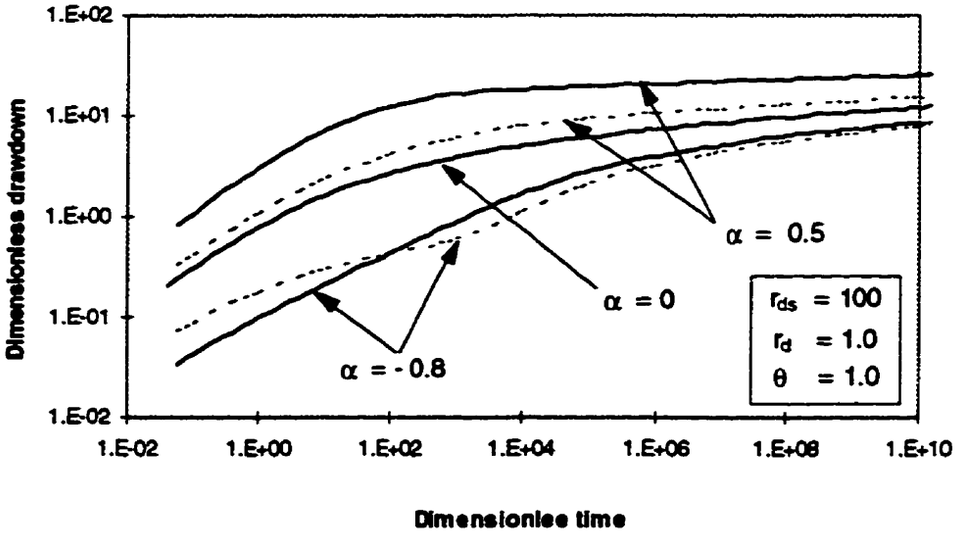

Figure 6.12 Comparisons of hydraulic head (drawdown) variations with time between the step permeability and power permeability models.

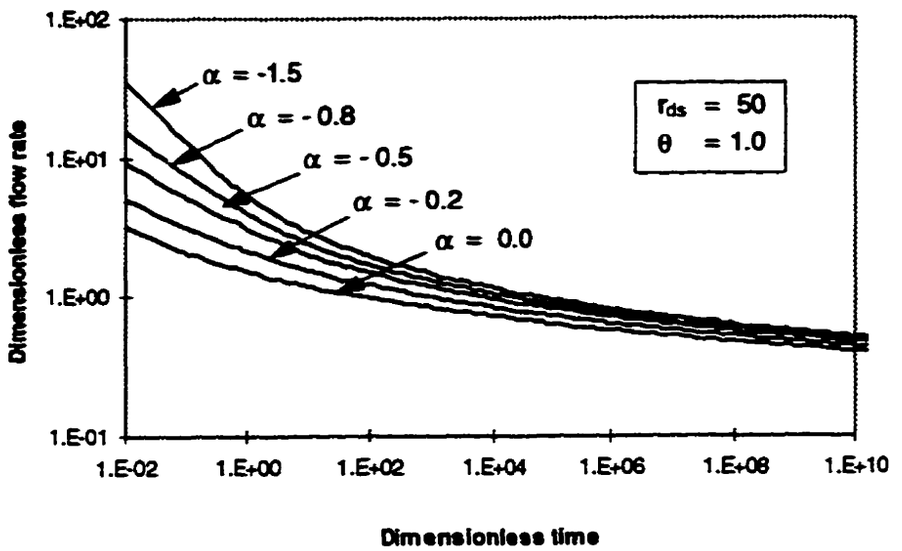

Figure 6.13 Well flow rate variations with time under constant well pressure conditions (improved reservoir).

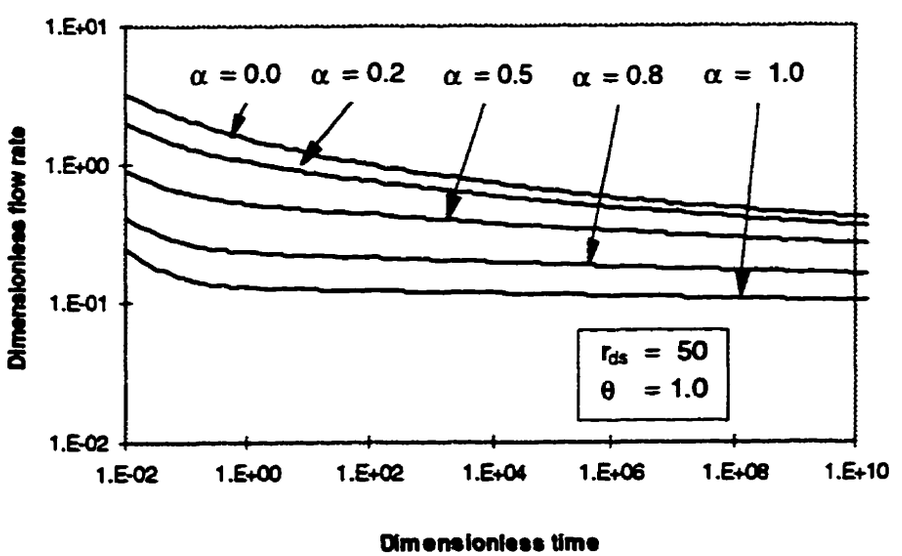

Figure 6.14 Well flow rate variations with time under constant well pressure conditions (damaged reservoir).

Chapter Seven

Research Summary and Conclusions

7.1 Research Summary

Several detailed analyses on application aspects of horizontal wells have been discussed in this thesis. Horizontal wells have become one of the most important tools in exploiting oil resources in the oil industry. The applications of horizontal wells in other engineering area such as contaminated groundwater cleanup is emerging. The traditional application of horizontal well in agriculture water table levelling and geotechnical dewatering can be systematically designed by the analytical results in this thesis. A horizontal well possesses many advantages compared to a conventional vertical well. In terms of productivity, a horizontal well usually is much better than a vertical well because of its longer contact length with the reservoir. Horizontal wells can lessen some of the conventional vertical well problems, such as gas or water coning and sand production. Horizontal wells also can greatly enhance gravity drainage processes because of the smaller pressure gradient required in production.

The productivity improvement from a horizontal well mainly comes from two parts; the longer contact length and the anisotropic permeability. The productivity increase is proportional to the well length for short wells ($L < 2h$), but the increase becomes a approximate logarithmic relationship when the well length becomes longer ($L >> h$). This indicates that, if the drilling cost is considered, increases of well length do not always mean an increase of production economically. The anisotropic permeability effect on well production can be approximately expressed as a relationship which is proportional to the square-root of the permeability ratio between vertical permeability k_z and well directional permeability k_α.

A slant well also can lead to a gain in production because of the inclination, besides the length and anisotropic permeability effects discussed above. Even though the productivity increase due to inclination is very small compared to the other two factors, it is worthwhile to note that the optimum productivity may come from a slant well rather than a horizontal well in thick and vertically less permeable reservoirs.

The reservoir parameters such as anisotropic permeability, formation compressibility and porosity are important in the evaluation of well productivity. The accuracy of these parameters directly affects the prediction of productivity and the design of well patterns in reservoir exploitation. Horizontal well test interpretation is one of the primary sources in obtaining these parameters. Therefore, it becomes another major objective of this thesis. Because well productivity is directly related to the permeability in the well direction, determination of k_α becomes an important task in well test interpretation. The new solutions derived in this thesis provide a way to determine the well directional permeability. The analyses available in the literature have not considered this parameter.

We also present new forms of the segmental solutions in terms of characteristic times, which makes the solutions simple, and convenient to use. The characteristic times for the boundary effect time t_b and well length effect time t_w usually can be determined directly from a derivative curve of a well test.

The true reservoir anisotropy can be determined by two directional permeabilities from the same reservoir using the relationship of (4.2.19). Two methods were discussed in the determination, a graphical method and a numerical method.

Wellbore storage and formation alteration often mask one or more flow regimes of a horizontal well test, which are the important data in the test interpretation. We discussed the effects of the storage on the segmental characteristic lines of different flow regimes. We also discussed ways to determine the end of the wellbore storage and formation alteration effects from both pressure and derivative curves. The formation alteration effects on a well test are not always possible to simulate by a skin term. If a large area is altered, such as in an sand producing reservoir, the alteration effect must be considered using an alteration model such as derived in Chapter 6.

Both wellbore storage and formation alteration effects can be evaluated by the curve matching method. However, to fully determine the anisotropic parameters of a reservoir, the wellbore storage effect should be minimized, such as by the use of a bottom-hole flow meter.

Even though horizontal wells have been the focus in this research, slant wells can be easily analyzed using the results presented in this thesis. All the solutions derived in this thesis are for general slant wells, the horizontal well solutions are only special situations of them. However, generally the slant solutions are more complicated than the horizontal well solutions, and therefore more numerical evaluation is required to use these solutions.

7.2 Conclusions and Discussion

7.2.1 Horizontal well productivity

Since the successful completion of the first modern horizontal well in the early 1970's, horizontal well applications have become extremely common and popular in the oil industry. Horizontal wells can provide a much larger drainage area than vertical wells under the same magnitude of pressure gradient because of a longer contact length with reservoirs. Horizontal wells also act as connecting conduits between vertical or inclined fractures in a reservoir.

Productivity prediction usually provides information for well pattern design in reservoir development. Productivity evaluation should therefore consider all important parameters such as 3-D anisotropic permeability, well orientation and inclination, and lateral boundary conditions. Borisov developed a productivity solution for horizontal wells in an isotropic reservoir which was modified later by Joshi to consider the reservoir anisotropy effect. However, Joshi only considered a two dimensional anisotropy by assuming $k_x = k_y$. This assumption makes his solution invalid in situations where k_x differs significantly from k_y. Neither solution considered the well inclination effect (slant well), which may lead to false conclusions for an optimum production design in thick reservoirs of small vertical permeability. To overcome these drawbacks, we presented a detailed analysis of the production evaluation of a slant well arbitrarily located in an 3-D anisotropic reservoir.

For a horizontal well, we find that the anisotropic permeability effects on well production can be approximately simulated by the following anisotropy-modified parameters:

$$L_i = L\sqrt{\frac{k_z}{k_\alpha}}, \quad r_{wi} = r_b\sqrt{\frac{k_\alpha k_z}{k_x k_y}}, \quad r_{el} = r_e\sqrt{\frac{k_z}{k_\alpha}} \tag{7.1}$$

From these parameters, we find that the modified well length L_i is proportional to the inverse square-root of the well direction permeability k_α. This indicates that a horizontal well drilled along the minimum permeability (k_y) direction can improve the well production in the same way as an increase in well length. Well radius has long been considered as sufficient by taking the permeability weighted average at the cross section in the evaluation of well productivity. However, from equation (7.1) we find that the additional terms such the axial permeability k_α also play a role and should be considered

in this weighting average. Considering the effect of k_α on well radius, we find that it is beneficial to the productivity if a well is drilled along the maximum (k_x) direction. However, because well radius has a very limited effect on well productivity, this anisotropy effect on the well radius may never be able to overcome the productivity decrease caused simultaneously by decreasing the modified well length L_s.

Increasing the vertical permeability k_z, by hydraulic fracturing for example, is equivalent to increase well length or wellbore radius (not linearly). Therefore, increasing the vertical permeability can improve productivity more than decreasing k_α. From equations in (7.1), we also find that the effect of vertical permeability can also be considered by using the anisotropy-modified well length L_l and well radius, which are proportional to the square-root of k_z.

7.2.2 Horizontal well test interpretation

Interpretation of a horizontal well test is more difficult than a vertical well test because of the many possible interactions between the well (orientation, elevation, inclination...) and reservoir (boundary condition, anisotropy...). The various flow regimes presented in a horizontal well test complicate the interpretation further.

Many well pressure transient solutions have been reported in the literature. These solutions are the basis of horizontal well test interpretation. However, there are several problems with those solutions. As we know, all these solutions assume that the well is parallel to the k_y direction which, however, is not always true. One drawback of this assumption is that the estimated permeability by these solutions is not the true reservoir anisotropy. A false anisotropy ellipse could lead a designed well to deviate significantly from the optimum productivity direction. Another common problem of the solutions in the literature is that the various characteristic times presented in a horizontal well test are not well formulated and used. The characteristic times are important in a test interpretation because they control the length of each flow regime as well as the test flow patterns identification (VLH or VSH).

A detailed horizontal well pressure analysis is given in Chapter 4. The solution is derived for a well with arbitrary orientation and inclination, and located in a three dimensional anisotropic reservoir. We discussed the horizontal well situation in much more detail than for the slant well because horizontal well tests are more common in the evaluation of reservoir characteristics, which is particularly true in the development period of a reservoir. However, a slant well test can also be interpreted similarly as a horizontal well test with the slant well solution developed in Chapter 4.

The logarithmic derivative of a horizontal well test is more useful than its pressure curve in test interpretation. This is because the derivative shows more distinguishable characteristics for each flow regime. The segmental solutions expressed in terms of the characteristic times in Chapter 4 in fact can lead to a simple and uniform solution form for the derivatives.

By simple derivation, we can find the following forms for the derivatives of the VLH flow pattern in oil field units:

$$\Delta p' = \frac{162.6\mu BQ}{hk_h}\sqrt{\frac{t_b}{t_w}} \qquad (t < t_b) \tag{7.2}$$

$$\Delta p' = \frac{162.6\mu BQ}{hk_h}\sqrt{\frac{t}{t_w}} \qquad (t_b < t < t_w) \tag{7.3}$$

$$\Delta p' = \frac{162.6\mu BQ}{hk_h}\sqrt{\frac{t_w}{t_w}} \qquad (t > t_w) \tag{7.4}$$

and for the VSH flow pattern:

$$\Delta p' = \frac{162.6\mu BQ}{hk_h}\sqrt{\frac{t_b}{t_w}} \qquad (t < t_w) \tag{7.5}$$

$$\Delta p' = \frac{162.6\mu BQ}{hk_h}\sqrt{\frac{t_b}{t}} \qquad (t_w < t < t_b) \tag{7.6}$$

$$\Delta p' = \frac{162.6\mu BQ}{hk_h}\sqrt{\frac{t_b}{t_b}} \qquad (t > t_b) \tag{7.7}$$

where $\Delta p'$ is the derivative and t_b and t_w are the characteristic times which have the following forms:

$$t_b = \frac{301.75h^2c_m\phi\mu}{k_z}, \qquad t_w = \frac{301.75L^2c_m\phi\mu}{k_\alpha} \tag{7.8}$$

In fact, the two characteristic times, t_b and t_w, themselves may be taken as two more representative and comprehensive parameters in describing the combined effects of a well interaction with a reservoir. First, the relative magnitudes of t_b and t_w determine the flow patterns, VLH or VSH; second, we note that t_b reflects the time at which the boundary effects are observed in the wellbore pressure, and t_w is the time at which the well length effect on the wellbore pressure transition becomes negligible. Also, the effects of well effective length, formation compressibility and porosity are included in these parameters, which are difficult to determine for the real test. Intuitively, if the productivity is to be evaluated during the transient period, t_b will be the time at which productivity shows a sudden decrease, and t_w is the time when productivity begins to gradually stabilize towards the steady-state production discussed in Chapter 3.

It is a simple task to estimate other reservoir parameters from (7.8) if t_b and t_w are obtained, except for k_x and k_y. The determination of horizontal anisotropic permeability k_x and k_y requires estimating of the permeability ellipsoid of a reservoir. We have discussed a detailed procedure to determine the horizontal anisotropic permeability ellipse from two horizontal wells in different orientations. Two methods were introduced in Chapter 4 to determine the true reservoir anisotropy: a graphical method and a numerical method. Each method has its advantages and disadvantages. The numerical method is more accurate than the graphical method but we need to figure out and eliminate the invalid intersections. The graphical method is easy to use but less accurate and a measuring net is required. In practical applications, if all three permeabilities $k_{\alpha 1}$, $k_{\alpha 2}$ and k_h are very close in magnitude, then it is possible that the reservoir is an isotropic reservoir; if $k_{\alpha 1}$ and $k_{\alpha 2}$ are close in magnitude but differ from k_h, then the spreadsheet method might be preferable; if $k_{\alpha 1}$ and $k_{\alpha 2}$ differ significantly, then the graphical method is convenient.

The flow patterns are the results of the combined effects from both the well geometry and reservoir characteristics. The flow pattern can be uniquely determined by the characteristic times t_b and t_w. Two primary flow patterns can be present in a horizontal well test performed in a infinite reservoir; the Vertical-Linear-Horizontal (VLH) flow pattern and the Vertical-Spherical-Horizontal (VSH) flow pattern. The two patterns differ in their relative magnitude between the boundary effect time t_b and well length effect time t_w. The segmental solutions simplified from the integrated solution become different for the two flow patterns, and the appropriate solutions need to be used in a horizontal well

test interpretation with a given flow pattern.

The solution expressions presented in Chapter 4 also provide a way to estimate the effective well length if the horizontal permeability is approximately isotropic, or if the well is in the average permeability direction i.e. $k_\alpha = k_h$. Under these conditions, the horizontal permeability k_h can be estimated from the horizontal radial flow regime, which is independent of the well length, and the well effective length can be determined from parameter t_w to obtain the following (in oil field units):

$$L_e = \frac{0.539BQt_w}{hc_m\phi\Delta p'_h} \tag{7.9}$$

where L_e is the effective well length and $\Delta p'_h$ is the pressure derivative at the horizontal radial flow regime.

The vertical permeability can be estimated from the early vertical radial regime or from t_b.

7.2.3 Wellbore storage and formation alteration effects

Wellbore storage effects on horizontal well tests are very similar to those of vertical well tests in terms of both type curves and derivative curves. However, depending on the magnitude of the storage coefficient, the early, middle, and even the late time flow regimes can be masked. Different from a vertical well test, horizontal well test masking can seriously damage the characteristics the segmental lines possess, which the test interpretation usually depends on. If this is the case, the interpretation quality will be limited, and most likely, only the storage coefficient can be determined from the storage masked segments. Therefore, if a large part of a test curve shows wellbore storage as dominant, the anisotropic parameters may become impossible to estimate.

Formation alteration also distorts the original characteristics of horizontal well test type curves and derivative curves. If the section of the type curve in which the alteration characteristics are present is not masked by the wellbore storage, it can be used to estimate the formation alteration parameters, such as alteration degree and alteration, by methods such as curve matching. The alteration size also can be estimated by using solution (6.4.1) because different alteration sizes give different intersections to the non-altered horizontal line in a derivative graph. However, if wellbore storage and formation alteration are combined, usually the alteration characteristics will be masked by the wellbore storage.

One thing we need to mention is that a improved formation sometimes can show a very similar effect to that of wellbore storage on a pressure or derivative curve, particularly if the formation permeability improvement is great ($\alpha < -0.5$). This similarity comes from the fact that both effects slow down the wellbore pressure decline rate. If this is the case, the slope of the affected line segments should be studied carefully to identify the cause of the dominant effect.

7.3 Future Research On Horizontal Well Analysis

We have focused on the analysis of productivity as well as parameter estimation for a horizontal well test throughout this research. However, many important issues related to horizontal well applications have been simplified, and sometimes over-simplified. Some other problems remain unsolved. The most important ones include the determination of horizontal well effective length, reservoir heterogeneity effects, moving boundaries, and productivity evaluation under multi-phase flow condition.

In the derivation of the solutions in Chapter 3 and 4 we assume that the flux entering the wellbore is the same along the whole length of the wellbore. This has over-simplified the real situation. Because of the viscosity effect, a certain amount of pressure gradient along the well axis is required in order for the fluid entering the wellbore to be transported to the well heel. The axial pressure gradient along the well also is not a constant; the gradient should be larger near the heel, and gradually decreases toward the toe. However, the actual pressure distribution along the well is unknown because it will be a function of the well length, orientation, total flow rate and reservoir characteristics. The reservoir pressure decline will also decrease from the area near the well heel to the area near the well toe. For a long horizontal well, it is very possible that the reservoir flux entering the wellbore is so small near the well toe area that the surrounding reservoir pressure decline becomes very small compared to the average. Under this condition, the effective well length which is receiving flux from reservoir will become less than the actual well length, and a effective well length must be used.

The effective well length can affect the magnitude of parameters estimated from a well test. Determination of well effective length is only possible from a well test if $k_a = k_h$, as discussed above. However, if this condition on the horizontal permeability can not be satisfied, it seems unlikely that the effective well length can be determined from a well test. Two possible ways might be considered in further research; the experimental method and numerical simulation.

The viscosity effect on the transportation of fluid within the wellbore disappears in a buildup test because no real wellbore flow exist in such cases. Therefore, we expect that the well length in a

buildup test should be approximately the same as the real well. This provides one possible way to estimate the effective well length by comparing the parameters estimated from both the drawdown and buildup test. However, because the effective well length depends on individual well configurations, the effect length obtained from a individual test may not be applicable to other wells in the same reservoir.

Another possibility in determining the effective well length is through numerical simulation. Two wellbore conditions may be used in such simulations. We may assume that the whole length of the well is filled up with fluid, but with varying densities due to the pressure difference along the well. The pressure and pressure gradient along the well can then be calculated easily. The calculated pressure is then assigned as the wellbore pressure conditions in the reservoir transient simulation. If the numerical simulated pressure is compared with the analytical pressure solution developed in Chapter 4, the effective well length can be estimated. Another possible way to simulate the effective length related problem may employ the assumption that, instead of a well, a cylinder of highly permeable material is located at the well location. Under this condition, only the pressure at the well heel need be simulated numerically. The pressure at other parts of the well will be determined by the flow conditions. This assumption may be closer to reality because the wellbore pressure will be determined automatically based on the simulation, which has the same mechanism as the real situation.

Reservoir heterogeneity is also an important factor in horizontal well test interpretation. In some situations, a horizontal well can be as long as 2000 to 3000 meters. In such a long section, it is almost certain that the porous medium properties will vary along the well. A well test in a heterogenous reservoir will reflect the combined characteristics along the whole effective length. This makes it difficult to identify the productive sections from the impaired sections. However, there are no obviously feasible methods which can address the problem. Observation points located along the wellbore may help by providing pressure distribution data, but this requires a complicated completion procedure or extra wells.

All the productivity and pressure analyses in this thesis assume that the reservoir is a layered reservoir with upper and lower impermeable boundaries. The situation of a gas cap or active bottom water reservoir will be much different from this assumption. Strictly speaking, the flow in such reservoirs will be multi-phase rather than single-phase flow. If the multi-phase character can be neglected, the moving boundary problem must be considered because the boundaries between the two phases will move toward the well during a well test or during production. This moving boundary problem is also important in the prediction of water or gas coning. It might be interesting to explore the relationship between the boundary effect time t_b and the moving boundary initiating time. There should exist some quantitative relationships because, intuitively, only after the boundary is detected by the pressure

propagation can the particles beyond the boundary begin to move.

Other problems related to horizontal well application analysis and applications also need to be addressed in future research. This may include a cost-optimized well productivity analysis by considering the cost in well drilling, completion and so on. Horizontal well test interpretation in fractured reservoirs also needs a more detailed study. Topics related to other engineering areas may include pressure decline analysis in water-table aquifers, important in dewatering design; water pressure distribution in a non-horizontally distributed initial pressure surface, a problem often encountered in slope stability analysis; and other environmental and petroleum related problems.

Chapter Eight

References

Abbaszadeh, M. and Kamal, M., 1989. "Pressure-transient testing of water-injection wells", SPE Reservoir Engineering, February, pp. 115-124.

Babu, D. K. and Odeh, Aziz S, 1989. "Productivity of a horizontal well", SPE Reservoir Engineering, November, pp. 417-421.

Bear, J., 1972. "Dynamics of Fluids in Porous Medium", Dover Publications Inc., New York.

Bennion, D.B. and Thomas, F.B., 1995. "Under-balanced drilling of horizontal wells: is it a total solution ?" J. Canada Petroleum Technology, November, pp. 34-41.

Borisov, Ju., P., 1984. "Oil production using horizontal and multiple deviation wells". Nedra, Moscow (1964). Translated by J. Strauss and S. D. Joshi (ed.), Phillips Petroleum Co., Bartlesville, USA, the R&D Library Translation.

Butler, R. M., 1994. "Horizontal wells for the reservoir of oil, gas and bitumen". Petroleum Society Monogrph Number 2.

Butler, R. M., 1989. "The potential for horizontal wells for petroleum production". J Canadian Petro. Tech., Vol. 28, No. 3, pp. 39-47.

Butler, J. J. Jr., 1988. "Pumping tests in nonuniform aquifers - the radially symmetric case", J. Hydrology, 101, pp. 15-30.

Carslaw, H. S. and Jaeger, J. C., 1959. "Conduction of Heat in Solids", Clarendon Press, Oxford.

Cinco, H., Miller, F. G. and Ramey, H. J., 1975. "Unsteady state pressure distribution created by a directional drilled well". JPT, November, pp. 1392-1400.

Daviau, F., Mouronval, G., Bourdarot, P. and Curutchet, P., 1988. " Pressure analysis for horizontal wells", SPE Formation Evaluation, December, pp. 716-724.

Domzalski, S., Yver, Jean-Pierre, 1992. " Horizontal well testing in the Gulf of Guinea", Oil Field Review, April, pp. 42-45.

Dusseault, M.B., 1994. "Borehole stability analysis", Proceedings 8th IACMAG, West Virginia; Balkema, Rotterdam, Vol.1, pp. 125-137 .

Dykstra, H. and Dickinson, W., 1992. "Oil recovery by gravity drainage into horizontal wells compared with recovery form vertical wells", SPE Formation Evaluation, September, pp. 255-260

Dullien, F.A.L., 1979, "Porous media fluid transport and pore structure", Acdemic Press.

Freeze R.A. and Cherry J.A., 1979 "GroundWater", Prentice-Hall Inc., Englewood Cliffs, New Jersey.

Frick, T.P., Economides, M.J., 1993. "Horizontal well damage characterization and removal", SPE Production and Faciliites, February, pp. 15-22.

Geilikman, M.B., Dusseault, M.B. and Dullien, F.A.L, 1994. "Sand production as a viscoplastic granular flow", SPE 27343, Int. Sym. Formation Damage Control, Lafayette, Louisiana, Feb. 9.

Goode, P. A. and Thambynayagam, R. K. M., 1987. " Pressure drawdown and build up analysis of horizontal wells", SPE Formation Evaluation, December, pp. 683-697.

Gringarten, A.C., Ramey, H.J. and Raghavan, R., 1974. "Unsteady-state pressure distributions created by a well with a single infinite-conductivity vertical fracture", SPE Engineers Journal, August, pp. 347-360.

Haitjema, H. M., 1985. "Modelling three-dimensional flow in confined aquifers by superposition of both two- and three-dimensional analytic functions". Water Resources Research, Vol. 21, No.10, pp. 1557-1566.

Hantush, M.S., 1966. "A method for analyzing a drawdown test in anisotropic aquifers", Water Resource Research, Vol.2, No. 2.

Hawkins, M. F., Jr., 1956. "A note on the skin effect", Trans. Am. Inst. Min. Metall. Pet. Eng., Vol. 207, pp. 356-367.

Howard,G. C. and Fast, C. R., 1970. "Hydraulic fracturing", SPE of AIME Monograph, Vol. 2.

Irmay, S., 1955. "Flow of fluid through cracked media", Bull. Res. Council of Israel No. 1, 5A, pp. 84.

Joshi, D., 1988. "Augmentation of well productivity with slant and horizontal wells". J. Petro. Tech. June, pp. 729-739.

Joshi, D., 1987. " A review of horizontal well and drainhole technology". SPE 16868, Soc. of Petro. Eng. preprint.

Kamal, M. M., Braden, J.C. and Park, H., 1992 "Use of transient testing to identify reservoir damage problems", SPE 24666, SPE Annual Fall Meeting, Washington, D.C.

Karakas, M., Yokoyama, Y. M. and Arima, E. M., 1991, "Well test analysis of a well with multiple horizontal drainholes", SPE 21424, SPE Middle East Oil Show, Bahrain, November, 16-19, pp. 715-734.

Kuchuk, F.J, Goode, P. A., Brice, B. W, and Thambynayagam, R.K., 1988. "Pressure transient analysis and inflow performance for horizontal wells", Paper SPE 18300, presented at the 1988 SPE Annual Technical Conf., Houston, October 2-5.

Kuchuk, F.J, Goode, P. A., Brice, B.W, Sherrard, D.W., and Thambynayagam, R.K., 1990. "Pressure-transient analysis for horizontal wells, JPT August, pp. 974-979-1028-1031.

Lee, S. H. and Milliken, W. J., 1993. "The productivity index of an inclined well in finite difference reservoir simulation". SPE 25247, 12th Symp. on Reservoir Simulation, New Orleans.

Lee, S. H., 1989. "Analysis of productivity of inclined wells and its implication for finite difference reservoir simulation". SPE Production Engineering, pp. 173-179.

Lien, S. C., Haldorsen, H.H. and Morten Manner, 1992. "Horizontal; wells: still appealing in formations with discontinuous vertical permeability barriers", JPT, Vol. 44, No. 12, pp. 1364-1370.

MacDonald, R. R., 1985. "Drilling at cold lake horizontal well pilot". SPE 14428, No. 2.

Marx, C. and Rahman, S.S., 1987. "Evaluation of formation damage caused by drilling fluids, specifically in pressure-reduced formations", JPT November, pp. 1449-1452.

Mattar, L. and Santo M., "A practical and systematic approach to horizontal well test analysis". JCPT, Nov., 1995, Vol. 34, No.9.

Matthews, C. S. and Russel, D. G., 1967. "Pressure buildup and flow test in wells", Monograph Series, 1967, SPE of AIME, Dallas, No. 1.

Michael, J., 1976. " A numerical integral code", Persional conminication

Moench, A. F., 1985. "Transient flow to a large-diameter well in an aquifer with storativity semiconfining layers", Water Resour. Res., 21(8), pp. 1121-1131.

Moench, A. F. Hsieh, P. A., 1985. "Analysis of slug test in a well with finite thickness skin", paper presented at the 17th international Congress, Int. Assoc. Hydrogeol. Tucson, Ariz., January.

Muskat, M., 1937. "The flow of homogeneous fluids through a porous media". Intl. Human Resources Development Corp., Boston.

Novakowski, K.S., 1993. "Interpretation of the transient flow rate obtained from constant-head tests conducted in situ in clays", Canadian Geotechnical Journal, Vol. 30, No. 4, pp. 600-606.

Novakowski, K.S., 1989. "A composite analytical model for analysis of pumping tests affected by wellbore storage and finite thickness skin", Water Resour. Res., Vol. 25(9), pp. 1937-1946.

Olarewaju, J.S., Lee, W.J., 1987. "A comprehensive application of a composite reservoir model to pressure transient analysis", SPE paper 16354, SPE California Regional Meeting, Ventura, April 8-10, pp. 227-243.

Ozkan, E., Raghavan, R. and Joshi, S., 1989. " Horizontal well pressure analysis". SPE Formation Evaluation, December, pp. 567-575.

Ozkan, E., Raghavan, R. and Joshi, S. D., 1987. "Horizontal well pressure analysis", SPE California Region Meeting, Ventura, California, April 8-10, pp. 511-529.

Papadopulos, I.S., Cooper, H.H., 1967. "Drawdown in well of large diameter", Water Resou. Res., Vol. 3, No. 1, pp. 241-244.

Peaceman, D. W., " 1983. "Interpretations of well block pressure in numerical reservoir simulation with nonsquare grid blocks and anisotropic permeability," SPEJ June, pp. 531-543.

Ranney, L., 1939. "The first horizontal well". Petroleum Engineering, June, pp. 25-30.

Robert, C. E. Jr., 1977. "Advances in well test analysis", SPE Monograph, Vol. 5, Henryl. Doherty Series.

Rosa A. J. and Souza Carvaho, R., 1989. " A mathematical model for pressure evaluation in an infinite-conductivity horizontal well", SPE Formation Evaluation, December, pp. 559-566.

Rumer, R.R, 1969. "Resistance to flow through porous media", Academica press, New York.

Russell, D. G., and Truitt, N. E.; 1964. "Transient pressure behaviour in vertically fractured reservoirs", J. Pet. Tech. (Oct. 1964) 1159-1170; Trans. AIME, Vol. 231.

Sabet. M.A., 1991. "Well test analysis", Gulf Publishing Company.

Scheidegger, A.E., 1960. "The physics of flow through porous media", 2nd ed., University of Toronto Press, Toronto.

Sherrard, D.W., Brice, B.W. and MacDonald, D.G., 1987. "Application of horizontal wells at Prodhoe Bay", SPE November, pp. 1417-1425.

Stehfest, H., 1977. "Numerical inversion of Laplace transforms", Communication of the ACM, 13(1), pp. 47-49.

Van Der Vlis, A. C., Duns, H. and Luque, R. F., 1979. "Increased well productivity in tight chalk reservoir". Proc. 10th Word Petroleum Cong., Bucharest Vol. 3 pp. 71-78.

Van Everdingen, A. F. and Meyer, L. J., 1971, "Analysis of buildup curves obtained after well treatment", J. Pet. Tech. (April 1971) 513-524; Trans. AIME Vol. 251.

Zhang, L. and Dusseault M.B., 1997. "Evaluation of formation damage from a constant-head borehole test", 36th U.S. Rick Mechanics Symposium, June 29-July 2.

Zhang, L., Dusseault, M.B., 1997. "Formation alteration characterization from well test interpretation", 9th IACMAG Conf. Nov 2-7, Wuhan, Hubei, People' Republic of China.

Zhang, L., Dusseault, M.B., 1996. "Anisotropic permeability estimation by horizontal well tests". 2nd Int. Conf. on Horizontal Well Technology, Calgary, 18-20 November.

Zhang, L., Dusseault, M.B. and Franklin, J.A., 1995. "Are horizontal wells always better producers than vertical wells", Canadian SPE/CIM/CANMET Int. Conf. on Recent Advances in Horizontal Well Applications, HWC94-27, March, 1994, Calgary, Canada.

Zhang, L. Dusseault, M.B. and Franklin, J.A. 1994. "Evaluation of horiozntal well productivity index", Proceedings 8th IACMAG, West Virginia; Balkema, Rotterdam, Vol. 3, pp 2201-2206.

Zhang, L. and Franklin, J.A., 1993. " Prediction of water flow into rock tunnels: an analytical solution assuming an hydraulic conductivity gradient", Int. J. Rock Mech. Min. Sci. & Geomech. Abstr. Vol. 30, No. 1, pp. 37-46.